Characterization, Comparison and Application of Two Types of Atmospheric Pressure Cold Argon Plasma Jets

Xiaomeng Fei

A THESIS SUBMITTED FOR THE DEGREE OF DOCTOR OF ENGINEERING

DEPARTMENT OF PRODUCTION SCIENCE AND TECHNOLOGY,

GRADUATE SCHOOL OF ENGINEERING

GUNMA UNIVERSITY

MARCH, 2011

CONTENTS

Chapter 1 General Introduction

1 Plasma classification

1.1 Thermal equilibrium plasma and non-thermal equilibrium plasma

Plasma is a more or less ionized gas. It is considered the fourth state of matter beside solid, liquid and gas. In fact, most of the observable matter (more than 99%) in the universe is in the plasma state. From a macroscopic point of view, plasma is electrically neutral. However, plasma is electrically conductive and a lot of free charge carriers are contained in it [1].

Depending on the amounts of energy transferred to the plasma, the plasma properties change in terms of electron density and electron temperature. These two parameters distinguish plasmas into different categories (see Fig. 1-1) [2]. Generally, plasmas are divided into two categories: thermal equilibrium plasma (thermal plasma) and non-thermal equilibrium plasma (cold plasma). In thermal plasma, transitions and chemical reactions are controlled by collisions and not by radiative processes. Moreover, collision phenomena are micro-reversible in thermal plasma, suggesting that each kind of collision is balanced by its inverse (excitation/de-excitation; ionization/recombination; kinetic balance) [3]. Therefore, in thermal plasma the electron temperature is equal to the gas temperature (depending on the temperature of heavy particles).

Non-thermal equilibrium plasma (cold plasma) can be described by two temperatures: electron temperature (T_e) and heavy particle temperature (T_h). Because of the huge mass difference between electrons and heavy particles, the plasma temperature (or gas temperature) is determined by T_h. On the other hand, the electron-induced de-excitation rate of the atom is generally lower than the corresponding electron-induced excitation rate because of a significant radiative de-excitation rate. Therefore, the density distribution of excited atoms in cold plasma is possible to depart from

Boltzmann distribution, suggesting that the gas temperature is much lower than the electron temperature [4-7].

1.2 Atmospheric pressure non-thermal equilibrium plasma

Fig. 1-2 shows effect of gas pressure on electron temperature (T_e) and gas temperature (T_g) [2]. It can clearly see that at a lower pressure ($10^{-4} \sim 10^{-2}$ kPa) gas temperature is much lower than electron temperature. The heavy particles are excited or ionized through inelastic collisions with electrons. These inelastic collisions do not raise the temperature of heavy particles. However, collisions in the plasma intensify when the gas pressure becomes higher. They lead to both plasma chemistry (by inelastic collisions) and heavy particles heating (by elastic collisions). Then, the difference between T_e and T_g decreases; plasma state is close to the thermal equilibrium state. How to prevent heavy particles from being heated is crucial to generate non-thermal equilibrium plasma at atmospheric pressure. It was found that the density of the feeding power affects the plasma state (thermal equilibrium or not) at a large extent. Namely, a high power density lead to atmospheric pressure thermal equilibrium plasma (e.g. arc plasma); a low density of feeding power or a pulsed power supply lead to atmospheric pressure non-thermal equilibrium plasma.

2 Dielectric barrier discharges (DBDs)

Dielectric barrier discharges have been known for more than one century. First experimental investigation was reported by Siemens in 1857 [8]. They concentrated on the generation of ozone by using DBDs. Nowadays, DBDs are widely used to generate atmospheric pressure non-equilibrium plasmas in a controllable way.

Generally, planar and cylindrical electrode arrangements are used in DBDs. (see Fig.1-3) [9]. No matter what kind of electrode arrangement is employed, the presence of one or more dielectric

layers between the metallic electrodes across the discharge gap is essential for the discharge. First, the dielectric is able to limit the discharge current and can avoid occurrence of the arcing transition. Second, the dielectric distributes microdischarges (streamers) randomly on the electrode surface since the formation of microdischarges is due to the electron accumulation on the dielectric layer. Typical materials for dielectric barriers are glass, quartz and ceramics. Plastic foils, teflon plates, silicone tube and other insulating materials can be used as well [9].

2.1 Filamentary mode barrier discharges

DBDs have been studied by many researchers [10-17]. There are two different modes of DBDs (filamentary mode and diffuse mode). DBD is generally operated in the filamentary mode. If the local electric field strength in the gas spacing gap reaches the ignition level, the breakdown occurs at many points followed by the development of filaments, named microdischarges. A large number of microdischarges were observed in most gases when the pressure is in the order of 10^5 Pa. The development of microdischarges can be sub-divided into three steps [9, 18]:

(1) The pre-breakdown phase. A negative space charge of electrons (or negative ions due to attachment) is accumulated in front of the anode (according to the polarity of the half cycle of applied voltage). The pre-breakdown phase lasts for at least 0.5 ms. Then, a high local electric field strength is formed in front of the anode. If it reaches a certain critical level, the breakdown starts from the anode surface.

(2) The propagation phase. This phase is controlled by an ionization wave (i.e. a wave of high local electric field strength) in the direction to the cathode. Pairs of ions and electrons are produced on the way of the ionization wave. This phase typically takes 1 ~ 2 ns.

(3) The decay phase. The decay phase is characterized by the charge accumulation on the dielectric

surface compensating the external electric field. Both the emission radiation and current pulses of the microdischarges decay in this phase.

The microdischarges are of nanosecond duration. They are uniformly distributed over the dielectric surface. In the next half cycle of the applied voltage, the formation of microdischarges renews inversely. The dielectric barrier limits the amount of the transferred charge and the energy deposited in a single microdischarge channel. Therefore, non-thermal equilibrium plasma is able to be generated at atmospheric pressure by DBD. Figure 1-4 shows the effect of the time constants on the relevant processes in the filamentary DBDs [9]. It can see that the development of microdischarge channels, which is characterized by the production of energetic electrons, takes place in the range of ns. However, the phase of plasma chemical reactions by atoms, radicals, excited species and short wave radiation typically starts within the minisecond scale. The production of active species is controlled by the properties of the microdischarges, namely by the reduced local electric field strength and electron density. The properties of the microdischarges in filamentary DBDs do not depend on the external driving circuit (e.g. the frequency, feeding voltage and waveform) over a wide range of operation conditions. They are mainly controlled by the feeding gas composition.

2.2 Diffuse (glow) mode barrier discharges

Under certain operating conditions, a diffuse (glow) mode of DBD can be obtained. In 1976, Donohoe investigated a uniform glow discharge with pulsed excitation in helium/ethylene mixtures [19]. In 1987, Okazaki and coworkers operated barrier glow discharges at 50 Hz sinusoidal feeding voltage, using an electrode configuration of two metal foils covered with a special metal mesh and ceramic dielectrics in helium, nitrogen and air etc. with and without certain organic additives [20-22].

They proposed the term “APGD” (atmospheric pressure glow discharge) for the first time. In 1992, Massines and co-workers investigated barrier glow discharges in helium and nitrogen in detail [23-25]. The generation of stable diffuse DBD at atmospheric pressure requires special operation conditions, which mainly depend on the properties of feeding gas. Comparing to the conditions of the filamentary mode DBD, effective pre-ionization, Penning ionization via metastables, and primary ionization in the low electric field are very important for the generation of diffuse mode DBD [9]. Additionally, the diffuse mode DBD is sensitive to impurities, admixtures, metastables and residual ions. The densities of residual species from the previous half period that can initiate the diffuse discharge in the next half cycle are dependent on the repetition frequency. Therefore, the feeding voltage frequency plays an important role in the transition to the diffuse mode. Some dielectric materials can trap considerable amounts of charges uniformly on the surface. When the electric field changes its polarity, the charge carriers are expelled from the surface and initiate a diffuse discharge [26]. The required operation conditions have been obtained in helium, neon and pure nitrogen gas.

Many efforts have been implemented to understand the formation mechanism of the diffuse DBD. So far, considerable progress was made to better understand the formation of diffuse DBD. The basic mechanisms of diffuse DBD are strongly affected by the properties of the feeding gas. This can be illustrated by the comparison of the DBD in helium and nitrogen. The dominant ionization and excitation mechanisms for both gases are quite different. In helium plasma, effective ionization and excitation processes occur in the electric field of the cathode region through direct collisions of atoms with energetic electrons or through three body processes, generating He^+ and He_2^+ ions [27, 28]. Penning ionization processes via nitrogen impurities in helium gas seems to be

important, too [28]. On the contrary, in nitrogen plasma ions and electrons are probably generated through another mechanism. Kinetic models of diffuse DBD in the nitrogen plasma come to the conclusion that Penning ionization through two body collisions of metastable nitrogen molecules producing N_4^+ ions and electrons are very important [29]. On the other hand, recent simulations showed that surface electrons should also be considered in the current balance for efficient primary ionization processes at low electric field strength, these surface electrons are expelled and initiate a diffuse discharge when the electric field changes its polarity [30]. Nitrogen metastable molecules as well as N_2 ($C^3\prod_u$) molecules are effectively generated by electron collisions. In the mixtures of nitrogen and oxygen, the nitrogen metastable molecules are quenched considerably by molecular oxygen, which results in a significant decreased in the densities of nitrogen metastables. Therefore, in nitrogen gas with an addition of trace of oxygen gas, the direct ionization of nitrogen molecules (E ≈ 18.7 eV) in the ground state by energetic electrons is dominant [31]. This process requires electrons with energy at least of 18.7 eV (i.e. much higher local field strength is needed). Therefore, when most of nitrogen metastables are quenched, there is no other way for the discharge development. It well explains that diffuse mode transits to filamentary mode when trace of O_2 gas is added into the nitrogen plasma [31].

3 Electrical and optical characterizations of atmospheric pressure cold plasmas

3.1 Electrical characterization of atmospheric pressure cold plasma

As discussed above, dielectric barrier discharges (DBDs) are widely used to produce non-equilibrium plasmas at atmospheric pressure. In order to understand the nature of DBDs, the important discharge parameters (such as discharge voltage, discharge current, transferred charge,

dissipated electric power etc.) must be characterized. Generally, the impedance of the entire load and not just of the discharge was measured electrically. To characterize the overall discharge behavior, an equivalent electric circuit can be used. An example of such a circuit is shown in Fig. 1-5 [9]. In this case, one side dielectric barrier discharge is employed. As long as the gap voltage (U_g) is smaller than the ignition voltage (breakdown voltage), there is no discharge and the plasma device acts as a series combination of two capacitances: the gap capacitance (C_g) and the capacitance (C_d) representing the dielectric. Then the total capacitance C is given by the expression:

$$C = \frac{C_d C_g}{C_d + C_g} = \frac{C_g}{1 + C_g / C_d} = \frac{C_g}{1 + d/(\varepsilon_r g)} \qquad (1\text{-}1)$$

Typically $g \approx d$, the term $C_g / C_d = d / (\varepsilon_r g) \approx U_d / U_g \ll 1$ (U_d represents the voltage across dielectric barrier). Therefore, the total capacitance (C) mainly depends on the capacitance of the gas gap (C_g). The gap voltage (U_g) is close to the feeding voltage. If U_g reaches the ignition voltage, microdischarges are initiated. Within every half cycle, the discharge voltage remains approximately constant, although the current flow through discharge gap is maintained by a large number of microdischarges. Figure 1-6 shows a general setup for electrical measurement of DBD [9]. Capacitance C represents the DBD fed by an applied voltage. The current pulse shape and the charge-voltage characteristic can be recorded alternatively using either a resistance R_{meas} ($R_{meas} \approx 50$ Ω) or a capacitance C_{meas} ($C_{meas} \approx 10$ nF) by using an oscilloscope. The applied high voltage is measured by a high-voltage probe. Using this measurement set up, the important electric operation parameters of DBDs, such as discharge voltage and discharge current can be measured. The discharge voltage (U_D) can be calculated by the following expression [9]. It is close to the measured voltage (U_{mea}) since $C_g / C_d = d / (\varepsilon_r g) \approx U_d / U_g \ll 1$.

$$U_D = U_{\text{mea}} \frac{1}{1 + C_g / C_d} \tag{1-2}$$

The dissipated electric energy consumed per voltage cycle (E_{el}) can be measured by the Lissajous figure (see Fig.1-7) [9, 32].

$$E_{el} = \int U(t) dQ = C_{meas} \int U(t) dU_{meas} = 4 C_d \frac{1}{1 + C_g / C_d} U_{\min}(U_{\max} - U_{\min}) \tag{1-3}$$

Obviously, the dissipated electric energy consumed per voltage cycle (E_{el}) is equal to the area of Q-U diagram shown in Fig. 1-7. Then, the dissipated electric power (consumed electric energy) can be estimated by the following expression:

$$\mathrm{P} = \frac{1}{T} E_{el} = f E_{el} \tag{1-4}$$

The number of microdischarge series per half cycle ($N_{T/2}$) can be derived under the assumption that all series transfer an identical charge ΔQ by the following expression.

$$N_{T/2} \approx \frac{2 C_d}{\Delta Q} \left(U_{\max} - U_{\min} \right) \tag{1-5}$$

Assuming that all microdischarges of one series (causing one single current pulse) have nearly identical properties, then $\Delta Q \approx nq$, where n is the number of microdischarges in a series and q is the charge transferred by one single microdischarge. The quantity of charge transfer is mainly determined by the categories of dielectric and the width of gap spacing [9].

3.2 Optical characterization of atmospheric pressure cold plasma (OES)

As we discussed above, heavy particles (gas molecules) are excited and ionized through the collisions with energetic electrons. However, the electron-induced de-excitation rate of the excited molecules, atoms or ions is generally lower than the corresponding electron-induced excitation rate in the non-equilibrium plasma. Therefore, the active species (excited molecules, atoms, and ions) in

plasma emits light through a significant radiative de-excitation. Optical emission spectroscopy (OES) is well known as a non-invasive and non-disturbing technique for plasma diagnostics [33-37]. In the OES measurement, light emitted from active species in the plasma is collected through a spectrometer. Using OES, active species in the plasma can be identified. We can explore the mechanism of plasma chemical reactions by monitoring the emission intensities of active species. Assuming that the plasma is local thermodynamic equilibrium, the gas temperature is equal to the rotational temperature of a certain active species. Therefore, OES can also be used to evaluate the gas temperature from the optical emission spectral profile shape of a certain molecular active species (e.g. N_2 or NO) [38-39]. Generally, a special OES simulation program is used to analyze the radiating species and thermodynamic characteristics of the plasma. Using this professional software, rotational and vibrational temperatures of excited molecules are obtained from the emission spectra by matching the experimental results with the simulation results. Recently, several research groups [40–43] focused on spatially and temporally resolved spectroscopic measurements. The measurement of temporally and spatially resolved spectra is the basis for the derivation of the electric field strength distribution. Nowadays, this technique is becoming the most promising tools for better understanding of physical and chemical processes in plasma.

4 Atmospheric pressure cold plasma jets and the applications

4.1 Glow to arc transition

Currently, a variety of atmospheric pressure cold plasma jets have been developed such as atmospheric pressure plasma jet (APPJ), cold plasma torch, one atmosphere uniform glow discharge plasma and micro-plasma etc. [44-49]. However, we have to confront some problems during the development of atmospheric pressure cold plasma jet. As we discussed above, atmospheric pressure

non-thermal equilibrium plasma only can be generated by either a low density of feeding power or a pulsed power supply. Therefore, if we simply increase the gas pressure in a low pressure glow discharge, the glow discharge will transit to arcing since atmospheric pressure glow discharges face a variety of instabilities [45, 46]. In order to understand the reason for this transition, we have to retrospect some important properties of glow discharge. At a given pressure, the current density and the discharge voltage in a normal glow discharge are constant. The total discharge current increases with the increasing coverage of the electrode. When the electrode is fully covered with the glow, a further increase in the current will cause an increase in the current density, which followed by an increase in the discharge voltage. The discharge with such characteristics is called an abnormal glow discharge. Hence, the minimum current density to sustain a glow discharge is the current density of a normal glow discharge [50]. For a given total current, the current density of the normal glow discharge is proportional with the square of the gas pressure. For example, an increase in the gas pressure from 1 Pa to atmospheric pressure would increase the normal current density by a factor of 10^{10}. In case of steel electrodes, the normal current density would grow up to almost 100 A/cm^2 in argon discharge [45]. These numbers give us an impression of the power density dissipated in the sheath of a normal glow discharge at atmospheric pressure, especially for argon atmospheric pressure cold plasma jet. Thus, we have to restrict the total current below this critical value, which avoids the glow-to-arc transition. Therefore, generally atmospheric pressure glow discharges only can be sustained with a small discharge scope, which is not efficient for the material processing. In order to develop atmospheric pressure cold plasma with wider discharge area, some measures must be taken, such as the forced cooling of electrodes, using helium as working gas since its normal current density is much lower than other gases [50]. Furthermore, we can restrict the discharge time

to a value below the time constant for glow-to-arc transition. This can be achieved by using a pulsed discharge or dielectric barrier discharge. Additionally, using high gas velocities is effective to reduce the residence time of the working gas in the discharge region [50].

4.2 RF discharges

Generally, uniform atmospheric pressure plasma jets can be generated by dielectric barrier discharges (DBDs) or RF discharges. We have discussed the DBDs above in details. In DBDs, dielectric materials are used to cover one or both electrodes; high voltage in the frequency range of several kHz is employed to ignite the discharge. Charge accumulation on the dielectric layer, which covers the electrodes, causes a drop of the voltage across the plasma. Therefore, DBDs are self-pulsed discharges that can restrict the discharge current and avoid arcing [50]. Radio frequency (RF) discharges have also been used to generate atmospheric pressure cold plasma jet with devices that are similar to DBDs or with devices where the electrodes are bare metal [51-53]. With bare metal electrodes, glow-to-arc transition occurs easily; therefore, the electrodes have to be cooled and the gas flow rate has to be adjusted to a certain level to minimize the risk of glow-to-arc transition. RF driven plasma devices require impedance matching between the power source and the plasma to optimize the dissipated power in the plasma and minimize the reflected power. Many studies were performed on the focus of the RF discharges [54-75]. It was found that two kinds of RF discharge modes were observed in atmospheric pressure cold plasma jets, the α-mode and the γ-mode [62]. In the α-mode, the discharge is sustained by the bulk ionization. The electrons oscillate with the drifting amplitude and are trapped in the bulk plasma region [50]. Then, the α-sheath forms since the electrodes serve as a tank for electrons. For helium atmospheric pressure plasma, the thickness of the α-sheath is in the order of 0.25 mm [50]. In the γ-mode, the discharge is sustained by secondary

electron emission from the electrode surface. The sheath thickness in the γ-mode is at least one order of magnitude smaller than that of the α-mode. Figure 1-8 shows the comparison of emission intensity profiles between electrodes for the α-mode and the γ-mode RF discharge in helium gas [50].

According to Raizer [77], when the product of gas spacing and gas pressure exceeds a critical value, the α-mode discharge becomes unstable and the α-mode discharge transits into the γ-mode or a coexisting α and γ mode discharge. Depending on the plasma device and the operating conditions, an upper discharge current or discharge power limit exists for the α-mode discharge, where the breakdown of the α-sheath occurs. The decrease in sheath thickness is followed by a decrease in the discharge voltage. When the voltage needed to sustain the γ-mode discharge is much lower than the voltage needed to sustain the α-mode discharge, only a pure γ-mode will be observed [51, 54, 63, 74]. However, when the γ-mode discharge voltage is comparable to the α-mode discharge voltage, then a coexisting α-mode and γ-mode discharge will be observed [51, 54].

4.3 Ejection mechanism of plasma jet

By DBDs or RF discharges, the issue of glow-to-arc transition has been overcome; and a variety of plasma devices have been developed to generate non-equilibrium plasma jets at atmospheric pressure. However, until now there have not been many studies to investigate the physical processes, which can explain the ejecting behavior of plasma jet. Intuitively, the jet is blown out the plasma device by flowing gas at flow rate of several liters per minute [49]. Generally, the jet is initiated and maintained in an atmospheric pressure environment. In most cases, the environment is the surrounding atmosphere. Theoretically, we should understand how the jet is ejected and maintained in the atmosphere where the electric field is very weak or even non-existent.

It was found that the traveling velocity of plasma jet is several orders of magnitude faster than the gas flow velocity [78]. Therefore, photo-induced ionization should be considered in the formation of plasma jet. Lu and Laroussi [78] proposed a photo-ionization-based model to explain how the jet is formed by their plasma device (a device driven by nanosecond pulsed high voltage). This model maybe is applicable to other plasma jets. In their model, they assumed that at a given instant time the cathode-directed streamer head is a sphere with radius r_0 and n^+ space charge. As the streamer head moves forward, it leaves behind a quasi-neutral ionized channel with a very low conductivity [49]. The head is not connected to the anode and only the streamer head is measurably luminous. This assumption is consistent with their experimental investigation [78]. Assume that a single photoelectron is created at a suitable distance r_1 from the center of the sphere because of photon emission from the streamer. With the influence of the electric field formed by the space charge, the electron is accelerated towards the sphere and an avalanche is initiated. In moving toward the sphere, from r_1 up to a certain point r_2, the electron forms an avalanche multiplication (n) and diffusion radius (r_0). The multiplication n and radius r_0 are expressed as follows [49]:

$$n = \exp \int_{r_2}^{r_1} \alpha \mathrm{dr} \,, \tag{1-6}$$

$$r_0 = \left(6 \int_{r_2}^{r_1} \frac{D}{v_d} dr \right)^{1/2} \,, \tag{1-7}$$

where α is Townsend's first ionization coefficient, D is the diffusion coefficient, and v_d is the electron drift velocity. If the multiplication up to the sphere is sufficient, the electrons neutralize the positive charge and leave behind a new positive region. In principle, the value of r_1 could be obtained from the number and the type of photons emitted from the sphere within a particular solid

angle. The absorption coefficients and ionizing efficiency should also be considered. Since the complete data on these quantities is not available, r_1 is taken as the distance at which the ionization and attachment rates are equal, where the reduced electric field is 30 V /cm^{-1}.$mmHg^{-1}$ (in air) [79]. According to Dawson and Winn [79], the following three requirements must be fulfilled for the streamer propagation under low or zero electric field. (1) The number of new positive ions created by the avalanche must be equal to the number of ions in the original sphere (n^+); (2) The diffusion radius of the avalanche head must be smaller than r_0; (3) the avalanche must reach the required amplification before the two charge regions begin to overlap, (i.e., $2r_0 \leq r_2$). Next, r_2 and r_0 are calculated as follows. First, a value of n^+ is given. Second, the electric field as a function of r from simple electrostatics is calculated from the following expression [49]:

$$E = \frac{Q}{4\pi\varepsilon_0 r^2} \tag{1-8}$$

As described above, the distance r_1 is determined as the distance at which the reduced electric field strength is equal to 30 V /cm^{-1}.$mmHg^{-1}$. r_2 is then calculated from Equation (1-6) when n is equal to n^+. The Townsend's first ionization coefficient α is calculated from the following expression [49, 80]:

$$\alpha = 15p \cdot \exp(-365\, p/E)_{cm^{-1}} \tag{1-9}$$

where p is the gas pressure and air is assumed to be the ambient gas. Finally, r_0 is calculated by using Equation (1-7) above, where D and v_d are determined from the following expressions, respectively [49, 80]:

$$D = \frac{2\times10^5}{p[torr]} cm^2 \cdot s^{-1} \tag{1-10}$$

$$\nu d = \frac{0.86\times10^6}{p[torr]} cm^2 \cdot V^{-1} \cdot s^{-1} \tag{1-11}$$

Table 1-1 shows the calculated r_2 and r_0 from different charge numbers (n^+) [78]. In these calculations, the values of D and v_d were determined for the case of helium plasma. According to the model described above, only when $2r_0$ is smaller than r_2 the streamer self-propagation can occur. From Tab. 1-1, it can be seen that when n^+ is less than 2×10^9, $2r_0$ is larger than r_2; suggesting that the streamer head can't self propagate under low or zero external electric field in this case. However, when n^+ is larger than 3×10^9, $2r_0$ is smaller than r_2; indicating that the streamer head can self-propagate. This is well in agreement with the experimental observations [78]. Using this model, it can explain why the traveling velocity of plasma jet is several orders of magnitude faster than the gas flow velocity. Therefore, the jet can travel up to several centimeters without the presence of an external electric field [49].

4.4 Applications of atmospheric pressure cold plasma jet

As pointed out in a previous section, non-thermal equilibrium plasmas are capable of producing charged particles, neutral metastable species, radicals and (V)UV radiation, which can be used for a variety of applications. Recently, there has been increased attention in using atmospheric pressure cold plasmas for material processing, since these plasmas do not require expensive vacuum systems. In particular, non-thermal atmospheric pressure plasma jets are playing an increasingly important role in various plasma processing applications [49]. This is because the plasma jet is not spatially bound or confined by electrodes. This capability is very desirable in many applications such as the treatment for complex shaped samples. On the other hand, comparing to other atmospheric pressure cold plasmas, APPJ (atmospheric pressure plasma jet) units are rather small, they are mobile and very easy to handle. Laroussi gave an overview of plasma sterilization by APGDs (atmospheric pressure glow discharges) [81]. It has been proven that APGDs can be effectively used to inactivate

bacteria. In respect to the sterilization by APGDs, the APPJ has a similar effect to other atmospheric pressure non-equilibrium plasmas. Therefore, disinfection and sterilization of medical instruments and implants are also possible. Using APPJ to treat the wounds and skin was reported by [82]. The inactivation of the biofilm-forming bacteria also opens an area of food treatment by APPJ. On the other hand, the APPJ can be used to enhance the hydrophilicity of polymer surface. APPJ can also be used for the cleaning of metal surface by using oxygen highly diluted in helium or argon gas [49]. The oxygen active species are capable to remove many organic materials on the metal surface with the release of water and carbon dioxide. Additionally, APPJ etching is widely used. It was reported that both Kapton and polyimide have been successfully etched by APPJ [83, 84]. The etching of oxides and metals has been demonstrated as well [85, 86, 87]. Carbon tetrafluoride (CF_4) as a reactive gas was added to helium or argon gas in the case of APPJ etching. APPJs were also used for PECVD (plasma-enhanced chemical vapor deposition). Moravej and Hicks made an excellent review about PECVD using APPJ [88]. It was reported that glass-like thin functional films have been successfully deposited by APPJ with oxygen highly diluted in helium or argon gas. The silicon containing precursor was diluted in main gas (He or Ar) and admixed downstream of the APPJ system. A large number of silicon containing precursors, such as tetraethoxysilane (TEOS), hexamethyldisilizane (HMDSN), hexamethyldisiloxane (HMDSO), tetramethyldisiloxane (TMDSO) and tetramethylcycotetrasiloxane (TMCTS) have been investigated [89-91]. Effects of precursors and reactive gas on the deposition rate and the properties of the deposited films were also widely studied [92]. Furthermore, the deposition of silicon nitride (Si_3N_4) was reported as well [93]. In this case, nitrogen gas as a reactive gas was highly diluted in helium, and SiH_4 was also added into the downstream of APPJ. Using an APPJ, the decontamination of chemical and biological warfare

agents has also been proven [94, 95]. In most cases, the exhaust gas from APPJ system is harmless and can exhaust to the atmosphere without further processing. As an environmental friendly technology, it is expected that APPJ will be more widely used in the future.

5 Objectives of this study

As mentioned above, atmospheric pressure cold plasma jets can be generated by DBDs or RF discharges. So far, though a variety of atmospheric pressure cold plasma jets have been developed, the discharge mechanisms are not clearly understood yet. On the other hand, in order to decrease the cost of plasma processing, argon gas is highly desirable to replace helium gas as the working gas since argon gas is much less expensive. A capacitive coupled RF plasma device was developed by Cresur Corporation of Japan. This plasma device has been commercialized under the name of "APC". Using APC, a cold Ar plasma jet is able to be generated at atmospheric pressure. On the other hand, we have successfully developed a plasma device that is able to generate a non-equilibrium atmospheric pressure Ar plasma jet of low temperature (22 to 35°C) using surface discharge fed by a high-voltage pulsed power source. This device has been commercialized under the name of "CAPPLAT" by Cresur Corporation of Japan. Though a variety of applications are being implemented, the electrical and the optical properties of these two atmospheric pressure cold Ar plasma jets had never been studied systematically. Therefore, to realize a wider applied field, it is highly desirable to get better understanding for the electrical and the optical properties of these two atmospheric pressure cold Ar plasma jets.

In chapter 2, the electrical and optical characterizations of APC Ar plasma jet are performed. Based on the electrical characterization, the discharge behavior of APC Ar plasma jet is verified and discussed. Active species in APC Ar plasma jet are also identified by using optical emission

spectroscopy (OES). According to the OES, the mechanism of chemical reactions in APC Ar plasma jet is proposed. In particular, effects of an additive gas (N_2 or O_2) on the electrical and optical properties of APC Ar plasma jet are investigated in detail.

In chapter 3, the electrical and optical characteristics of CAPPLAT Ar plasma jet are investigated. The aim is to characterize the discharge behavior and to explore the discharge mechanism of this Ar plasma jet by using a high-voltage probe and a current monitor. On the other hand, the active species in this Ar plasma jet are identified by using optical emission spectroscopy (OES). According to the OES, the mechanism of plasma chemical reactions in CAPPLAT Ar plasma jet is proposed. In particular, effects of an additive gas (N_2 or O_2) on the electrical and optical properties of CAPPLAT Ar plasma jet are investigated in detail.

In chapter 4, the physical and chemical properties (such as jet length, jet temperature, discharge behavior and the mechanism of plasma chemical reactions) of CAPPLAT Ar plasma jet and APC Ar plasma jet are compared. In particular, effects of an additive gas (N_2 or O_2) on the physical and chemical properties of these two Ar plasma jets are compared and discussed in detail. To demonstrate an application of these two Ar plasma jets, high-density polyethylene (HDPE) surface is treated using the two Ar plasma jets, respectively. In particular, effects of an additive gas (N_2 or O_2) on HDPE surface treatment are investigated and compared in detail. According to the experimental results, a probable process of HDPE surface treatment by the two Ar plasma jets is proposed.

References

[1]C. Tendero, C. Tixier, P. Tristant, Spectrochimica Acta Part B, 2006, 61, 2.

[2] M. I. Boulos, P. Fauchais, E. Pfender, Thermal Plasmas: Fundamental and Applications. Volume I, Plenum Press, New York, ISBN: 0-306-44607-3, 1994, 452.

[3] M. Moisan, M. D. Calzada, A. Gamero, A. Sola, J. Appl. Phys. 1996, 80, 46.

[4] R. H. Huddlestone, S. L. Leonard, Plasma Diagnostic Techniques, Academic Press, New York, 1965.

[5] H. R. Griem, Plasma Spectroscopy, McGraw-Hill, New York, 1964.

[6] W. Lochte-Holtgreven, Plasma Diagnostics, North-Holland, Amsterdam, 1968.

[7] M. Mitchner, C. H. Kruger, Partially Ionized Gases, Wiley, New York, 1973.

[8] U. Kogelschatz, Plasma Chem. Plasma Process. 2003, 23, 1.

[9] H-E. Wagner, R. Brandenburg, K. V. Kozlov, A. Sonnenfeld, P. Michel, J. F. Behnke, Vacuum 2003, 71, 417.

[10] B. Eliasson, U. Kogelschatz. IEEE Trans. Plasma Sci. 1991, 19, 309.

[11] V. I. Gibalov, G. J. Pietsch. J. Phys. D: Appl. Phys. 2000, 33, 2618.

[12] G. J. Pietsch, Contrib. Plasma Phys. 2001, 41, 620.

[13] B. Eliasson, M. Hirth, U. Kogelschatz, J. Phys. D: Appl. Phys. 1987, 20, 1421.

[14] D. Braun, U. Kuchler, G. J. Pietsch, J. Phys. D: Appl. Phys. 1991, 24, 564.

[15] D. Braun, V. Gibalov, G. Pietsch, Plasma Sources Sci. Technol. 1992, 1, 166.

[16] V. I. Gibalov, V. G. Samoilovich, Y. V. Filippov, Russ. J. Phys. Chem. 1981, 55, 471.

[17] K. Yoshida, H. Tagashira. Memoirs Kitami Inst. Technol. 1986, 18, 11.

[18] K. V. Kozlov, H-E. Wagner, R. Brandenburg, P. Michel, J. Phys. D: Appl. Phys. 2001, 34, 3164.

[19] K. G. Donohoe, PhD thesis, California Institute of Technology, Pasadena, CA, 1976.

[20] S. Kanazawa, M. Kogoma, T. Moriwaki, S. Okazaki, International Symposium on Plasma Chemistry, Tokyo (Japan), 1987, 1844.

[21] S. Kanazawa, M. Kogoma, T. Moriwaki, S. Okazaki, J. Phys. D: Appl. Phys. 1988, 21, 838.

[22] S. Okazaki, M. Kogoma, M. Uehara, Y. Kimura, J. Phys. D: Appl. Phys. 1993, 26, 889.

[23] F. Massines, C. Mayoux, R. Messaoudi, A. Rabehi, P. Segur. International Conference on Gas Discharges and Their Applications, Swansea (UK), 1992, 730.

[24] F. Massines, A. Rabehi, P. Decomps, R. B. Gadri, P. Segur, C. Mayoux, J. Appl. Phys. 1998, 83, 2950.

[25] N. Gherardi, G. Gouda, A. Ricard, F. Massines, Plasma Sources Sci. Technol. 2000, 9, 340.

[26] J. Tepper, M. Lindmayer, J. Salge, Proceedings of the Sixth International Symposium on High Pressure Low Temperature Plasma Chemistry, HAKONE VI, Cork (Ireland), 1998, 123.

[27] A. Ricard, P. Decomps, F. Massines. Surf. Coatings 1999, 112, 1.

[28] Y. B. Golubovski, A. Maiorov, J. Behnke, J. F. Behnke, Proceedings of the Eighth International Symposium on High Pressure, Low Temperature Plasma Chemistry, HAKONE VIII, Puhajarve (Estonia), 2002, 48.

[29] P. Segur, F. Massines, Proceedings of the International Conference on Gas Discharges and Their Applications, Glasgow (UK), 2000, 15.

[30] Y. B. Golubovskii, V. A. Maiorov, J. Behnke, J. F. Behnke, J. Phys. D: Appl. Phys. 2002, 35, 751.

[31] H-E. Wagner, R. Brandenburg, P. Michel, F. Massines, K. V. Kozlov, Proceedings of the seventh International Symposium on High Pressure Low Temperature Plasma Chemistry, HAKONE VII, Greifswald (Germany), 2000, 93.

[32] U. Kogelschatz, Process Technologies for Water Treatment, New York: Plenum press, 1988, 87.

[33] A. Ricard, T. Czerwiec, Thin Solid Films 1999, 341, 1.

[34] A. Fateev, F. Leipold, Plasma Process. Polym. 2005, 2, 193.

[35] A. Simon, S. D. Anghel, Nucl. Instr. Methods in Phys. Res. B 2009, 267, 438.

[36] J. R. Roberts, J. Res. Natl. Inst. Stand. Technol. 1995, 100, 353.

[37] P. Jamroz, W. Zyrnicki, Vacuum 2010, 84, 940.

[38] J. K. Rhee, D. B. Kim, Thin Solid Films 2007, 515, 4909.

[39] Y. Kubota, R. Ichiki, T. Hara, J. Plasma Fusion Res. Series 2009, 8, 740.

[40] C. Hudon, R. Bartnikas, M. R. Wertheimer, IEEE Trans. Electr. Insul. 1993, 28, 1.

[41] R. Brandenburg, K.V. Kozlov, N. Gherardi, P. Michel, C. Khampan, H-E. Wagner, F. Massines, Proceedings of the Eighth International Symposium on High Pressure, Low Temperature Plasma Chemistry, HAKONE VIII, Puhajarve (Estonia), 2002, 28.

[42] D. Trunec, R. Brandenburg, P. Michel, D. Pasedag, H-E. Wagner, Z. Navratil, Proceedings of the International Symposium on High Pressure, Low Temperature Plasma Chemistry, HAKONE VIII, Puhajarve (Estonia), 2002, 63.

[43] V. Poenariu, M. R. Wertheimer, R. Bartnikas, Plasma Process. Polym. 2006, 3, 17.

[44] J. R. Roth, ‘‘Industrial Plasma Engineering: Applications to Non-thermal Plasma Processing’’, Vol. 2, IOP Publishing, Bristol 2001.

[45] Y. P. Raizer, ‘‘Gas Discharge Physics’’, Springer, Heidelberg 1991.

[46] E. E. Kunhardt, IEEE Trans. Plasma Sci. 2000, 28, 189.

[47] A. Schutze, J. Y. Jeong, S. E. Babayan, J. Park, G. S. Selwyn, R. F. Hicks, IEEE Trans. Plasma Sci. 1998, 26, 1685.

[48] K. H. Becker, K. H. Schoenbach, J. G. Eden, J. Phys. D 2006, 39, R55.

[49] M. Laroussi, T. Akan, Plasma Process. Polym. 2007, 4, 777.

[50] J. Laimer, H. Stŏri Plasma Process. Polym. 2007, 4, 266.

[51] J. Laimer, H. Stŏri Plasma Process. Polym. 2006, 3, 573.

[52] J. J. Shi, M. G. Kong, IEEE. Trans. Plasma Sci. 2005, 33, 624.

[53] J. Park, I. Henins, H. W. Herrmann, G. S. Selwyn, J. Appl. Phys. 2001, 89, 20.

[54] J. Laimer, S. Haslinger, W. Meissl, J. Hell, H. Stori, Vacuum 2005, 79, 209.

[55 J. J. Shi, M. G. Kong, Phys. Rev. Lett. 2006, 96, 105009.

[56] S. Wang, V. Schultz von der Gathen, H. F. Dobele, Appl. Phys. Lett. 2003, 83, 3272.

[57] G. S. Selwyn, H. W. Herrmann, J. Park, I. Henins, Contrib. Plasma Phys. 2001, 6, 610.

[58] J. Park, I. Henins, H. W. Herrmann, G. S. Selwyn, J. Y. Jeong, R. F. Hicks, D. Shim, C. S. Chang, Appl. Phys. Lett. 2000, 76, 288.

[59] J. Park, I. Henins, H. W. Herrmann, G. S. Selwyn, J. Appl. Phys. 2001, 89, 15.

[60] M. Moravej, X. Yang, G. R. Nowling, J. P. Chang, R. F. Hicks, J. Appl. Phys. 2004, 96, 7011.

[61] X. Yang, M. Moravej, G. R. Nowling, J. P. Chang, R. F. Hicks, IEEE Trans. Plasma Sci. 2005, 33, 294.

[62] J. J. Shi, X. T. Deng, R. Hall, J. D. Punnett, M. G. Kong, J. Appl. Phys. 2003, 94, 6303.

[63] X. Yang, M. Moravej, G. R. Nowling, S. E. Babayan, J. Panelon, J. P. Chang, R. F. Hicks, Plasma Sources Sci. Technol. 2005, 14, 314.

[64] X. Yang, M. Moravej, S. E. Babayan, G. R. Nowling, R. F. Hicks, Plasma Sources Sci. Technol. 2005, 14, 412.

[65] S. E. Babayan, G. Ding, G. R. Nowling, X. Yang, R. F. Hicks, Plasma Chem. Plasma Process. 2002, 22, 255.

[66] M. Moravej, X. Yang, M. Barankin, J. Penelon, S. E. Babayan, R. F. Hicks, Plasma Sources Sci. Technol. 2006, 15, 204.

[67] K. Niemi, V. Schulz von der Gathen, H. F. Dobele, Plasma Sources Sci. Technol 2005, 14, 375.

[68] J. Park, I. Henins, H. W. Herrmann, G. S. Selwyn, Phys. Plasmas 2000, 7, 3141.

[69] X. Yuan, L. L. Raja, Appl. Phys. Lett. 2002, 81, 814.

[70] X. Yuan, L. L. Raja, IEEE Trans. Plasma Sci. 2003, 31, 495.

[71] J. J. Shi, M. G. Kong, IEEE Trans. Plasma Sci. 2005, 33, 278.

[72] J. J. Shi, M. G. Kong, Appl. Phys. Lett. 2005, 87, 201501.

[73] J. Y. Jeong, J. Park, I. Henins, S. E. Babayan, V. J. Tu, G. S. Selwyn, G. Ding, R. F. Hicks, J. Phys. Chem. A 2000, 104, 8027.

[74] S. Y. Moon, R. K. Rhee, D. B. Kim, W. Choe, Phys. Plasmas 2006, 13, 033502.

[75] T. Kimura, T. Hanai, Jpn. J. Appl. Phys. 2006, 45, 4219.

[76] W-C. Zhu, B-R. Wang, Z-X. Yao, Y-K. Pu, J. Phys. D: Appl. Phys. 2005, 38, 1396.

[77] Y. P. Raizer, M. N. Shneider, N. A. Yatsenko, ‘‘Radio-Frequency Capacitive discharge’’, CRC, Boca Raton 1995.

[78] X. Lu, M. Laroussi, J. Appl. Phys. 2006, 100, 063302.

[79] G. A. Dawson,W. P. Winn, Zeitschrift fur Physik 1965, 183, 159.

[80] R. P. Yuri, ‘‘Gas Discharge Physics’’, Springer, New York 1991.

[81] M. Laroussi, Plasma Process. Polym. 2005, 2, 391.

[82] M. Vleugels, G. Shama, X. T. Deng, E. Greenacre, T. Brocklehurst, M. G. Kong, IEEE Trans Plasma Sci. 2005, 33, 824.

[83] J. Y. Jeong, S. E. Babayan, V. J. Tu, J. Park, R. F. Hicks, G. S. Selwyn, Plasma Sources Sci.

Technol. 1998, 7, 282.

[84] J. Y. Jeong, S. E. Babayan, A. Schu¨tze, V. J. Tu, J. Park, I. Henins, G. S. Selwyn, R. F. Hicks, J. Vacuum. Sci. Technol A 1999, 17, 2581.

[85] V. J. Tu, J. Y. Jeong, A. Schutze, S. E. Babayan, G. Ding, G. S. Selwyn, R. F. Hicks, J. Vacuum Sci. Technol. A 2000, 18, 2799.

[86] X. Yang, M. Moravej, S. E. Babayan, G. R. Nowling, H. R. Hicks, J. Nucl. Mater. 2004, 324, 134.

[87] Y. Kim, J. Park, L. A. Rosocha, H. L. Teslow, Appl. Phys. Lett. 2005, 87, 011502.

[88] M. Moravej, R. F. Hicks, Chem. Vap. Depos. 2005, 11, 469.

[89] S. E. Babayan, J. Y. Jeong, V. J. Tu, J. Park, G. S. Selwyn, R. F. Hicks, Plasma Sources Sci. Technol. 1998, 7, 286.

[90] G. R. Nowling, M. Yajima, S. E. Babayan, M. Moravej, X. Yang, W. Hoffman, R. F. Hicks, Plasma Sources Sci. Technol. 2005, 14, 477.

[91] S. E. Babayan, J. Y. Jeong, A. Schu¨tze, V. J. Tu, M. Moravej, G. S. Selwyn, R. F. Hicks, Plasma Sources Sci. Technol. 2001, 10, 573.

[92] M. Moravej, S. E. Babayan, G. R. Nowling, X. Yang, R. F. Hicks, Plasma Sources Sci. Technol. 2004, 13, 8.

[93] G. R. Nowling, S. E. Babayan, V. Jankovic, R. F. Hicks, Plasma Sources Sci. Technol. 2002, 11, 97.

[94] H. W. Herrmann, I. Henins, J. Park, G. S. Selwyn, Phys. Plasmas 1999, 6, 2284.

[95] H. W. Herrmann, G. S. Selwyn, I. Henins, J. Park, M. Jeffery, J. M. Williams, IEEE Trans. Plasma Sci. 2002, 30, 1460.

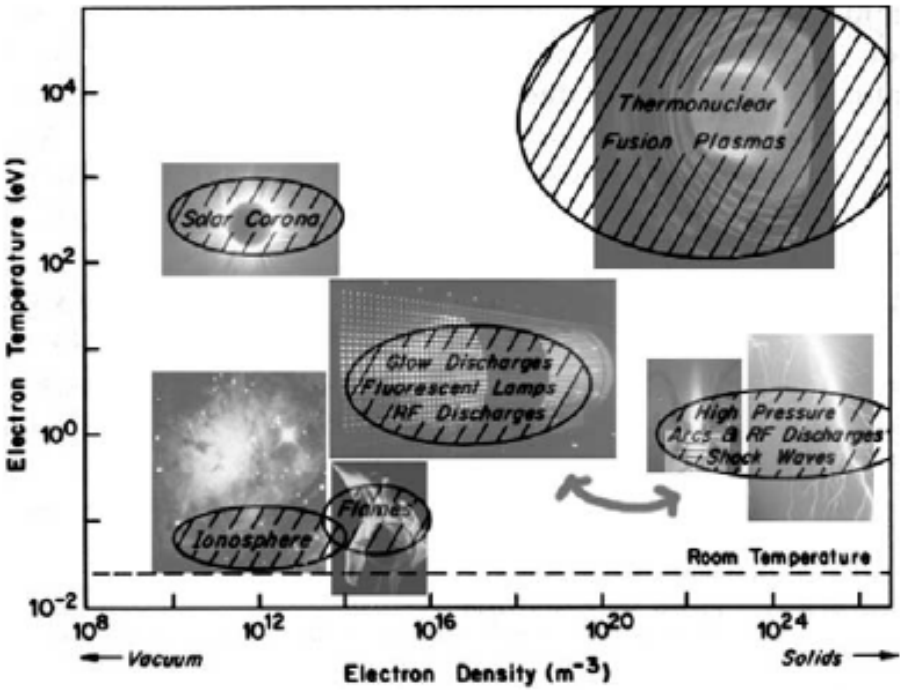

Fig. 1-1 Schematic of plasma classification (electron temperature versus electron density). Taken from reference [2].

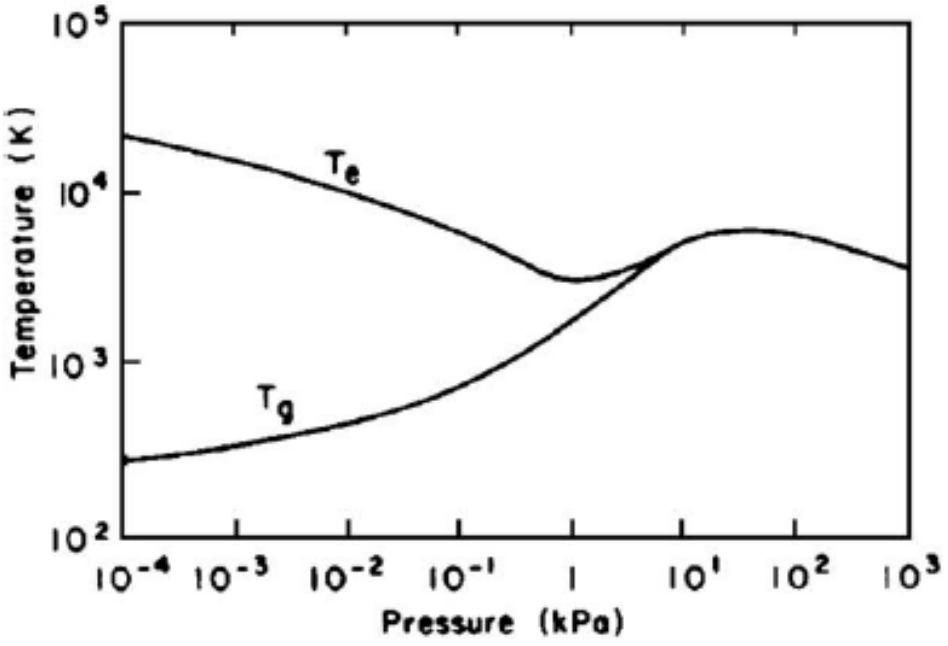

Fig. 1-2 Dependence of electron temperature and gas temperature on gas pressure in a mercury arc plasma. Taken from reference [2].

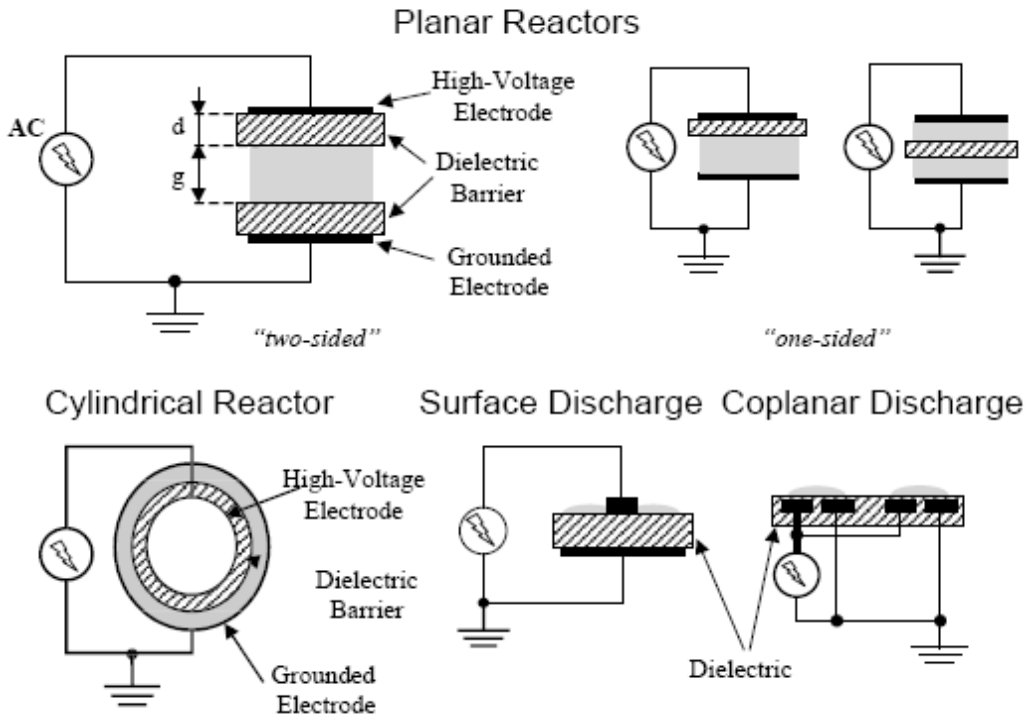

Fig. 1-3 Typical electrode arrangements of dielectric barrier discharges. Taken from reference [9].

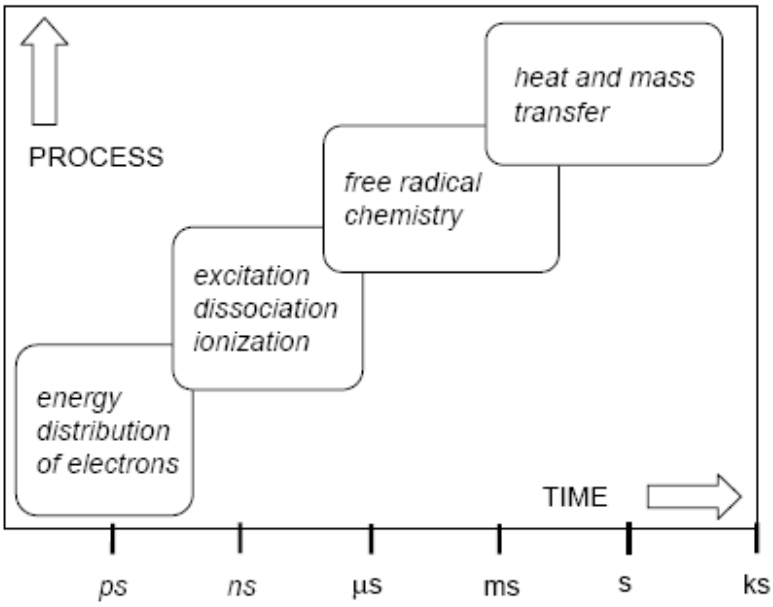

Fig. 1-4 Time scales of relevant processes in filamentary barrier discharges. Taken from reference [9].

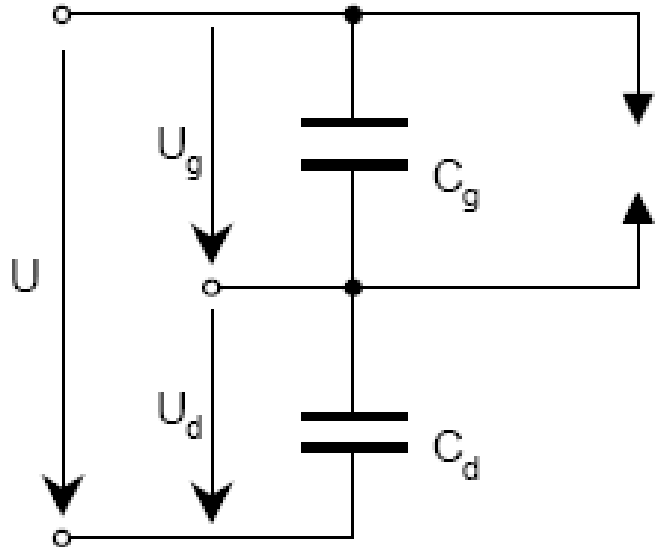

Fig. 1-5 Equivalent circuit used for DBD. Taken from reference [9].

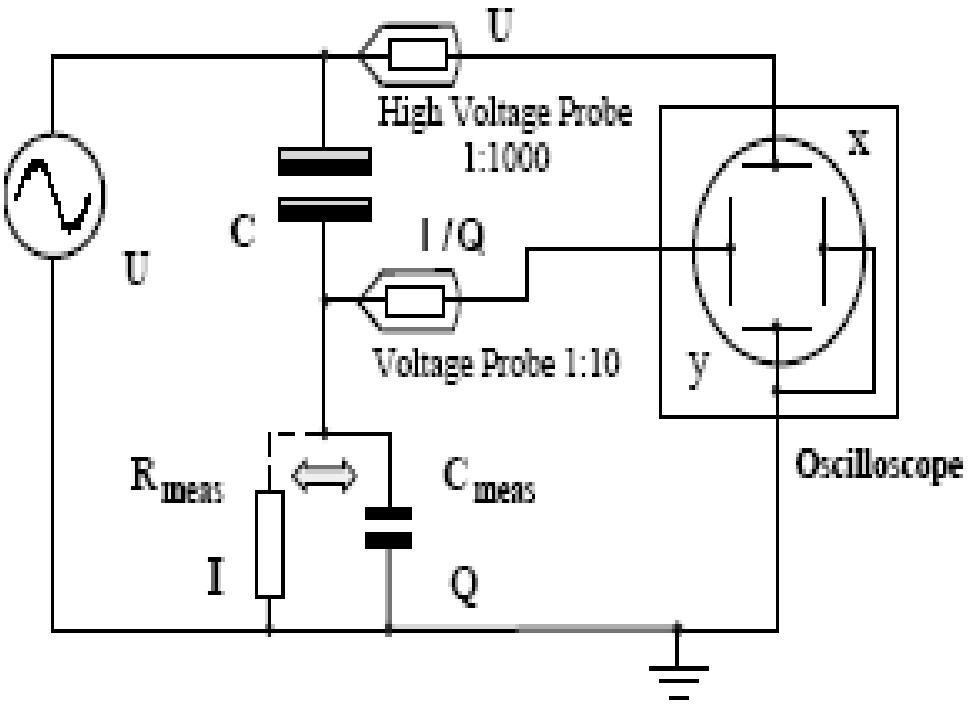

Fig. 1-6 Experimental setup for discharge voltage, discharge current and charge transfer measurements alternatively. Using Rmeas for current measurement (broken line); using Cmeas for charge transfer measurement (solid line). Taken from reference [9].

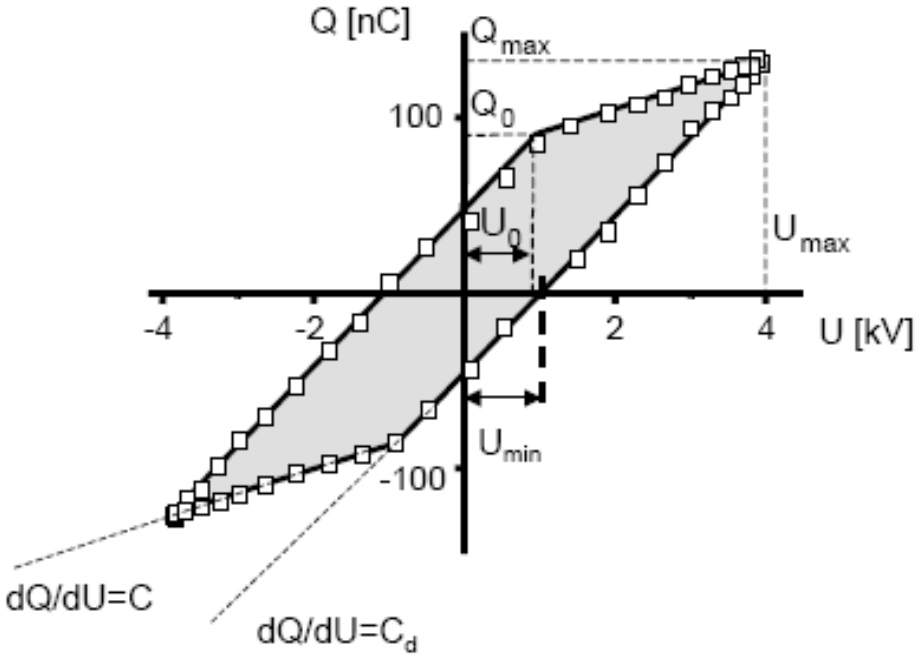

Fig. 1-7 Idealized Q-U diagram (Lissajous figure) for measurement of dissipated electric energy per voltage cycle. Taken from reference [9].

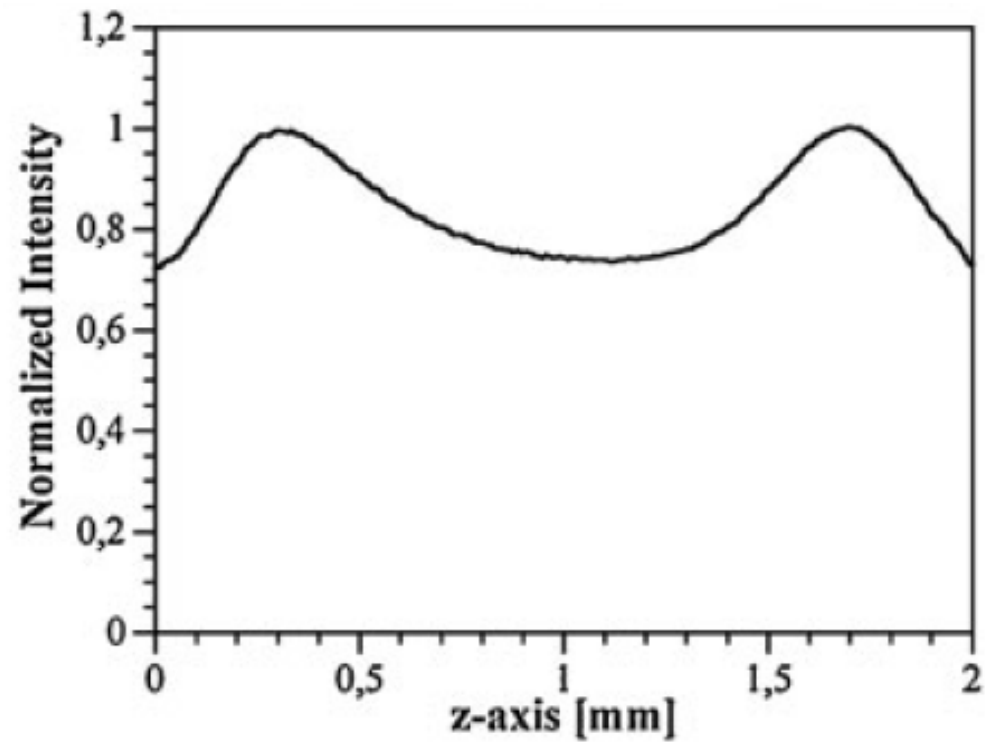

(a)

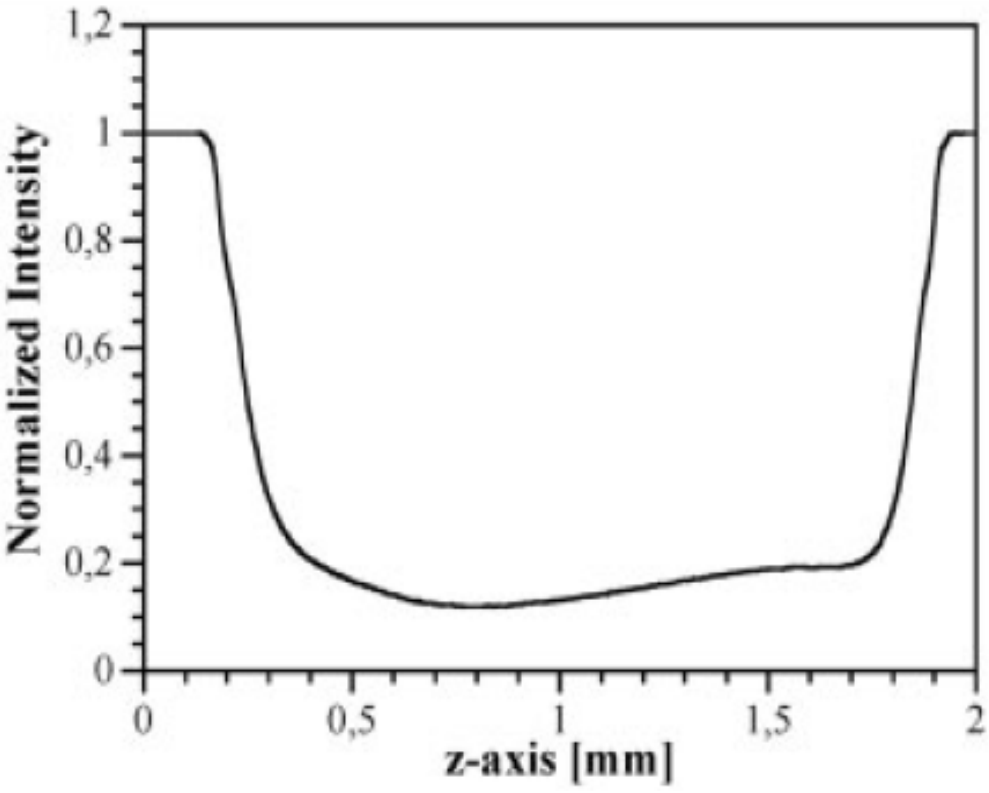

(b)

Fig. 1-8 Emission intensity profiles between electrodes in RF helium discharge with a gap spacing of 2 mm. (a): α-mode discharge; (b): γ-mode discharge. Taken from reference [50].

Tab. 1-1 Calculated radius (r_0 and r_2) for different original space charge numbers. Taken from reference [49].

Radius (cm)	**Number of original positive charges (n^+)** ($\times 10^9$)				
	1	2	3	4	5
r_2	0.02	0.1	0.17	0.23	0.3
r_0	0.056	0.068	0.075	0.080	0.085

Chapter 2 Electrical and Optical Characterization of RF Capacitive Atmospheric Pressure Cold Argon Plasma Jet

1 Introduction

Recently, several novel atmospheric pressure plasma sources have been developed. These sources show a promising potential to replace low pressure plasma devices for some existing applications and to create new applications. These sources include the atmospheric pressure plasma jet, the cold plasma torch and the one atmosphere uniform glow discharge plasma. All these plasma sources produce discharges with a low gas temperature [1-10].

In this study, electrical properties of a RF capacitive cold Ar plasma jet were characterized using a high-voltage probe and a current probe. According to the waveforms of discharge voltage and RF current, the discharge behavior was confirmed. Further, optical emission spectrometry (OES) was employed to identify the active species in this Ar plasma jet. Based on the electrical and optical characterization, the reaction mechanism of active species in this RF capacitive Ar plasma jet was proposed. In particular, the effects such as additive gas (N_2 or O_2), torch diameter, and feeding gas flow rate on the electrical and optical properties of this Ar plasma jet were investigated in detail.

2 Experimental setup and methods

2.1 Plasma device

The RF capacitive plasma device used in the experiments is called APC plasma developed by Cresur Corporation of Japan. The inner diameter of the plasma torch is 25 mm. Two parallel perforated Al electrodes are consisted in the plasma torch. The diameter of the perforated holes is 1.3 mm; the distance between the holes is 3.2 mm. Ceramics is used as an insulator between the two electrodes. The gap spacing between the two electrodes is 1.5 mm. The inner electrode is connected

to the original RF power source with a frequency of 27.12 MHz through an impedance matching box, and the outer electrode is grounded. The schematic of the plasma torch is shown in Fig. 2-1. In the discharge experiment, Ar gas was working gas at flow rates of 5~20 SLPM (standard liter per minute), RF powers were maintained at 25~100 W without reflection, N_2 or O_2 as an additive gas was added into the Ar plasma jet at flow rates of 0~30 SMLPM (standard miniliter per minute), respectively. All flow rates were controlled by a mass flow controller.

2.2 Electrical measurement

The voltage applied to the discharge was measured using a 10:1 voltage probe (Tektronix P6139 10X Passive Probe 063-0870-05); the RF current was monitored using a wide band current monitor (PearsonTM current monitor) manufactured by Pearson Electronics Inc., Palo Alto, California, U.S.A. Further, a Tektronix TDS3012C digital phosphor oscilloscope was employed to obtain the voltage and current waveforms.

2.3 Optical emission spectroscopy (OES)

The optical emission spectrum of the plasma jet was collected perpendicular to the jet using an Ocean Optics USB4000 spectrometer (spectral range of 350–950 nm) with a resolution of 0.2 nm full width at half-maximum (FWHM); this was achieved using a personal computer equipped with relevant software (SpectraSuite) for both driving and acquisition. Prior to the OES measurement, the USB4000 spectrometer was calibrated using a standard halogen light source. Therefore, absolute irradiance of the active species in the plasma was obtained. During the measurement of the optical emission spectra, the exposure time was 100 ms. Emission intensities of the active species were collected at an axial position of the plasma jet (5 mm from the end of the torch), through an optical fiber with a diameter of 100 μm. The experimental setup for OES and electrical measurement is

shown in Fig. 2-2.

3 Results and discussion

3.1 Electrical characterization of APC Ar plasma jet

3.1.1 Current and voltage (I – V) characteristics

Figure 2-3 shows the current-voltage (I – V) curve for the pure Ar discharge with different input RF powers. It can be seen that at a lower input RF power (below 40 W), the discharge voltage increased with the increase in the RF current, indicating that the discharge is an abnormal glow discharge [11]. At a medium input RF power (40 W ~ 60 W), the discharge voltage increased slightly while the RF current increased remarkably, indicating the discharge became a normal glow discharge. At a higher input RF power (60 W ~ 105 W), the discharge became an abnormal glow discharge again. This abnormal glow operating regime has been observed in other studies of the atmospheric pressure plasma [12-18]. This abnormal glow is an α-mode discharge. We have explained the properties of the α-mode discharge in chapter 1.

Figure 2-4 shows waveforms of the discharge voltage (red line) and the RF current (blue line) in a pure Ar discharge. Both the voltage and the current waveforms are smooth and nearly sinusoidal, indicating a mostly linear response of the discharge. Additionally, the capacitive essence of the discharge is clearly shown as the current waveform leads the voltage waveform by about 85°, indicating the capacitive essence of the α-mode discharge [19].

3.1.2 Effect of Ar flow rate on electrical properties

Figure 2-5 shows waveforms of the discharge voltage (red line) and the RF current (blue line) in a pure Ar discharge at Ar flow rate of 5 SLPM. Compared with the waveforms of the discharge voltage and the RF current shown in Fig. 2-5 above, both the discharge voltage and the current

scarcely changed, suggesting that APC Ar plasma jet is a stable α-mode discharge when the Ar flow rate is in the experimental range of 5 SLPM to 20 SLPM.

3.1.3 Effect of torch diameter on electrical properties

Figure 2-6 shows waveforms of the discharge voltage (red line) and the RF current (blue line) in a pure Ar discharge with the torch diameter of 10 mm and RF power of 100 W. Compared with the waveforms of the discharge voltage and the RF current shown in Fig. 2-4 above, the discharge voltage increased and the RF current decreased slightly. However, considering the difference in the discharge areas of the two APC plasma torches, the current density increased with the decrease in the torch diameter, which leads to a stronger electric field.

3.1.4 Effect of additive gas (N_2 or O_2) on electrical properties

Effect of additive gas (N_2 or O_2) on electrical properties of APC Ar plasma jet was investigated. It was found that the waveforms of the discharge voltage and the RF current scarcely changed with the addition of additive gas. However, the values of discharge voltage and the current changed with the addition of additive gas. Figure 2-7 shows the Effects of additive gas (N_2 or O_2) on the discharge voltage and the RF current of APC Ar plasma jet. It can be seen that the discharge voltage decreased and the current increased with the increasing concentration of the additive gas. The similar phenomena were observed in the He discharge by J. Park et al [20]. However, so far, there is no clear understanding for this phenomenon. We conceive that the ionization of additive gas molecules through collisions with energetic electrons results to the increase in the RF current, which will decrease the impedance of the plasma. Therefore, the discharge is able to be sustained at a lower discharge voltage. On the other hand, the RF impedance matching was disturbed with the addition of the additive gas, which could also lead to the change in the discharge voltage and the RF current.

We monitored the plasma temperature by using a thermocouple set at the exit of the plasma jet. Changes in plasma temperature with the addition of additive gas are shown in Fig. 2-8. It can be seen that the temperature increased with the increasing concentration of added N_2 or O_2 gas. As discussed above, the RF impedance matching was disturbed with the addition of the additive gas, which causes the change in the dissipated RF power in the plasma. Mean power density dissipated in the discharge can be calculated from the following formula [21]:

$$P = [I_{mrs} \times V_{mrs} \times \cos(\theta_v - \theta_i)] / A,$$

where I_{mrs} and V_{mrs} are the values of mean root square of the discharge current and the discharge voltage, respectively; θ_v and θ_i mean the phase angles of the discharge voltage and the discharge current, respectively; A represents the discharge area.

In the experiments, we noted that the phase angle between the current and the voltage decreased slightly with the increasing concentration of additive gas (N_2 or O_2). From the formula above, we can see that the decrease in the phase angle between the current and the voltage will lead to an increase in the mean power density. Therefore, we assume that the increase in the mean power density leads to the increase in the plasma temperature. In the future, we intend to calculate the mean power density dissipated in APC plasma jet quantitatively, using the equivalent circuit model reported by H. Stori, et al. [11, 12, 22].

3.2 Optical characterization of APC Ar plasma jet

3.2.1 Typical optical emission spectrum

A typical optical emission spectrum (OES) of APC Ar plasma jet in the wavelength range of 350–950 nm is shown in Fig. 2-9. It can be seen that the peaks belonging to the excited Ar atoms (4p-4s transitions) are predominant in APC Ar plasma jet (in the wavelength range of 690–950 nm)

[23, 24]. Surprisingly, peaks at 357 and 380 nm belonging to the N_2 second positive system (N_2 ($C^3\prod_u$ — $B^3\prod_g$)) were also observed. However, peaks belonging to the N_2 first negative system ((N_2^+ ($B^2\Sigma^+_u$ — $X^2\Sigma^+_g$)) were not detected. Additionally, an O atom peak was detected at 777 nm [25, 26]. Both nitrogen and oxygen active species were detected in the pure Ar discharge because the impurities (N_2 and O_2 molecules) from the Ar gas or from the atmosphere are excited and dissociated. Emission intensities and assignments of all active species (in the wavelength range of 350–950 nm) detected in the APC Ar plasma jet are summarized in Table 2-1.

As is well known, in Ar discharge, numerous Ar metastable atoms are generated through collisions with energetic electrons. And then, the Ar metastables are excited to a higher excitation level through the successive collisions with energetic electrons. The excited Ar atoms emit light when they return to the lower excitation level. This process can be expressed by the following reactions:

$$e^* + Ar^0 \rightarrow Ar^m + e \quad (2\text{-}1)$$

$$e^* + Ar^m \rightarrow Ar^* (4p) + e \quad (2\text{-}2)$$

$$Ar^* (4p) \rightarrow Ar^* (4s) + h\nu \quad (2\text{-}3)$$

These reactions can be used to explain the emission lines of excited Ar atoms. On the other hand, it was previously reported that Ar metastables hold roughly 11.5 eV of energy, which is close to the excitation energy of N_2 second positive system (N_2 ($C^3\prod_u$ — $B^3\prod_g$)) ($E \approx 11.1$ eV) [23, 24]. Therefore, a resonant reaction easily occurs between the Ar metastables and ground-state molecular N_2.

$$Ar^m + N_2 (X_1\Sigma^+_g) \rightarrow Ar^0 + N_2 (C^3\prod_u) \quad (2\text{-}4)$$

The above resonant reaction is the main channel for the generation of N_2 ($C^3\prod_u$).

$$N_2 (C^3\prod_u) \rightarrow N_2 (B^3\prod_g) + h\nu \quad (2\text{-}5)$$

These reactions help explain why the emissions corresponding to the N_2 second positive system ($N_2 (C^3\prod_u — B^3\prod_g)$) were observed.

Additionally, it was reported that the most probable channel for the formation of O atoms was through collisions between the oxygen molecular ions (O_2^+) and electrons [27]. Oxygen molecular ions (O_2^+) are generated mainly through the Penning ionization of O_2 molecules. Apparently, Ar metastables have insufficient energy for the generation of O_2 molecular ions (O_2^+) ($E \approx 18.2$ eV) through the Penning ionization [23]. However, in the Ar discharge, the excited O atoms at 777 nm can probably be generated through the following channels [23, 28-30]:

$$Ar^* + O_2 (X^3\Sigma^-_g) \rightarrow O (^1D) + O (^3P) + Ar^0 \quad (2\text{-}6)$$

$$e^* + O_2 (X^3\Sigma^-_g) \rightarrow e + [O (^1D) \text{ or } O (^1S)] + O (^3P) \quad (2\text{-}7)$$

$$e^* + O_2 (X^3\Sigma^-_g) \rightarrow 2e + O_2^+ (b^4\Sigma^-_g) \quad (2\text{-}8)$$

$$e^* + O_2^+ (b^4\Sigma^-_g) \rightarrow 2O (^3P) \quad (2\text{-}9)$$

As we discussed above, it can be seen that reaction (2-8) and reaction (2-9) are the main channel for the formation of O atoms in APC Ar plasma jet. These reactions may explain the detection of excited O atoms at 777 nm in APC Ar plasma jet.

3.2.2 Effect of Ar flow rate on OES

Effect of Ar flow rate on emission intensities of active species in APC Ar plasma jet is shown in Fig. 2-10. It can be seen that the emission intensities of excited Ar and O atoms increased significantly with the increase in the Ar flow rate. However, the emission intensity of $N_2 (C^3\prod_u — B^3\prod_g)$ decreased with the increase in the Ar flow rate. It was reported that the transport of active species depends critically on the gas flow rate. Lower gas flow rates will decrease the concentrations

of active species at distant positions from the nozzle since the active species in plasma jet decay quickly in the atmosphere [31]. Therefore, a higher Ar flow rate leads to a faster velocity of the Ar stream, which is very helpful for the transport of the active species. Consequently, more active species reached to a certain position from the exit (a distance of 5 mm in the experiment) at a higher Ar flow rate. This is why the emission intensities of excited Ar and O atoms increased significantly with the increase in the Ar flow rate. However, the observed N_2 ($C^3\prod_u$ — $B^3\prod_g$), generated through reaction (2-4), mainly comes from the afterglow zone. It is because N_2 ($C^3\prod_u$) in the discharge region will transform to N_2^+ ($B^2\Sigma^+_u$) quickly through the successive collisions with energetic electrons. And then N_2^+ ($B^2\Sigma^+_u$) will be trapped in the discharge region by a very fast polarity change (details about this will be discussed in section 3. 2. 4). Therefore, though a higher Ar flow rate is helpful for the transport of Ar metastables, the entry of N_2 (from the atmosphere) into the Ar stream becomes difficult with the increase in the Ar flow rate. It will restrict the rate of reaction (2-4). This may be helpful to explain why the emission intensities of N_2 ($C^3\prod_u$ — $B^3\prod_g$) decreased with the increase in the Ar flow rate.

3.2.3 Effect of torch diameter on OES

Effect of torch diameter on optical emission spectrum of APC Ar plasma jet is shown in Fig. 2-11. It can be seen that the plasma radiation increased with the decrease in the torch diameter. We have discussed the effect of torch diameter on electrical properties of APC Ar plasma jet in section 3.1.3. It was found that for a constant input RF power, the current density increased with the decrease in the torch diameter. Therefore, the electric field strength is stronger in case of the 10-mm-diameter plasma torch, which leads to a higher electron density. From the reactions above, it can see that the increased electron density will lead to an increase in the plasma radiation. On the

other hand, as we discussed above, the velocity of the Ar stream increased with the decrease in torch diameter, which is helpful for the transport of active species and will lead to an increase in the emission intensities of active species.

3.2.4 Effect of additive gas (N_2 or O_2) on OES

Changes in emission intensities of active species in APC Ar plasma jet with different flow rates of additive gas (N_2 or O_2) are shown in Fig. 2-12. From Fig. 2-12 (a), it can be clearly seen that the emission intensities of excited Ar and O atoms decreased with the increasing concentration of added N_2 gas. The quenching effect of the added N_2 gas causes the decrease in the emission intensities of excited Ar and O atoms. On the other hand, the emission intensities of N_2 ($C^3\prod_u$ — $B^3\prod_g$) increased only slightly with the addition of N_2 gas. From Fig. 2-12 (b), similar to the N_2 addition, it can be clearly seen that the emission intensities of excited Ar atoms and N_2 ($C^3\prod_u$ — $B^3\prod_g$) decreased with the increasing concentration of added O_2 gas. The quenching effect of added O_2 gas causes the decrease in the emission intensities of excited Ar atoms and N_2 ($C^3\prod_u$ — $B^3\prod_g$). Additionally, the emission intensity of O atoms increased significantly with the addition of O_2 gas. A maximum emission intensity of O atoms was observed at the added O_2 flow rate of 15 smlpm. More than 15 smlpm of O_2 addition causes the decrease in the emission intensity of O atoms because of the quenching effect.

Comparison of emission intensities of active species before and after the addition of N_2 or O_2 is shown in Fig. 2-13. It can be seen that the emission intensities of N_2 ($C^3\prod_u$ — $B^3\prod_g$) increased only slightly with the addition of N_2 gas. Additionally, with the N_2 gas addition, the total emission intensity decreased more remarkably than with the same amount of O_2 gas addition. However, it was reported that the quenching rate by O_2 molecules is much faster than by N_2 molecules [27]. On the

other hand, as we discussed in the above section of 3.1.4, the RF current increased with the addition of N_2 gas, suggesting the occurrence of collision ionization of the added N_2 gas. Therefore, we assume that new ionic species (such as $N_2^+(B^2\Sigma^+_u)$) are formed. In the Ar discharge, the nitrogen molecular ions ($N_2^+(B^2\Sigma^+_u)$) can probably be generated through the following channels [24, 32].

$$e^* + N_2(X^1\Sigma^+_g) \rightarrow N_2^+(B^2\Sigma^+_u) + 2e \quad (2\text{-}10)$$

$$e^* + N_2(C^3\prod_u) \rightarrow N_2^+(B^2\Sigma^+_u) + 2e \quad (2\text{-}11)$$

$$Ar^+ + N_2(X^1\Sigma^+_g) \rightarrow Ar^0 + N_2^+(X^2\Sigma^+_g) \quad (2\text{-}12)$$

$$N_2^+(X^2\Sigma^+_g) + e^* \rightarrow N_2^+(B^2\Sigma^+_u) + e \quad (2\text{-}13)$$

Considering the reaction constant rates of the above reactions and the concentrations of active species, reaction (2-11) is the main reaction for the generation of $N_2^+(B^2\Sigma^+_u)$ in Ar discharge.

However, we never detected the emission from $N_2^+(B^2\Sigma^+_u — X^2\Sigma^+_g)$ in the afterglow zone of the plasma jet since the ions are trapped in the electric field (discharge region) by a very fast polarity change (at a frequency of 54.24 MHz). As we well known, the ionization extent in the He plasma is quite high because the He metastables hold a very high energy ($E \approx 19.8$ eV), which is almost capable to ionize any gas molecules through the Penning ionization. We have attempted the He discharge with APC plasma torch. Nearly no plasma jet was observed because ionic species are trapped in the discharge region. This result is well in agreement with our assumption.

4 Conclusions

In this study, in order to get better understanding for the RF capacitive atmospheric pressure cold Ar plasma jet, electrical and optical characterizations of APC Ar plasma jet were performed by using electrical diagnostics and OES technique. Electrical characterizations showed that the discharge of APC Ar plasma jet is an abnormal glow discharge at a lower input RF power (below 40 W); then the

discharge became a normal glow discharge with the increasing input RF power (40 ~ 60 W); the discharge became the abnormal glow discharge again when the input RF power is higher than 60 W. When the input RF power is in the range of 60 to 100 W, APC Ar plasma jet is a stable abnormal glow discharge (the α-mode discharge). We did not observed the transition from the α-mode discharge to the γ-mode discharge in the APC Ar plasma jet since the maximum input RF power is 105 W for our RF power source. Additionally, we investigated the effects of Ar flow rate, additive gas (N_2 or O_2) and the torch diameter on the discharge behavior of APC Ar plasma jet. It was shown that the discharge behavior scarcely changed with different Ar flow rates and different torch diameters. Interestingly, the discharge voltage decreased and the RF current increased with the increasing concentration of additive gas (N_2 or O_2). Until now, we do not have clear understanding for this interesting phenomenon. We assumed that the ionization of additive gas molecules through collisions with energetic electrons leaded to the increase in the RF current, which would decrease the impedance of the plasma. Therefore, the discharge was able to be sustained at a lower discharge voltage. Additionally, the RF impedance matching was disturbed by the addition of additive gas, which could lead to the change in the discharge voltage and the RF current.

OES characterizations of APC Ar plasma jet revealed that Ar active species belonging to the excited Ar atoms (4p-4s transition) were predominant in this plasma jet (in the wavelength range of 690–950 nm). Peaks belonging to the N_2 second positive system (N_2 ($C^3\prod_u$ — $B^3\prod_g$)) were also observed. N_2 ($C^3\prod_u$) (E ≈ 11.1 eV) were generated through a resonant reaction between Ar metastables (E ≈ 11.5 eV) and ground state molecular N_2. However, peaks belonging to the N_2 first negative system ((N_2^+ ($B^2\Sigma^+_u$ — $X^2\Sigma^+_g$)) (E ≈ 18.7 eV) were not detected. Additionally, an O atom peak was detected at 777 nm. Both the nitrogen and oxygen active species were detected in the pure

Ar discharge because the impurities (N_2 and O_2 molecules) from the Ar gas or from the atmosphere were entrained into the plasma. In particular, we investigated the effects of additive gas (N_2 or O_2) on the OES of APC Ar plasma jet. It was shown that the emission intensities of excited Ar atoms and N_2 ($C^3\prod_u$ — $B^3\prod_g$) decreased with the increasing concentration of added O_2 gas because of the quenching effect. Meantime, the emission intensity of O atoms increased significantly after the addition of O_2 gas. A maximum emission intensity of O atoms was observed at the added O_2 flow rate of 15 smlpm. Similar to the O_2 addition, the emission intensities of excited Ar and O atoms decreased with the increasing concentration of added N_2 gas. However, the emission intensities of N_2 ($C^3\prod_u$ — $B^3\prod_g$) increased only slightly after the addition of N_2 gas. We assumed that the generated N_2 ($C^3\prod_u$) transformed to N_2^+ ($B^2\Sigma^+_u$) quickly through the successive collisions with energetic electrons, and then the newly created N_2^+ ($B^2\Sigma^+_u$) was trapped in the electric field (discharge region) by the very fast polarity change.

References

[1] Y. Duan, C. Huang, Q. Yu, IEEE Trans. Plasma Sci. 2005, 33, 328.

[2] S. Forster, C. Mohr, W. Viol, Surface Coat. Technol. 2005, 200, 827.

[3] J. Zhang, J. Sun, D. Wang, X. Wang, Thin Solid Films 2006, 506, 404.

[4] J. L. Walsh, J. J. Shi, M. G. Kong, Appl. Phys. Lett. 2006, 88, 171501.

[5] M. Laroussi, X. Lu, Appl. Phys. Lett. 2005, 87, 113902.

[6] A. Schu¨tze, J. Y. Jeong, S. E. Babayan, J. Park, G. S. Selwyn, R. F. Hicks, IEEE Trans. Plasma Sci. 1998, 26, 1685.

[7] J. Janca, M. Klima, P. Slavicek, L. Zajickova, Surface Coat. Technol. 1999, 116, 547.

[8] E. Stoffels, A. J. Flikweert, W. W. Stoffels, G. M. W. Kroesen, Plasma Sources Sci. Technol. 2002, 11, 383.

[9] R. Foest, E. Kindel, A. Ohl, M. Stieber, K. D. Weltmann, Plasma Phys. Controlled Fusion 2005, 47, 525.

[10] R. Stonies, S. Schermer, E. Voges, J. A. C. Broekaert, Plasma Sources Sci. Technol. 2004, 13, 604.

[11] J. Laimer, H. Stŏri, Plasma Process. Polym. 2007, 4, 266.

[12] J. Laimer, H. Stŏri, Plasma Process. Polym. 2006, 3, 573.

[13] J. Park, I. Henins, H. W. Herrmann, G. S. Selwyn, Appl. Phys. Lett. 2000, 76, 288.

[14] S. Y. Moon, R. K. Rhee, D. B. Kim, W. Choe, Phys. Plasmas 2006, 13, 033502.

[15] J. J. Shi, X. T. Deng, R. Hall, J. D. Punnett, M. G. Kong, J. Appl. Phys. 2003, 94, 6303.

[16] J. J. Shi, M. G. Kong, Phys. Rev. Lett. 2006, 96, 105009.

[17] X. Yang, M. Moravej, S. E. Babayan, G. R. Nowling, R. F. Hicks, Plasma Sources Sci. Technol. 2005, 14, 314.

[18] X. Yang, M. Moravej, S. E. Babayan, G. R. Nowling, R. F. Hicks, Plasma Sources Sci. Technol. 2005, 14, 412.

[19] J. Laimer, S. Haslinger, W. Meissl, J. Hell, H. Stŏri, Vacuum 2005, 79, 209.

[20] J. Park, I. Henins, H. W. Herrmann, G. S. Selwyn, J. Appl. Phys. 2001, 89, 20.

[21] Y. H. Choi, J. H. Kim, K. H. Paek, W. T. Ju, Y. S. Hwang, Surf. Coat. Technol. 2005, 193, 319.

[22] S. Haslinger, J. Laimer, H. Stŏri, Vacuum 2008, 82, 142.

[23] Q. S. Yu, H. K. Yasuda, Plasma Chem. Plasma Process. 1998, 18, 461.

[24] M. C. García, M. Varo, P. Martínez, Plasma Chem. Plasma Process. 2010, 30, 241.

[25] A. F. Bublievskii, A. A. Galinovskii, A. V. Gorbunov, S. A. Zhdanok, V. A. Koval, L. I. Sharakhovskii, G. V. Dolgolenko, D. S. Skomorokhov, J. Eng. Phys. Thermophys. 2006, 79, 629.

[26] V. Poenariu, M. R. Wertheimer, R. Bartnikas, Plasma Process. Polym. 2006, 3, 17.

[27] V. Léveillé, S. Coulombe, Plasma Process. Polym. 2006, 3, 587.

[28] C. Lee, D. B. Graves, M. N. Lieberman, D. W. Hess, J. Electrochem. Soc. 1994, 141, 1546.

[29] B. Eliasson, U. Kogelschatz, ‘‘Basic Data for Modeling of Electrical Discharge in Gases: Oxygen’’, Research, Asea Brown Boveri Corporate, KLR-11C CH5405, 1986.

[30] D. Lee, J. Park, S. H. Hong,Y. Kim, IEEE Trans. Plasma Sci. 2005, 33, 949.

[31] K. Niemi, V. Schulz von der Gathen, H. F. Dŏbele, Plasma Sources Sci. Technol 2005, 14, 375.

[32] V. Nemchinsky, J. Phys. D: Appl. Phys. 2005, 38, 3825.

Tab. 2-1 Summary of active species (wavelength range of 350-950 nm) detected in APC Ar plasma jet at a distance of 5 mm from the end of the torch. Discharge conditions: Ar flow rate of 20 SLPM, input RF power of 100 W.

Species	**λ** (nm)	**Absolute irradiance** ($\mu W/cm^2/nm$)	**Transition**
N_2 2^{nd} positive system	357.51	0.01717	$C^3\prod_u \rightarrow B^3\prod_g$
	375.51	0.00466	
	380.27	0.01208	
	405.79	0.00339	
Ar atoms	696.53	0.03763	4p → 4s
	707.60	0.00764	
	728.03	0.01234	
	739.22	0.01902	
	751.67	0.03472	
	764.06	0.13171	
	773.03	0.08964	
	795.47	0.02952	
	801.91	0.04615	
	812.00	0.13457	
	827.13	0.10463	
	842.87	0.08260	
	852.57	0.02274	
	867.57	0.00504	
	912.68	0.22457	
	922.70	0.03411	
O atoms	777.87	0.02543	3p → 3s

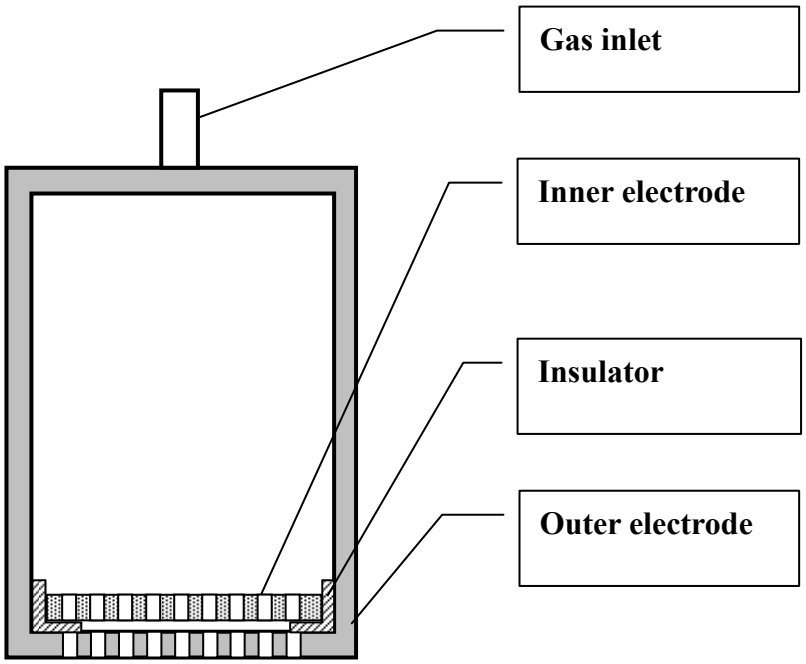

Fig. 2-1 Schematic illustration for APC plasma torch.

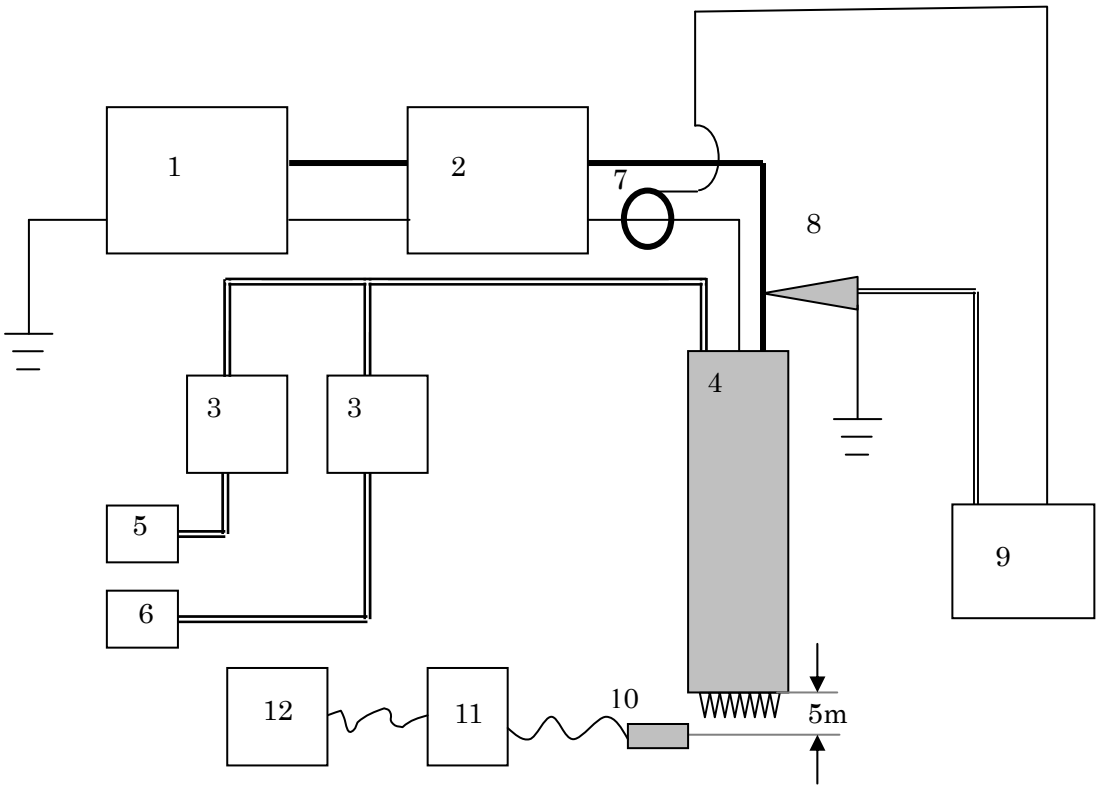

1. RF power source; 2. Matching box; 3. Mass flow controller; 4. APC plasma torch; 5. Ar gas; 6. Additive gas (N_2 or O_2); 7. Current probe; 8. High-voltage probe; 9. Oscilloscope; 10. Optical fiber; 11. Spectrometer; 12. Personal computer.

Fig. 2-2 Schematic illustration for experimental setup of OES and electrical measurement.

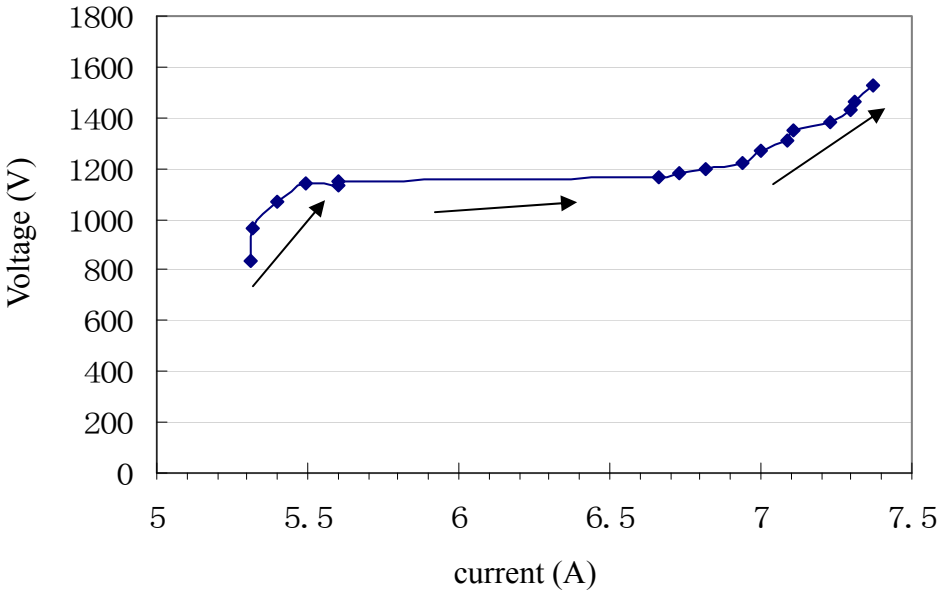

Fig. 2-3 I-V curve for APC pure Ar plasma jet with the arrow showing the sequence of operating conditions employed. In the discharge experiments, input RF power was increased from 25 W to 105 W with a step of 5 W at Ar flow rate of 20 SLPM. Note: peak to peak values of the discharge voltage and the RF current are given in the figure.

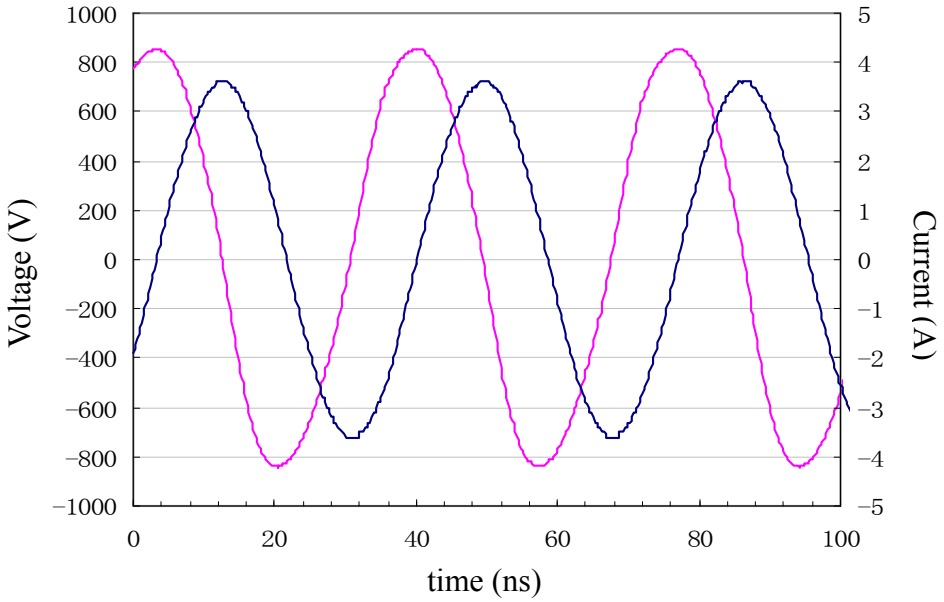

Fig. 2-4 Waveforms of discharge voltage (red line) and RF current (blue line) for APC pure Ar plasma jet with RF power of 100 W at Ar flow rate of 20 SLPM.

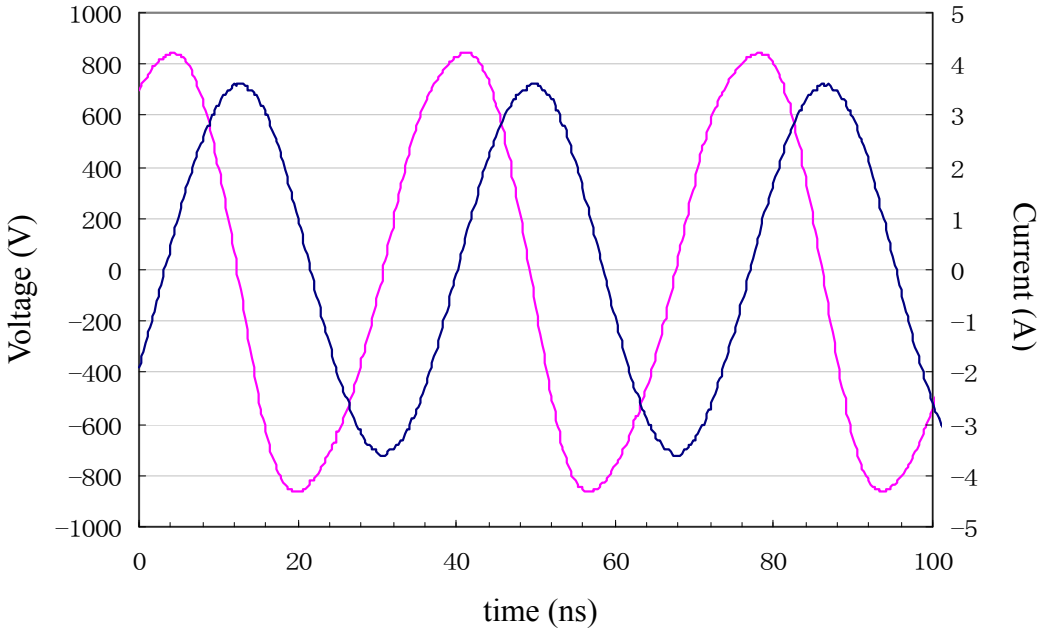

Fig. 2-5 Waveforms of discharge voltage (red line) and RF current (blue line) for APC pure Ar plasma jet with RF power of 100 W at Ar flow rate of 5 SLPM.

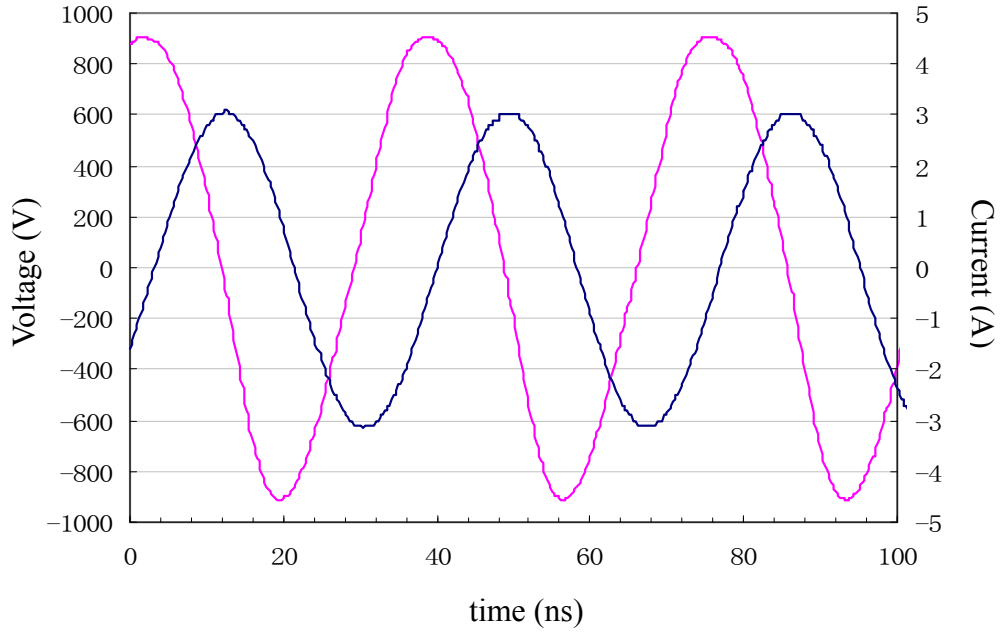

Fig. 2-6 Waveforms of discharge voltage (red line) and RF current (blue line) for APC pure Ar plasma jet with 10-mm-diameter plasma torch, at RF power of 100 W and Ar flow rate of 20 SLPM.

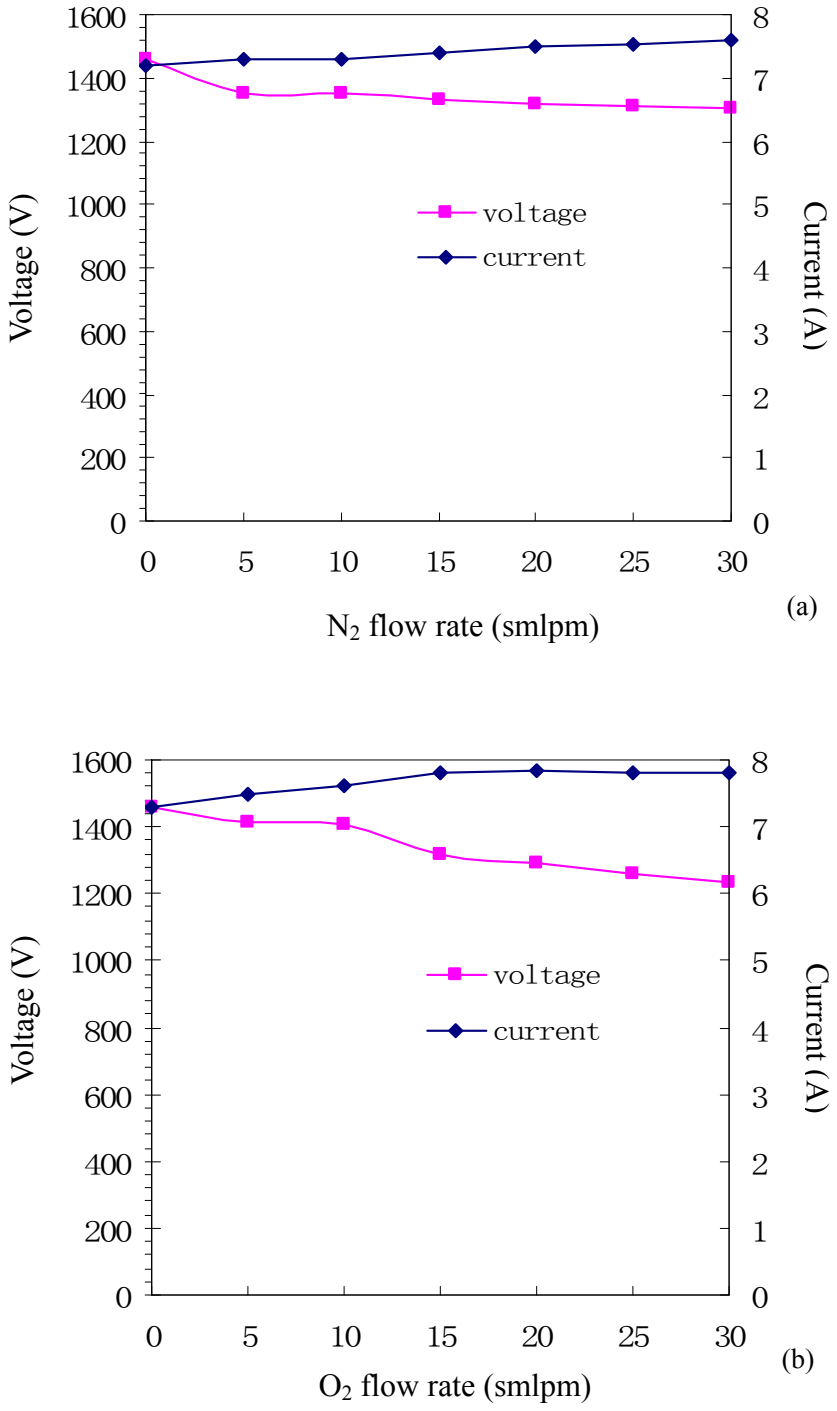

Fig. 2-7 Changes in discharge voltage and RF current for APC Ar plasma jet with increasing concentration of additive gas. (a): N_2 addition; (b): O_2 addition. Discharge conditions: input RF power of 100 W, Ar flow rate of 20 SLPM. Note: peak to peak values of the discharge voltage and the RF current are given in the figure.

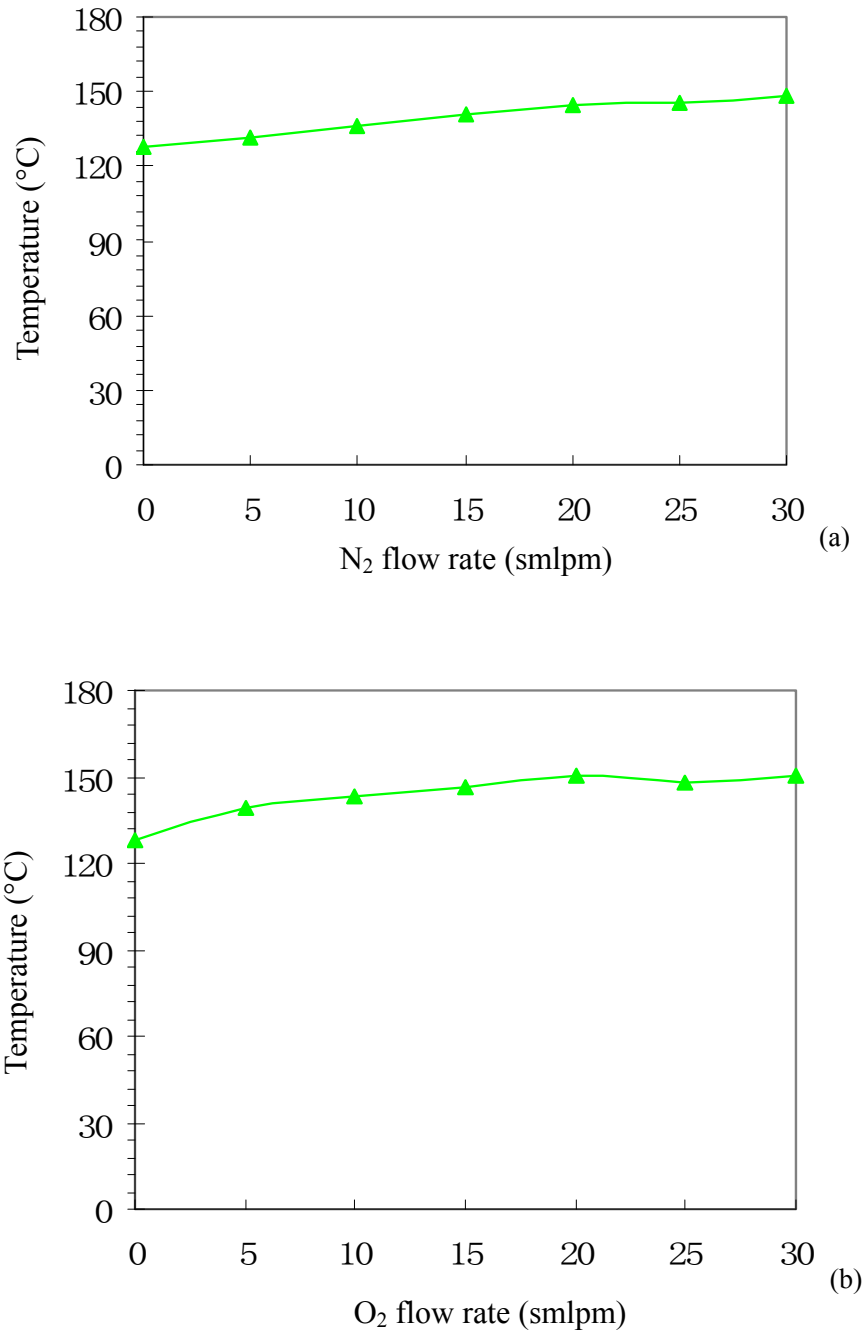

Fig. 2-8 Changes in APC Ar plasma temperature with increasing concentration of additive gas. (a): N_2 addition; (b): O_2 addition. Discharge conditions: input RF power of 100 W, Ar flow rate of 20 SLPM. Note: plasma temperatures were monitored at the end of the plasma torch using a thermocouple.

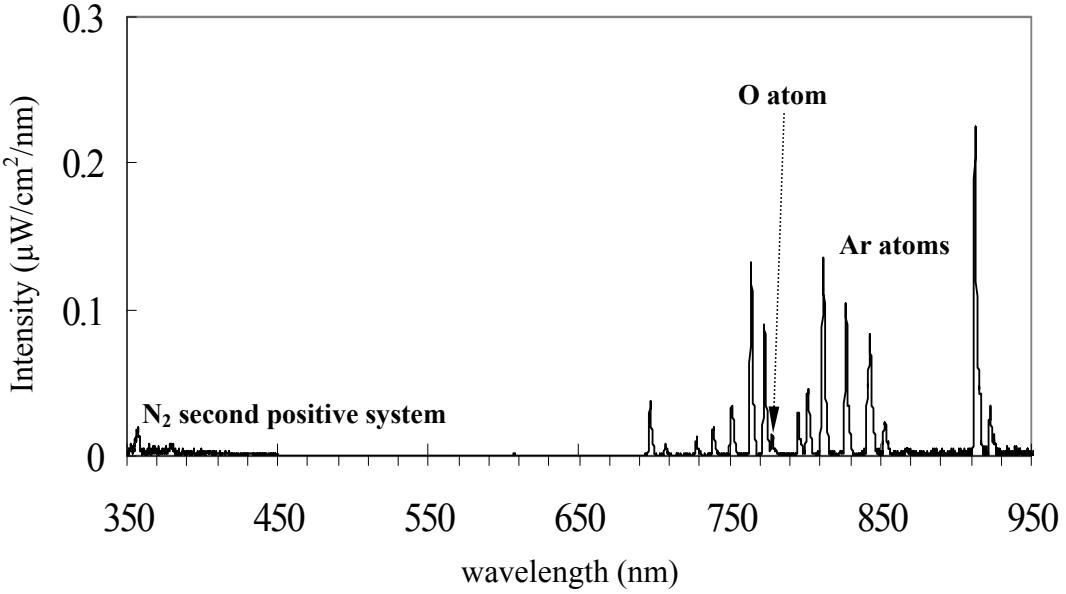

Fig. 2-9 Typical optical emission spectrum of APC Ar plasma jet measured by USB4000 spectrometer at a distance of 5 mm from the end of the torch. Discharge conditions: Ar flow rate of 20 SLPM, input RF power of 100 W.

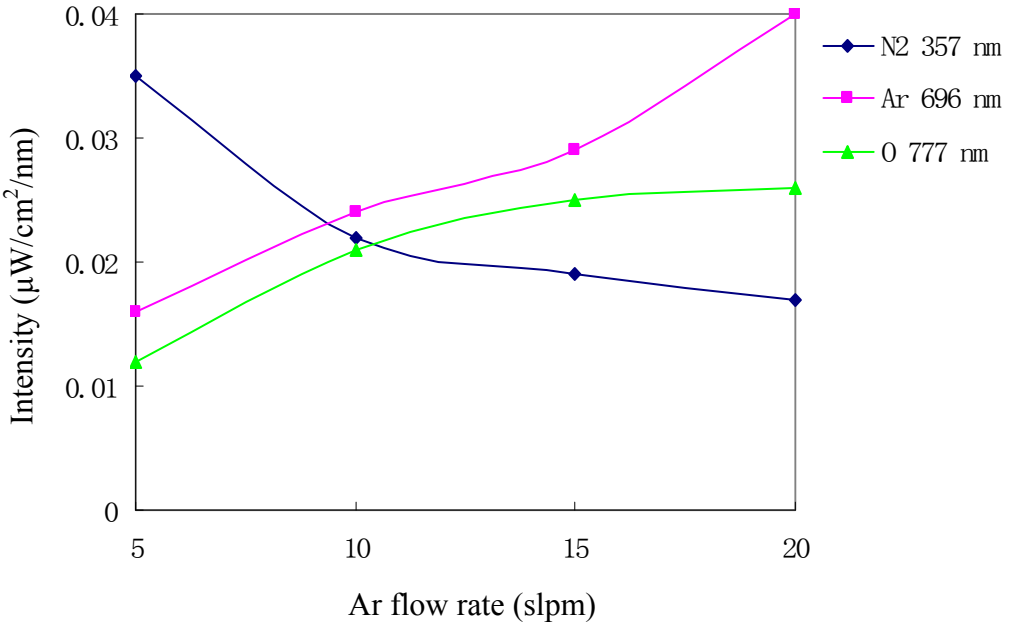

Fig. 2-10 Changes in emission intensities of active species in APC Ar plasma jet with increasing concentration of Ar flow rate. OES was measured at a distance of 5 mm from the end of the plasma torch. In the discharge experiments, RF power was maintained at 100 W. Note: N_2 ($C^3\prod_u$ — $B^3\prod_g$) at 357 nm and excited Ar atoms at 696 nm are selected as representatives for N_2 second positive system and excited Ar atoms, respectively.

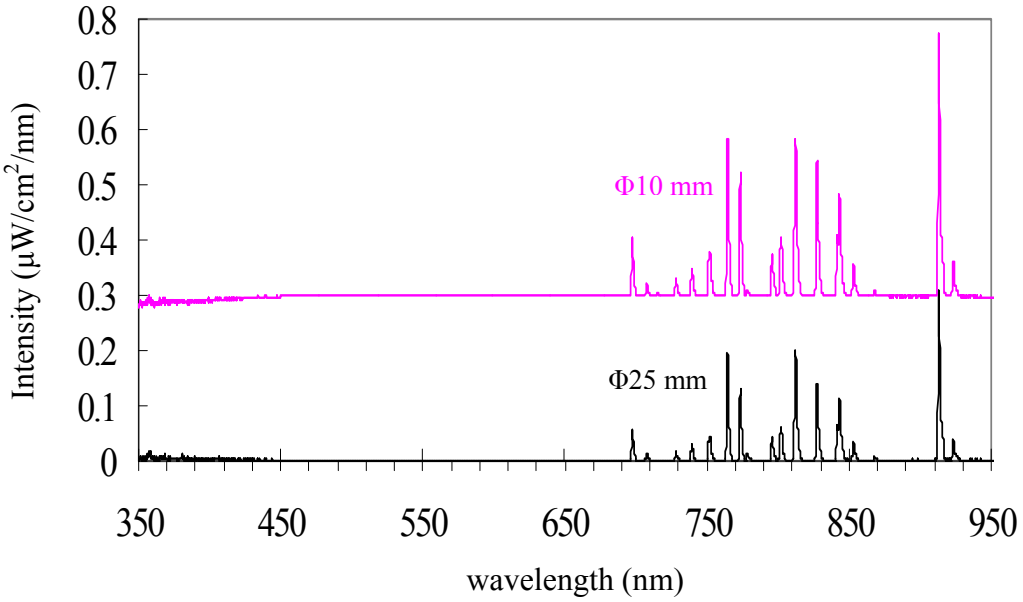

Fig. 2-11 Comparison of typical optical emission spectra of APC Ar plasma jets with different diameter plasma torches. OES were measured by USB4000 spectrometer at a distance of 5 mm from the end of the torch. Discharge conditions: Ar flow rate of 20 SLPM, input RF power of 100 W.

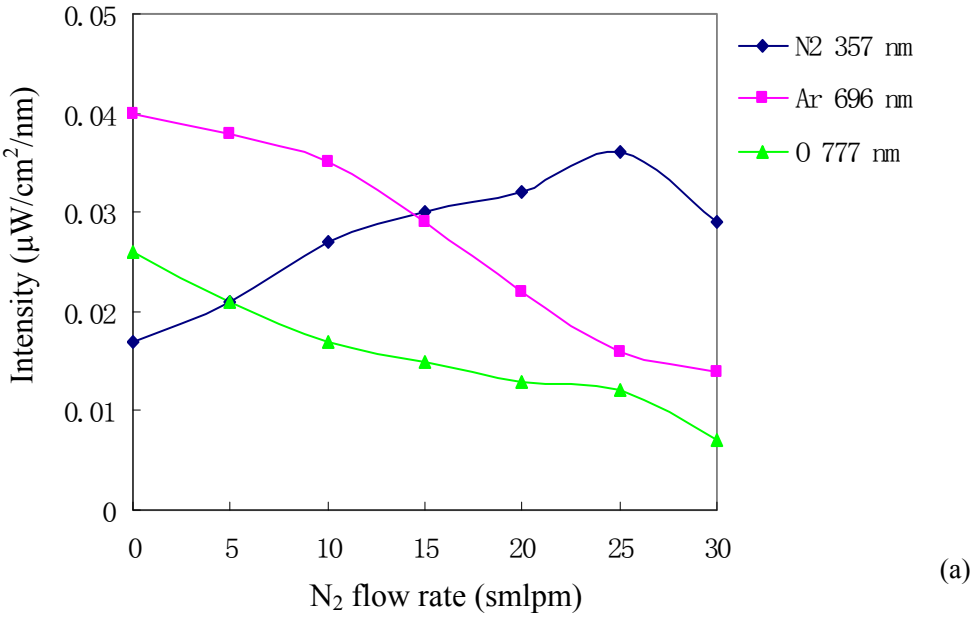

(a)

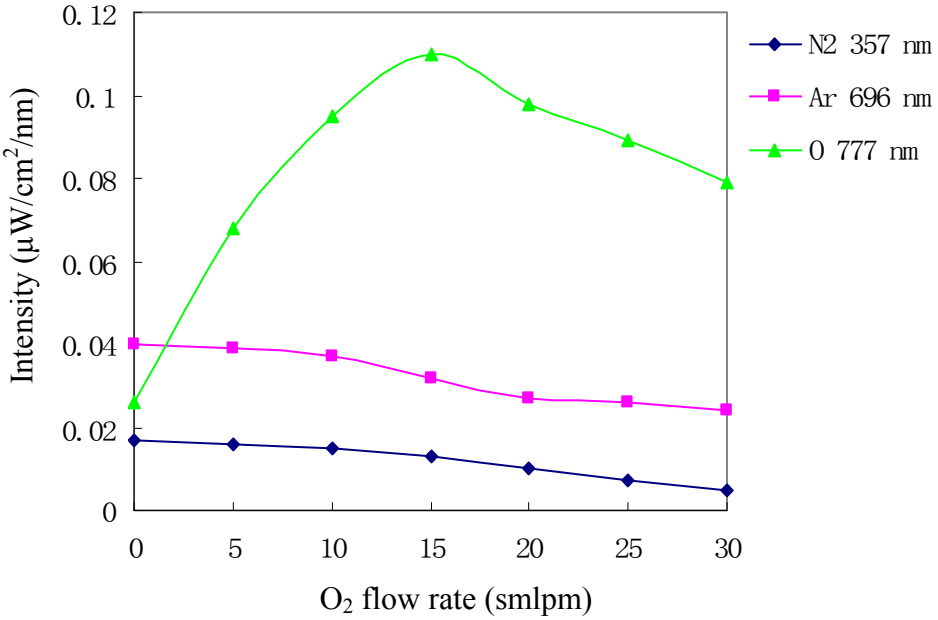

(b)

Fig. 2-12 Changes in emission intensities of active species in APC Ar plasma jet with increasing concentration of additive gas. OES was measured at a distance of 5 mm from the end of the plasma torch. (a): N_2 addition, (b): O_2 addition. Discharge conditions: input RF power of 100 W, Ar flow rate of 20 SLPM. Note: N_2 ($C^3\prod_u$ — $B^3\prod_g$) at 357 nm and excited Ar atoms at 696 nm are selected as representatives for N_2 second positive system and excited Ar atoms, respectively.

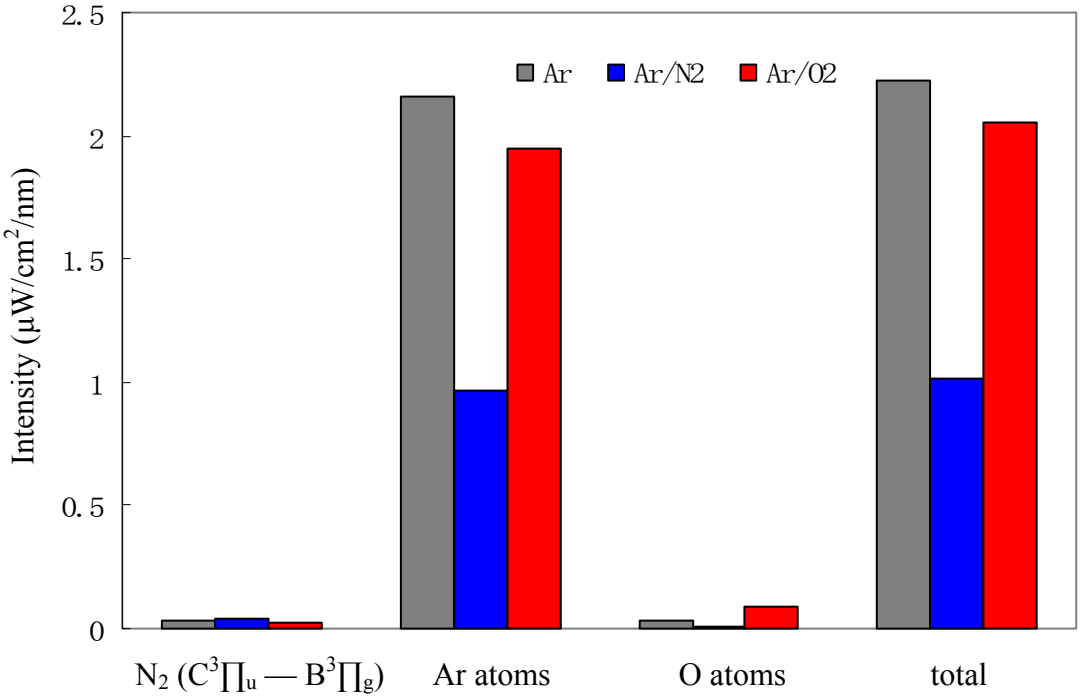

Fig. 2-13 Comparison of emission intensities of active species in APC Ar plasma jet before and after the addition of additive gas (N_2 or O_2). OES was measured at a distance of 5 mm from the end of the plasma torch. Discharge conditions: Ar flow rate of 20 SLPM, additive gas flow rate of 30 smlpm, input RF power of 100 W. Note: only active species in the wavelength range of 350–950 nm are counted in the total emission intensity.

Chapter 3 Electrical and Optical Characterization of Surface Discharge Non-equilibrium Atmospheric Pressure Argon Plasma Jet

1 Introduction

Non-equilibrium plasmas have been used in various fields such as materials processing and biomedicine and in processes such as surface coating and plasma enhanced chemical vapor deposition (PECVD) [1-5]. Previously, non-equilibrium plasmas were typically employed at pressures between 0.1 and 500 Pa. Sophisticated vacuum equipment was therefore needed to maintain the low pressure that was required for the discharge. In order to reduce costs, it was highly desirable to eliminate the need for expensive vacuum systems and operate plasmas at atmospheric pressure. Recently, several novel atmospheric pressure discharge sources have been developed; examples include the atmospheric pressure plasma jet, cold plasma torch, one atmosphere uniform glow discharge plasma, and microplasma. All these plasma sources produce discharges with a low gas temperature at atmospheric pressure [6-13].

We have successfully developed a device that is able to generate a non-equilibrium atmospheric pressure plasma jet of low temperature (22 to 35°C) fed by a high-voltage pulsed power source. This device has been commercialized under the name of "CAPPLAT" by Cresur Corporation of Japan [14]. Both He and Ar can be used as working gas with this plasma device. This plasma jet has previously been used for both chemical vapor deposition (CVD) and polymer surface treatment [15-18]. In this study, electrical properties of CAPPLAT Ar plasma jet were characterized using a high-voltage probe and a current probe. Further, optical emission spectrometry (OES) was used to identify the active species in this Ar plasma jet. In particular, the effects of additive gas (N_2 or O_2) on the electrical and optical characteristics of this Ar plasma jet were investigated in detail.

2 Experimental setup and methods

2.1 Plasma device

The plasma device (CAPPLAT) used in the experiments is a hand-made cold atmospheric pressure plasma torch. The plasma torch comprises two co-axial cylindrical electrodes. With the normal connection mode, the inner electrode (copper pipe) is connected to a high-voltage pulsed power source with a frequency of several tens of kilohertz. The outer electrode (aluminum foil) is grounded. If without specific illustration, the normal connection mode was employed in the experiments. A Laboran® silicone tube (thickness: 2 mm) acts as a dielectric barrier between the two electrodes. The outer and inner diameters of the torch are 10 mm and 6 mm, respectively. The schematic illustration of the torch is shown in Fig. 3-1. Further details of the configuration of this plasma torch are provided in our previous papers [17, 18]. Discharge experiments were performed under normal conditions by applying invariable voltage (±8.0 kV) with a square-wave amplitude at a 50% duty cycle and a constant frequency of 20 kHz. Ar gas was employed as the working gas. N_2 or O_2 gas was introduced as the additive gas into the Ar stream. The flow rates of the Ar gas were set to 5 ~ 10 SLM (standard liters per minute). The flow rates of additive gas were set to 30 ~ 500 smlpm (standard milliliters per minute), respectively. All flow rates were controlled using a mass flow controller. It should be noted that N_2 additive gas was injected directly into the Ar gas. We tried to adopt this injection approach even for O_2 additive gas; however, no plasma jet was generated by such direct injection, because of the considerable quenching effect of O_2. Therefore, we developed a new injection method. We added O_2 to the afterglow zone of the plasma jet through a glass capillary placed at the center of the torch (see Fig. 3-1). In this case, O_2 mixes with the Ar plasma in the afterglow zone. We also added N_2 to the plasma afterglow zone through the glass capillary; however,

in this case, the effects of N_2 addition on the Ar plasma jet were negligible in terms of both the electrical and the optical properties. The difference in the injection approaches for the N_2 and O_2 additive gases is shown in Fig. 3-2.

2.2 Electrical measurement

The high voltage applied to the discharge was measured using a 1000:1 high-voltage probe (Tektronix P6015A); the discharge current was monitored using a wide band current monitor (Pearson^{TM} current monitor) manufactured by Pearson Electronics Inc., Palo Alto, California, U.S.A. Further, a Tektronix TDS3012C digital phosphor oscilloscope was employed to obtain the voltage and current waveforms. The setup for electrical measurement is shown in Fig. 3-3.

2.3 Optical emission spectroscopy (OES)

The optical emission spectra of the plasma jet were collected perpendicular to the jet using an Ocean Optics USB4000 spectrometer (spectral range of 350–950 nm) with a resolution of 0.2 nm full width at half-maximum (FWHM); this was achieved using a personal computer equipped with relevant software (SpectraSuite) for both driving and acquisition. Prior to the OES measurement, the USB4000 spectrometer was calibrated using a standard halogen light source. Therefore, absolute irradiance of the active species in the plasma jet was obtained. During the measurement of the optical emission spectra, the exposure time was 100 ms. Emission intensities of the active species were collected at an axial position of the plasma jet, through an optical fiber with a diameter of 100 μm.

3 Results and discussion

3.1 Electrical characterization of CAPPLAT Ar plasma jet

3.1.1 Current and voltage (I – V) characteristics

Generally, electrical measurements allow for the determination of the impedance of the entire load and not just of the plasma itself. A simple electrical equivalent circuit model can be used to evaluate the discharge characteristics of this plasma jet. This equivalent circuit model was reported in many literatures [19-21]. In this study, an equivalent R-C parallel circuit was employed to evaluate the discharge characteristics of this plasma jet, C is the capacitance representing the silicone dielectric between the two electrodes and R is the resistance of the discharge. It should be noted that the sheath was not considered in this study, because CAPPLAT plasma jet is based on surface discharge. The equivalent R-C parallel circuit is shown in Fig. 3-4. The total current (current 1) and capacitive current (current 2) were measured on the basis of the equivalent R-C circuit model by using a current monitor (see Fig. 3-4). For simplicity, we assume that the total current in the circuit is equal to the sum of the capacitive current and the discharge current. Therefore, the discharge current can be roughly calculated from the total current and the capacitive current.

Figure 3-5 (a) shows typical waveforms of the applied voltage (black line) and total current (red line) recorded by an oscilloscope. It is apparent that the actual applied high voltage is only about 14.5 kV (peak to peak), although the nominal voltage is 16.0 kV (peak to peak). In addition, a large and instantaneous pulse current was observed when the high voltage was applied and switched off. As mentioned earlier, the temperature of the plasma jet is 22–35°C as the duration of application of both voltage and current is quite short in a single period. Figure 3-5 (b) shows waveforms of the total current (current 1), capacitive current (current 2), and discharge current during polarity change. The calculated discharge current was found to be about 60 mA and the pulse width was about 1 μs. On the other hand, it should be noted that current pulses due to a series of microdischarges [22] were not observed here. Therefore, we inferred that the discharge of this plasma jet is glow-like (diffuse)

barrier discharge and not filamentary barrier discharge. Until now, rare studies were performed to study the glow discharge mechanism in Ar gas at atmospheric pressure. However, glow discharge mechanisms in He or N_2 gas at atmospheric pressure were reported by a few studies [23-26]. It was reported that the glow barrier discharge only occurs at very typical operating conditions. The effective ionization and excitation processes are very important for the glow barrier discharge. On the other hand, the electrons on the dielectric surface play an important role in the current balance for efficient primary ionization processes at low electric field strength. Analogously, we assume that the effective ionization and excitation of Ar molecules are critical for the atmospheric pressure glow-like discharge in Ar gas. Additionally, the quantity of "seed electrons" on the barrier surface, remaining from the previous half period, is quite important for the ionization and excitation of Ar molecules in the next half cycle. When the seed electrons are overabundant the diffuse barrier mode (glow mode) will transit to the filamentary barrier mode since the memory effect of microdischarges increased. On the other hand, the diffuse barrier mode (glow mode) is not able to occur when the seed electrons are not abundant for the primary ionization and excitation of Ar molecules in the next half cycle.

Figure 3-6 shows the dependence of discharge current on the nominal applied voltage. It can be clearly seen that the discharge current increased significantly with the increase in the nominal applied voltage, suggesting the increase in the electron density.

3.1.2 Effect of Ar flow rate on electrical properties

Figure 3-7 shows waveforms of the total current (current 1), capacitive current (current 2), and discharge current during polarity change at Ar flow rate of 5 SLPM. Compared to the waveforms shown in Fig. 3-5 (b) above, both the total current and the discharge current scarcely changed,

suggesting that the Ar flow rate scarcely affected the discharge behavior of CAPPLAT Ar plasma jet in the experimental range (Ar flow rates were set from 5 SLPM to 20 SLPM).

3.1.3 Effect of dielectric thickness on electrical properties

In order to investigate effects of the thickness of silicone tube on the electrical properties of CAPPLAT Ar plasma jet, silicone tubes with different thicknesses were used in the experiments. Figure 3-8 shows waveforms of the total current (current 1), capacitive current (current 2), and discharge current during polarity change at Ar flow rate of 10 SLPM with the different thicknesses of silicone tubes. It can be clearly seen that the total current in the circuit increased significantly with the decrease in the thickness of the dielectric (silicone tube). However, the discharge current increased slightly with the decrease in the thickness of the silicone tube, since the increase in the total current mainly attributes to the increase in the capacitive current (see Fig. 3-8 (a)). As we well known, the breakdown voltage decreases when the thickness of the dielectric is reduced. Therefore, the displacement current through the dielectric increases with the decrease in the dielectric thickness. On the other hand, the total current decreased with the increase in the thickness of the silicone tube. However, in this case, the discharge current changed slightly as well (see Fig. 3-8 (b)). All of these suggest that the discharge current is weakly dependent on the thickness of the barrier.

3.1.4 Effect of torch diameter on electrical properties

In order to investigate the effect of torch diameter on the electrical properties of CAPPLAT Ar plasma jet, a mini-CAPPLAT plasma torch was used. The inner and the outer diameter of the mini-CAPPLAT plasma torch are 3 mm and 5 mm, respectively. Figure 3-9 shows waveforms of the total current (current 1), capacitive current (current 2), and discharge current of mini-CAPPLAT plasma jet during polarity change at Ar flow rate of 10 SLPM. Compared to the waveforms of the

total current and the discharge current shown in Fig. 3-8 (a) above, the capacitive current decreased remarkably with the decrease in the torch diameter, which shows the essence of surface discharge. However, the discharge current changed slightly with the change in the torch diameter. Considering the difference in the discharge areas, the current density increased with the decrease in the torch diameter, which will lead to a stronger electric field.

3.1.5 Effect of additive gas (N_2 or O_2) on electrical properties

In order to investigate the effects of additive gas (N_2 or O_2) on the electrical properties of CAPPLAT Ar plasma jet, N_2 or O_2 was injected into the Ar plasma jet at different flow rates, respectively. Comparisons of waveforms of the total current (current 1) before and after the addition of the additive gas are shown in Fig. 3-10 (a) and (b), respectively. Surprisingly, the total current (current 1) in the circuit decreased only slightly after the addition of N_2 or O_2, although the injection approach was quite different in the case of these two gases. It is also apparent that injecting N_2 gas directly into the Ar stream or adding O_2 gas to the plasma afterglow zone through a glass capillary caused only a slight change in the electrical properties of this Ar plasma jet. Additionally, we monitored the plasma temperature at the exit of the plasma jet before and after the addition of additive gas using a thermometer. It was shown that the plasma temperature scarcely changed as well. All of these suggest that the ionization of additive gas molecules through collisions with energetic electrons is negligible in CAPPLAT Ar plasma jet.

On the basis of this result, a simple discharge mechanism is proposed here. First, Ar molecules are excited and ionized through collisions with energetic electrons. In this step, energy is transferred to the Ar particles and Ar active species (Ar metastable atoms) are produced. Second, N_2 or O_2 molecules are excited through collisions with energetic Ar metastable atoms. Nitrogen active species

(N_2 ($C^3\prod_u$)) and oxygen active species (O atoms) are then generated. Additionally, the peak width of the current increased slightly after the injection of N_2 (see Fig. 3-10 (a)). However, this increase was not observed when O_2 was added (see Fig. 3-10 (b)). This suggests that the plasma jet became more homogenous after N_2 injection. We also noted that with the N_2 injection, the plasma was strongly modified and the whitish Ar plasma jet became a stable, homogenous pink jet. However, the appearance of the plasma jet changed only slightly after O_2 was added to the plasma afterglow zone through the glass capillary.

3.1.6 Effect of connection mode on electrical properties

Besides the normal connection mode, the reverse connection mode was also attempted with CAPPLAT plasma device. As we mentioned in section of 2.1, in the normal connection mode the inner electrode is connected to the high-voltage power supplier and the outer electrode is grounded. However, in the reverse connection mode the outer electrode is connected to the high-voltage power supplier and the inner electrode is grounded. Figure 3-11 shows waveforms of the total current (current 1), capacitive current (current 2), and discharge current with the reverse connection mode during polarity change at Ar flow rate of 10 SLPM. It can be clearly seen that comparing to the normal connection mode, the discharge current decreased dramatically, though the nominal applied voltage is identical in the two cases. We assume that the distribution and the strength of electric field inside the plasma torch are quite different from the normal connection mode. It is presumed that the electric field strength and the electric field energy density reduce from the high-voltage electrode to the ground electrode. Thus, the electric field strength and the electric field energy density are quite weak around the grounded electrode. Therefore, with the reverse connection mode (the inner electrode is grounded), the strength and the energy density of electric field are very weak inside the

plasma torch, which leads to a very low energy transfer to the Ar gas. This assumption can explain why the discharge current is very low with the reverse connection mode. Additionally, we note that the air around the outer electrode is discharged with the reverse connection mode. It is completely consistent with our assumption for the distribution of the electric field strength and the energy density.

3.2 Optical characterization of CAPPLAT Ar plasma jet

3.2.1 Typical optical emission spectrum

A typical optical emission spectrum of CAPPLAT Ar plasma jet in the wavelength range of 350–950 nm is shown in Fig. 3-12. It can be seen that peaks belonging to the excited Ar atoms (4p-4s transition) are predominant in this plasma jet (in the wavelength range of 690–950 nm) [27, 28]. Surprisingly, peaks at 357, 380, and 406 nm belonging to the N_2 second positive system (N_2 ($C^3\prod_u$ — $B^3\prod_g$)) were also observed with relatively strong emission intensities. However, peaks belonging to the N_2 first negative system ((N_2^+ ($B^2\Sigma^+_u$ — $X^2\Sigma^+_g$)) were not detected. Additionally, an O atom peak at 777 nm was detected with rather weak emission intensity [29, 30]. Both nitrogen and oxygen active species were detected in the pure Ar discharge because the impurities (N_2 and O_2 molecules) from the Ar gas or from the atmosphere were excited and dissociated. Emission intensities and assignments of all active species (in the wavelength range of 350–950 nm) detected in CAPPLAT Ar plasma jet are summarized in Table 3-1.

As discussed above, in CAPPLAT plasma jet, the Ar metastable atoms are generated through collisions with energetic electrons. And then, the Ar metastables are excited to a higher excitation level through the successive collisions with energetic electrons. The excited Ar atoms emit light when they return to the lower excitation level. On the other hand, these species are the main energy

carriers that generate N_2 ($C^3\prod_u$) and O atoms, through collisions with N_2 or O_2 molecules. As we discussed in chapter 2, N_2 ($C^3\prod_u$) is mainly generated through a resonant reaction between Ar metastables and ground-state molecular N_2. This reaction helps explain why relatively strong emission intensities corresponding to the N_2 second positive system (N_2 ($C^3\prod_u$ — $B^3\prod_g$)) were observed. On the other hand, it was reported that the generation of the N_2 first negative system ((N_2^+ ($B^2\Sigma^+_u$ — $X^2\Sigma^+_g$)) was primarily based on the Penning ionization of N_2 molecules [28]. Obviously, the Ar metastables have insufficient energy to generate the N_2 first negative system (E ≈ 18.7 eV) through the Penning ionization [27]. As we discussed in chapter 2, N_2^+ ($B^2\Sigma^+_u$) may probably be generated through the following channels in Ar discharge [28, 31]:

$$e^* + N_2 (X^1\Sigma^+_g) \rightarrow N_2^+ (B^2\Sigma^+_u) + 2e \quad (3\text{-}1)$$

$$e^* + N_2 (C^3\prod_u) \rightarrow N_2^+ (B^2\Sigma^+_u) + 2e \quad (3\text{-}2)$$

$$Ar^+ + N_2 (X^1\Sigma^+_g) \rightarrow Ar^0 + N_2^+ (X^2\Sigma^+_g) \quad (3\text{-}3)$$

$$e^* + N_2^+ (X^2\Sigma^+_g) \rightarrow N_2^+ (B^2\Sigma^+_u) + e \quad (3\text{-}4)$$

However, as abovementioned, the ionization of additive gas molecules through collisions with energetic electrons is negligible in CAPPLAT Ar plasma jet, since the electron density and the electron energy are relatively low. Thus, no peaks belonging to the N_2 first negative system ((N_2^+ ($B^2\Sigma^+_u$ — $X^2\Sigma^+_g$)) were detected. On the other hand, it was reported that the most probable channel for the formation of O atoms was through collisions between the oxygen molecular ions (O_2^+) and electrons [32]. Oxygen molecular ions (O_2^+) are mainly generated through the Penning ionization of O_2 molecules. Apparently, Ar metastables have insufficient energy for the generation of O_2 molecular ions (O_2^+) (E ≈ 18.2 eV) through the Penning ionization [27]. However, as we mentioned in chapter 2, oxygen atoms can probably be generated through the following channels in Ar

discharge [27, 33-35]:

$$Ar^* + O_2 (X^3\Sigma^-_g) \rightarrow O (^1D) + O (^3P) + Ar^0 \quad (3\text{-}5)$$

$$e^* + O_2 (X^3\Sigma^-_g) \rightarrow e + [O (^1D) \text{ or } O (^1S)] + O (^3P) \quad (3\text{-}6)$$

$$e^* + O_2 (X^3\Sigma^-_g) \rightarrow 2e + O_2^+ (b^4\Sigma^-_g) \quad (3\text{-}7)$$

$$e^* + O_2^+ (b^4\Sigma^-_g) \rightarrow 2O (^3P) \quad (3\text{-}8)$$

Considering the electron density and the electron energy, reaction (3-5) is the only channel for the generation of O atoms in CAPPLAT Ar plasma jet. This may explain the detection of rather weak emission intensity of excited O atoms at 777 nm in CAPPLAT Ar plasma jet.

3.2.2 Effect of Ar flow rate on OES

Comparison of optical emission spectra of CAPPLAT Ar plasma jets with different Ar flow rates is shown in Fig. 3-13. Similar to APC Ar plasma jet, it can be seen that the emission intensities of excited Ar and O atoms increased significantly with the increase in the Ar flow rate. As we discussed in chapter 2, it is because a higher Ar flow rate leads to a faster velocity of the Ar stream, which is very helpful for the transport of the active species [36]. Interestingly, opposite to the APC Ar plasma jet, the emission intensity of N_2 ($C^3\prod_u$ — $B^3\prod_g$) increased with the increase in the Ar flow rate in case of CAPPLAT Ar plasma jet. In case of APC Ar plasma, the observed N_2 ($C^3\prod_u$ — $B^3\prod_g$) mainly comes from the afterglow zone. It was because N_2 ($C^3\prod_u$) in the discharge region transformed to N_2^+ ($B^2\Sigma^+_u$) quickly and was trapped in the discharge region by a very fast polarity change. However, in case of CAPPLAT Ar plasma jet, N_2 ($C^3\prod_u$ — $B^3\prod_g$) from the discharge region is also able to be observed since N_2 ($C^3\prod_u$) can not be transformed to N_2^+ ($B^2\Sigma^+_u$) and be trapped in the discharge region. Thus, similar to excited Ar and O atoms, more N_2 ($C^3\prod_u$) can reach to a certain distant position from the exit (a distance of 5 mm in the experiment) at a higher Ar flow rate. On the

other hand, at the same Ar flow rate, the velocity of Ar stream in case of CAPPLAT plasma is much slower than APC plasma. Therefore, the change in Ar flow rate affects the entry of N_2 (from the atmosphere) into the plasma jet only slightly in case of CAPPLAT Ar plasma jet.

3.2.3 Effect of dielectric thickness on OES

Comparisons of optical emission spectra of CAPPLAT Ar plasma jets with different thicknesses of silicone tube are shown in Fig. 3-14. It can be seen that the plasma radiation changed only slightly with the change in the thickness of dielectric. It was because the discharge properties are weakly dependent on the thickness of barrier. These results are consistent with the electrical characterization in section 3.1.3.

3.2.4 Effect of torch diameter on OES

Comparison of optical emission spectra of CAPPLAT Ar plasma jets with different torch diameters is shown in Fig. 3-15. It can be seen that the plasma radiation increased remarkably with the decrease in the torch diameter. As we discussed in section 3.1.4, considering the difference in the discharge areas, the current density increased significantly with the decrease in the torch diameter, although the discharge current changed slightly with the change in the torch diameter. On the other hand, the velocity of the Ar stream increased with the decrease in the torch diameter, which is helpful for the transport of active species. All of these may probably be used to explain the increase in the plasma radiation with the decrease in the torch diameter.

3.2.5 Effect of additive gas (N_2 or O_2) on OES

Changes in emission intensities of excited Ar atoms at 696 nm, N_2 ($C^3\prod_u$ — $B^3\prod_g$) at 357 nm, and excited O atoms at 777 nm with the increasing concentration of N_2 gas are shown in Fig.3-16 (a), (b), and (c), respectively. The plasma jet was strongly modified when N_2 gas was injected directly into

the Ar stream. From Fig. 3-16 (a), it is seen that the emission intensities of excited Ar atoms decreased considerably after the addition of N_2 gas. As discussed above, electron collisions were dominant and Ar metastables were highly quenched by the resonant reaction with N_2 molecules. Therefore, the emission intensities of excited Ar atoms decreased dramatically when N_2 gas was injected directly into the Ar stream. Nearly all excited Ar atoms are quenched by the added N_2 molecules when the N_2 addition is more than 300 smlpm. From Fig. 3-16 (b), it is seen that the emission intensities of N_2 ($C^3\prod_u$ — $B^3\prod_g$) increased significantly when trace of N_2 was added. However, their emission intensities decreased drastically with the N_2 addition of more than 100 smlpm because of the quenching effect. From Fig. 3-16 (c), it is seen that similar to the excited Ar atoms, the emission intensity of O atoms decreased with the increasing N_2 addition. As described above, Ar metastables play an important role in the generation of O atoms. When N_2 gas is injected directly into the Ar stream, the N_2 molecules quench the Ar metastables to a large extent. Consequently, this leads to a decrease in the generation of O atoms.

Changes in emission intensities of excited Ar atoms at 696 nm, N_2 ($C^3\prod_u$ — $B^3\prod_g$) at 357 nm, and excited O atoms at 777 nm with the increasing concentration of O_2 gas are shown in Fig. 3-17 (a), (b), and (c), respectively. From Fig. 3-17 (a), it is seen that the emission intensities of excited Ar atoms decreased only slightly after the addition of O_2 gas. When O_2 gas was added to the plasma afterglow zone through a glass capillary, no significant quenching effect was observed. It is because that electrons and ions are not present in the plasma afterglow zone. From Fig. 3-17 (b), it is seen that the emission intensities of N_2 ($C^3\prod_u$ — $B^3\prod_g$) were scarcely affected with the concentration of added O_2 gas. As discussed above, N_2 ($C^3\prod_u$ — $B^3\prod_g$) is mainly generated through a resonant reaction between Ar metastables and ground-state molecular N_2. However, the concentration of Ar

metastables scarcely changed when O_2 gas was added to the plasma afterglow zone through a glass capillary, since the Ar metastables are generated through collisions with energetic electrons in the electric field (discharge region). This can be used to explain why the emission intensities of N_2 ($C^3\prod_u$ — $B^3\prod_g$) were scarcely affected with the increasing concentration of added O_2 gas. From Fig. 3-17 (c), it is seen that the emission intensity of O atoms decreased with the increasing concentration of added O_2 gas. We have to note that when O_2 gas was added to the plasma afterglow zone, the emission intensities of both excited Ar atoms and O atoms decreased (see Fig. 3-17 (a) and (c)). This suggests that a new active species is probably created. We presume that newly generated O atoms were quickly transformed to O_3 through combination with the added O_2 molecules; this presumption is based on the fact that we identified a much stronger ozone smell during the experiment. This helps explain why the number of O atoms decreased with the increasing concentration of added O_2. In the future, we intend to measure the density of ozone quantitatively by using absorption spectroscopy.

On the other hand, we investigated the decay of active species at the axial direction of the plasma jet. Changes in emission intensities of excited Ar atoms at 696 nm, N_2 ($C^3\prod_u$ — $B^3\prod_g$) at 357 nm, and excited O atoms at 777 nm in Ar, Ar/N_2, and Ar/O_2 plasmas at different axial positions are shown in Fig. 3-18 (a), (b), and (c), respectively. From Fig. 3-18 (a), it is seen that the emission intensities of excited Ar atoms in Ar and Ar/O_2 plasmas decreased gradually along the axial direction. The tendency of excited Ar atoms to decay in Ar/O_2 plasma is almost the same as that in Ar plasma. This suggests that the decay of excited Ar atoms along the axial direction is mainly due to the collisions with molecules in the atmosphere. However, their emission intensities scarcely changed with differing axial positions in Ar/N_2 plasma. From Fig. 3-18 (b), it is seen that after N_2 gas was injected, the emission intensities of N_2 ($C^3\prod_u$ — $B^3\prod_g$) increased at positions close to the exit of the

plasma jet and decayed more quickly along the axial direction. As mentioned above, most Ar metastables are quenched by N_2 molecules and N_2 ($C^3\prod_u$ — $B^3\prod_g$) become the main energy carrier after the injection of N_2 gas. Therefore, in this case, N_2 ($C^3\prod_u$ — $B^3\prod_g$) decayed more quickly through collisions with molecules in the atmosphere. On the other hand, in Ar and Ar/O_2 plasmas, the emission intensities of N_2 ($C^3\prod_u$ — $B^3\prod_g$) decayed slightly along the axial direction. From Fig. 3-18 (c), it is seen that the emission intensity of excited O atoms scarcely decayed along the axial direction. It suggests that the concentration of O atoms in the plasma jet scarcely changed along the axial direction.

3.2.6 Effect of connection mode on OES

Comparison of optical emission spectra of CAPPLAT Ar plasma jets with different connection modes is shown in Fig. 3-19. It can be seen that comparing to the normal connection mode the plasma radiation became quite weak with the reverse connection mode, although the nominal applied voltage is identical in these two cases. As we discussed in section 3.1.6, for the normal and the reverse connection modes, the distributions of the electric field strength inside the plasma torch are quite different from each other. It was found that the discharge current decreased dramatically with the reverse connection mode, suggesting that the energy transfer to the Ar gas is quite low in this case. On the other hand, as we well known, the generation of active species is mainly controlled by the properties of the discharge, namely by the reduced local electric field strength and electron density. This can probably be used to explain why the plasma radiation is quite weak with the reverse connection mode.

4 Conclusions

We have developed a surface discharge plasma device (CAPPLAT) that is able to generate a

non-equilibrium atmospheric pressure Ar plasma jet. An Ar/N_2 plasma jet was successfully generated by injecting N_2 gas directly into the Ar stream. However, no plasma jet was generated when the O_2 gas was added by such direct injection, because of the considerable quenching effect of O_2. Therefore, we developed a new injection method by which we added O_2 gas to the plasma afterglow zone through a glass capillary. Through this new injection method, we also successfully obtained an Ar/O_2 plasma jet.

In this study, the electrical and optical properties of CAPPLAT Ar plasma jet were characterized. In particular, the effects of dielectric thickness, torch diameter, Ar flow rate and additive gas (N_2 or O_2) on these properties were investigated in detail. First, a simple equivalent R-C parallel circuit model was employed to evaluate the discharge characteristics of CAPPLAT Ar plasma jet. Using this equivalent circuit, the discharge current was roughly calculated from the total current and the capacitive current. According to the observed waveforms of the applied voltage and the discharge current, it was concluded that the discharge of CAPPLAT Ar plasma jet was a glow-like discharge. The electrical properties scarcely changed with the injection of the additive gas either directly into the Ar stream or into the plasma afterglow zone through a glass capillary. On the basis of this observation, a simple discharge mechanism was proposed. According to this mechanism, in the first step, Ar molecules are excited and ionized through collisions with energetic electrons. In this step, energy is transferred to the Ar particles, and Ar metastable atoms are generated. In the second step, Ar metastable atoms, the main energy carriers, are used to generate N_2 ($C^3\prod_u$) and O atoms through collisions with N_2 or O_2 molecules. Additionally, it was found that the glow-like discharge scarcely changed with the change in dielectric thickness, torch diameter, and Ar flow rate.

OES characterization revealed that Ar active species belonging to excited Ar atoms (4p-4s

transition) were predominant in the CAPPLAT Ar plasma jet (in the wavelength range of 690–950 nm). Peaks belonging to the N_2 second positive system (N_2 ($C^3\prod_u$ — $B^3\prod_g$)) were also observed. N_2 ($C^3\prod_u$ — $B^3\prod_g$) (E ≈ 11.1 eV) were generated through a resonant reaction between Ar metastables (E ≈ 11.5 eV) and ground-state molecular N_2. However, peaks belonging to the N_2 first negative system ((N_2^+ ($B^2\Sigma^+_u$ — $X^2\Sigma^+_g$)) (E ≈ 18.7 eV) were not detected, since the excitation energy was insufficient. Additionally, an O atom peak was detected at 777 nm, with rather weak emission intensity. A small quantity of O atoms was generated through collisions between the excited Ar atoms and molecular O_2. The plasma radiation was strongly modified when N_2 gas was injected directly into the Ar stream. In this case, Ar metastables were highly quenched. This resulted in a marked decrease in the emission intensities of excited Ar and O atoms. Additionally, after the injection of N_2 gas, N_2 ($C^3\prod_u$) became the main energy carrier, since most of Ar metastables were quenched by the N_2 molecules. When O_2 gas was added to the plasma afterglow zone through a glass capillary, no significant quenching effect was observed, since electrons and ions are not present in the afterglow zone. In this case, the emission intensities of excited Ar atoms decreased only slightly. Interestingly, the emission intensity of excited O atoms decreased with increasing concentration of added O_2. We presumed that the newly generated O atoms were quickly transformed to O_3 through combination with the added O_2 molecules.

Finally, we attempted the reverse connection mode with CAPPLAT plasma device. It was found that both the electrical and the optical properties of the plasma jet changed significantly with the reverse connection mode. With reverse connection mode the discharge current became very low, although a higher applied voltage was employed. On the other hand, the plasma radiation is quite weak with reverse connection mode. We assumed that the distribution of the electric field strength

inside the plasma torch is quite different from the normal connection mode. It was presumed that the electric field strength and the energy density reduce from the high-voltage electrode to the ground electrode. Therefore, with the reverse connection mode (in this case, the inner electrode is grounded), the electric field strength and the energy density are quite weak inside the plasma torch. It resulted in a very low discharge current and rather weak plasma radiation.

References

[1] S. Yang, H. Yin, Plasma Chem. Plasma Process. 2007, 27, 23.

[2] R. B. Gadri, J. R. Roth, T. C. Montie, K. K. Wintenberg, P. P. Y. Tsai, D. J. Helfritch, P. Feldman, D. M. Sherman, F. Karakaya, Z. Chen, Surf. Coat. Technol. 2000, 131, 528.

[3] S. Martin, F. Massines, N. Gherardi, C. Jimenez, Surf. Coat. Technol. 2004, 177-178, 693.

[4] M. Walker, K. M. Baumgărtner, J. Feichtinger, M. Kaiser, A. Schulz, E. Răuchle, Vacuum 2000, 57, 387.

[5] M. F. Dubreuil, E. M. Bongaers, Surf. Coat. Technol. 2008, 202, 5036.

[6] J. Park, I. Henins, H. W. Herrmann, G. S. Selwyn, J. Appl. Phys. 2001, 89, 20.

[7] M. Laroussi, T. Akan, Plasma Process. Polym. 2007, 4, 777.

[8] Y. H. Kim, Y. H. Choi, J. K. Park, W. T. Ju, K. H. Paek, Y. S. Hwang, Surf. Coat. Technol. 2006, 174-175, 535.

[9] L. Xu, P. Liu, R. J. Zhan, X. H. Wen, L. L. Ding, M. Nagatsu, Thin Solid Films 2006, 506, 400.

[10] J. Zhang, J. Sun, D. Wang, X. Wang, Thin Solid Films 2006, 506, 404.

[11] Y. Tanaka, S. Iizuka, Thin Solid Films 2006, 506, 436.

[12] C. Cheng, L. Zhang, R. J. Zhan, Surf. Coat. Technol. 2006, 200, 6659.

[13] F. Massines, P. Ségur, N. Gherardi, C. Khamphan, A. Ricard, Surf. Coat. Technol. 2003, 174-175, 8.

[14] http://www.cresur.com

[15] A. Kuwabara, S. Kuroda, H. Kubota, Plasma Sources Sci. Technol. 2006, 15, 328.

[16] T. P. Kasih, S. Kuroda, H. Kubota, Chem. Vap. Depos. 2007, 13, 1.

[17] A. Kuwabara, S. Kuroda, H. Kubota, Plasma Sci. Technol. 2007, 9, 181.

[18] A. Kuwabara, S. Kuroda, H. Kubota, Plasma Chem. Plasma Process. 2008, 28, 263.

[19] J. Laimer, H. Stŏri, Plasma Process. Polym. 2006, 3, 573.

[20] J. Laimer, H. Stŏri, Plasma Process. Polym. 2007, 4, 266.

[21] H. P. Li, W. T. Sun, H. B. Wang, G. Li, C. Y. Bao, Plasma Chem. Plasma Process. 2007, 27, 529.

[22] H. E. Wagner, R. Brandenburg, K. V. Kozlov, A. Sonnenfeld, P. Michel, J. F. Behnke, Vacuum 2003, 71, 417.

[23] F. Massines, A. Rabehi, P. Decomps, R. B. Gadri, P. Segur, C. Mayoux, J. Appl. Phys. 1998, 83, 2950.

[24] P. Segur, F. Massines, Proceedings of the International Conference on Gas Discharges and Their Applications, Glasgow (UK), 2000, 15.

[25] Y. B. Golubovskii, V. A. Maiorov, J. Behnke, J. F. Behnke, J. Phys. D: Appl. Phys. 2002, 35, 751.

[26] A. Ricard, P. Decomps, F. Massines. Surf. Coatings 1999, 112, 1.

[27] Q. S. Yu, H. K. Yasuda, Plasma Chem. Plasma Process. 1998, 18, 461.

[28] M.C. García, M. Varo, P. Martínez, Plasma Chem. Plasma Process. 2010, 30, 241.

[29] A. F. Bublievskii, A. A. Galinovskii, A. V. Gorbunov, S. A. Zhdanok, V. A. Koval, L. I.

Sharakhovskii, G. V. Dolgolenko, D. S. Skomorokhov, J. Eng. Phys. Thermophys. 2006, 79, 629.

[30] V. Poenariu, M. R. Wertheimer, R. Bartnikas, Plasma Process. Polym. 2006, 3, 17.

[31] V. Nemchinsky, J. Phys. D: Appl. Phys. 2005, 38, 3825.

[32] V. Léveillé, S. Coulombe, Plasma Process. Polym. 2006, 3, 587.

[33] C. Lee, D. B. Graves, M. N. Lieberman, D. W. Hess, J. Electrochem. Soc. 1994, 141, 1546.

[34] B. Eliasson, U. Kogelschatz, ‘‘Basic Data for Modeling of Electrical Discharge in Gases: Oxygen’’, Research, Asea Brown Boveri Corporate, KLR-11C CH5405, 1986.

[35] D. Lee, J. Park, S. H. Hong,Y. Kim, IEEE Trans. Plasma Sci. 2005, 33, 949.

[36] K. Niemi, V. Schulz von der Gathen, H. F. Dŏbele, Plasma Sources Sci. Technol 2005, 14, 375.

Tab. 3-1 Summary of active species (wavelength range of 350–950 nm) detected in CAPPLAT Ar plasma jet at a distance of 5 mm from the end of torch. Discharge conditions: pure Ar discharge at a flow rate of 10 SLM, dielectric thickness of 2 mm, nominal applied voltage of 16.0 kV (peak to peak) with 50% duty cycle, discharge frequency of 20 kHz.

Species	**λ** (nm)	**Absolute irradiance** ($\mu W/cm^2/nm$)	**Transition**
N_2 2^{nd} positive system	357.52	0.0513	$C^3\prod_u \rightarrow B^3\prod_g$
	380.27	0.0191	
	405.79	0.0065	
Ar atoms	696.53	0.0836	4p → 4s
	707.60	0.0049	
	728.03	0.0239	
	739.22	0.0124	
	751.67	0.0484	
	764.06	0.2036	
	773.03	0.1764	
	795.47	0.0295	
	801.91	0.0489	
	812.00	0.1031	
	827.13	0.1889	
	842.87	0.0709	
	852.57	0.0192	
	867.57	0.0021	
	912.68	0.2654	
	922.70	0.0351	
O atoms	777.87	0.0032	3p → 3s

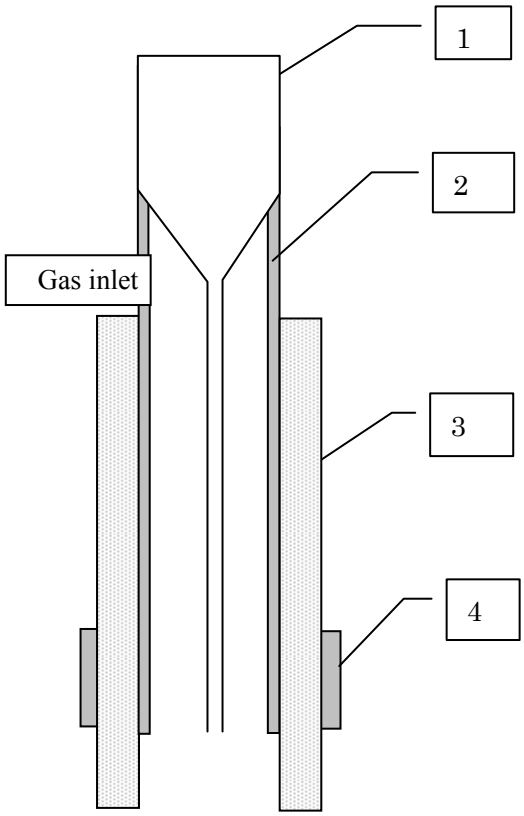

(a)

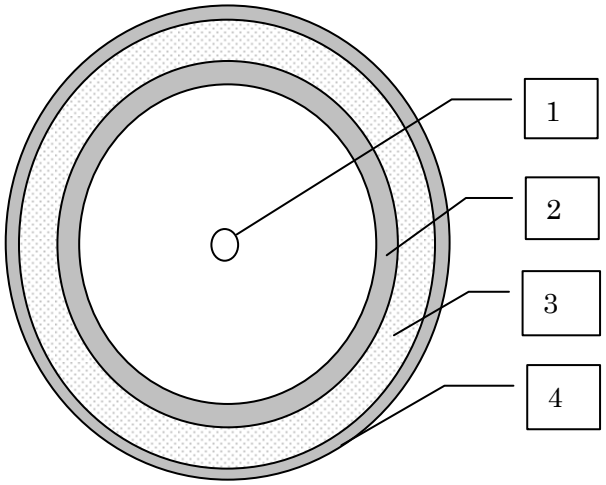

(b)

Fig. 3-1 Schematic illustration of CAPPLAT plasma torch. (a): front view; (b): top view. 1: glass capillary; 2: inner electrode; 3: dielectric; 4: outer electrode.

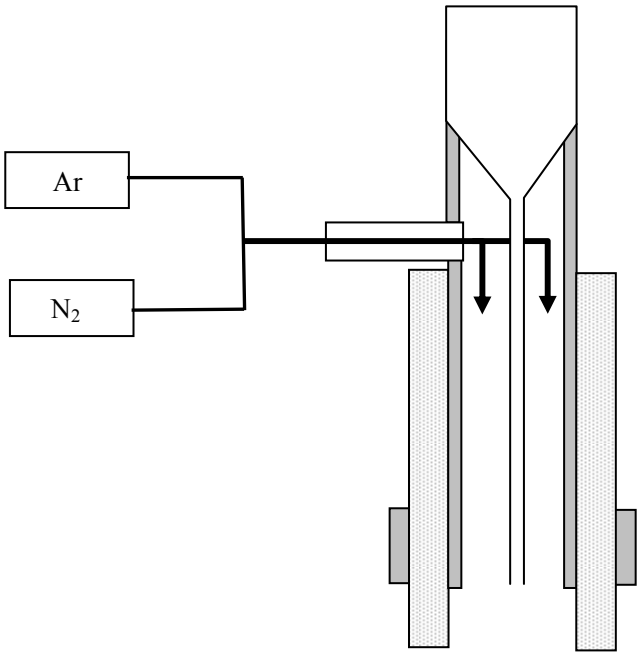

(a)

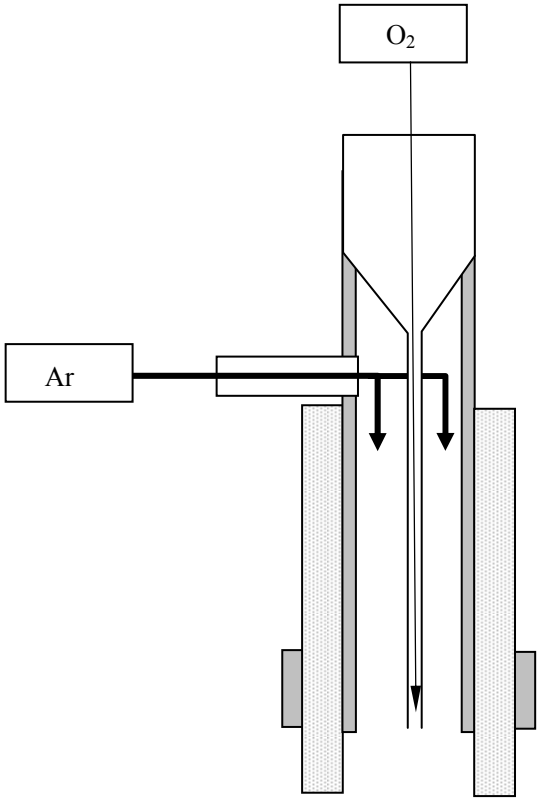

(b)

Fig. 3-2 Schematic of addition process of additive gas. (a): N_2 addition; (b): O_2 addition.

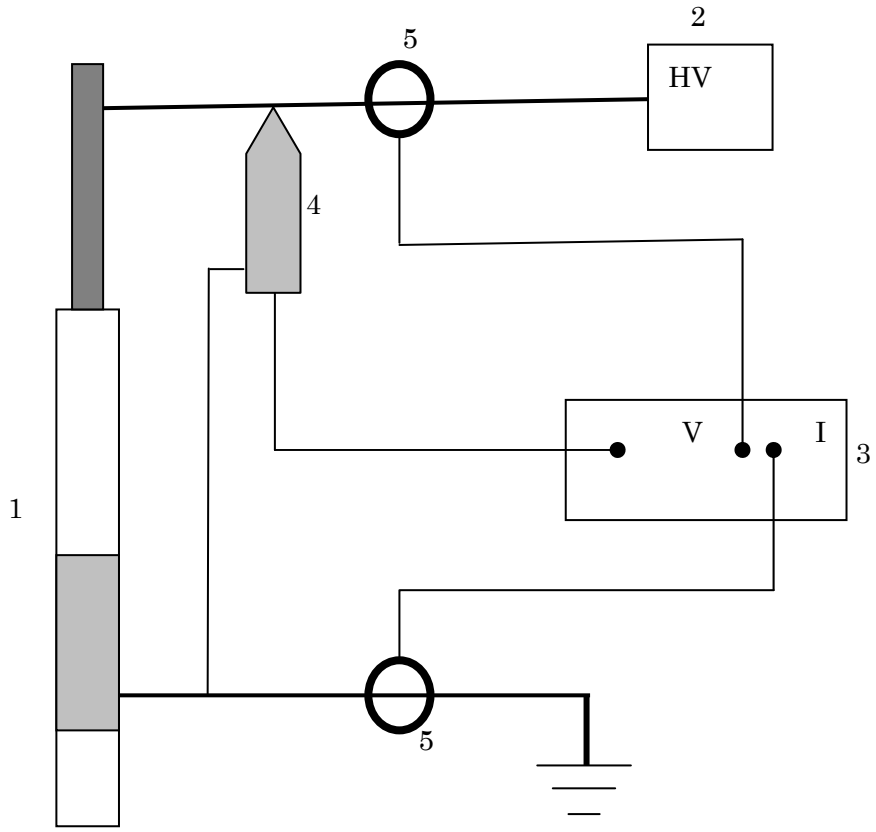

Fig. 3-3 Electrical measurement setup for CAPPLAT Ar plasma jet. 1: CAPPLAT plasma torch; 2: High-voltage pulsed power source; 3: Oscilloscope; 4: High-voltage probe; 5: Current probe.

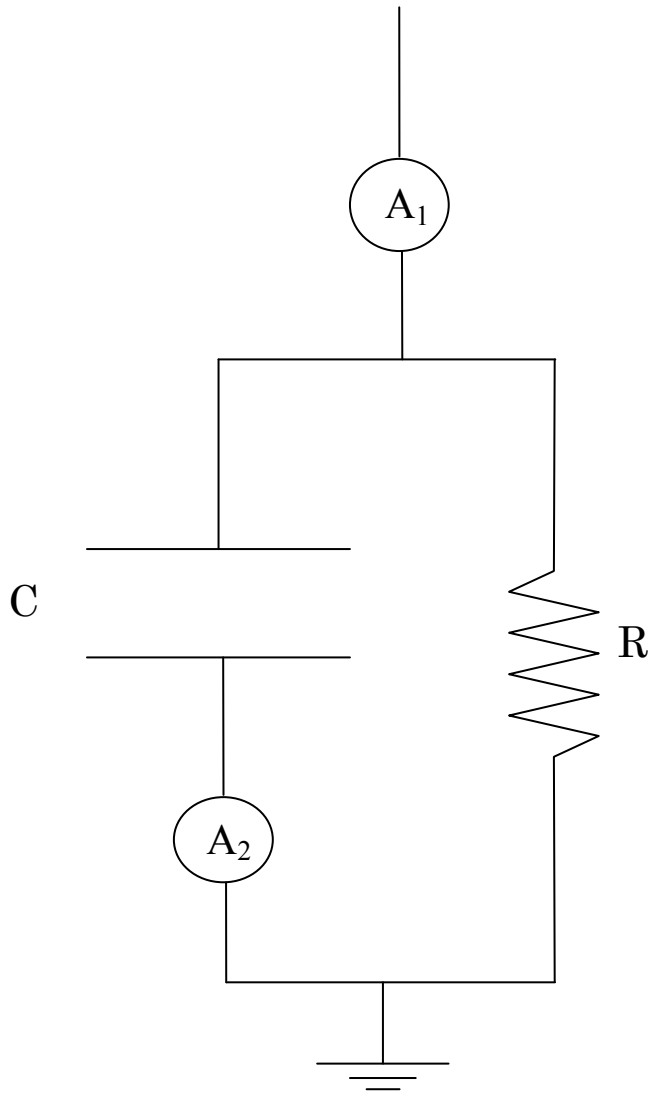

Fig. 3-4 Schematic of equivalent circuit model for CAPPLAT Ar plasma jet.

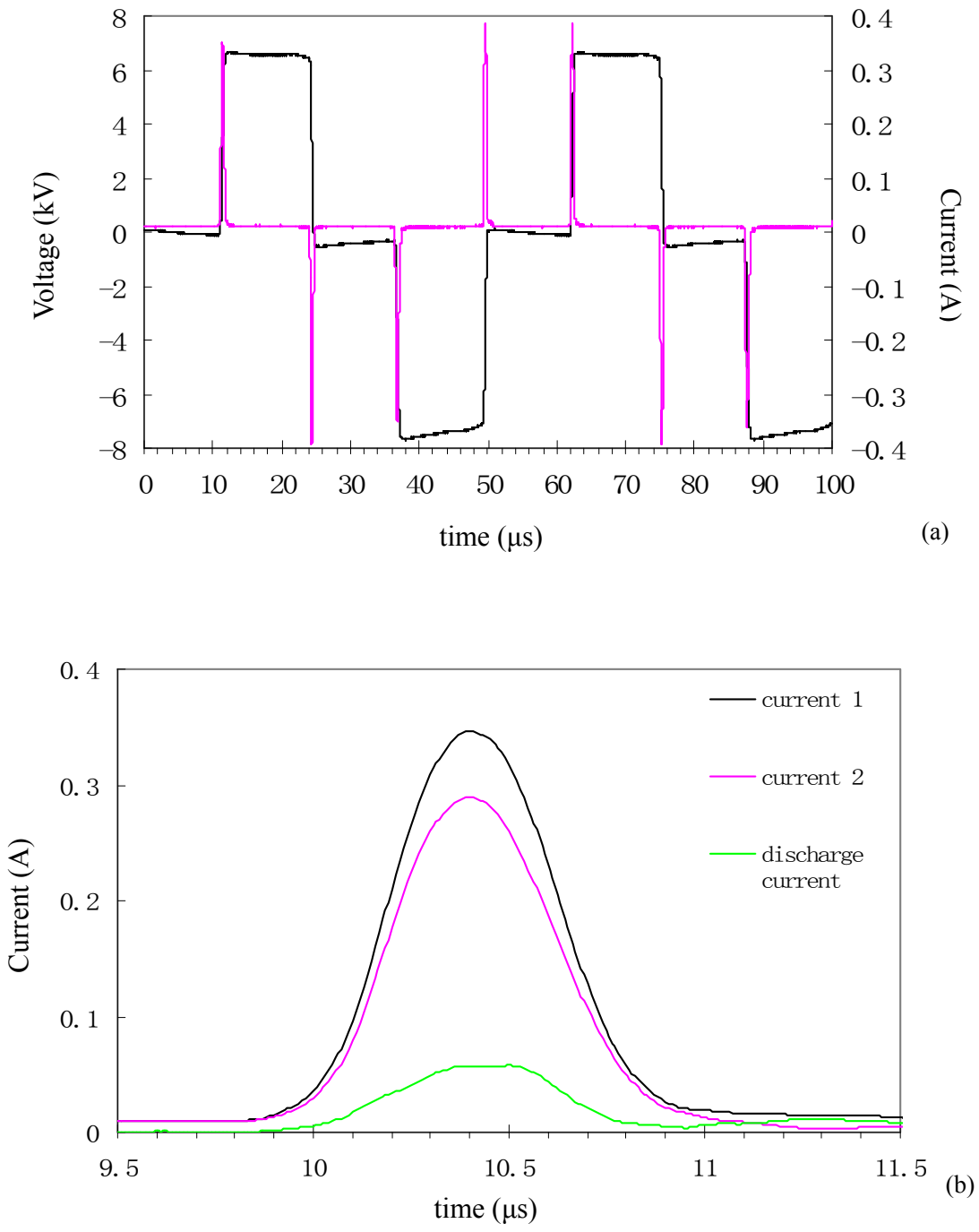

Fig. 3-5 (a): Typical waveforms of applied voltage (black line) and total current (red line); (b): Waveforms of total current (current 1), capacitive current (current 2), and discharge current during polarity change. Discharge conditions: pure Ar discharge at a flow rate of 10 SLPM, dielectric thickness of 2 mm, nominal applied voltage of 16.0 kV (peak to peak) with 50% duty cycle, discharge frequency of 20 kHz.

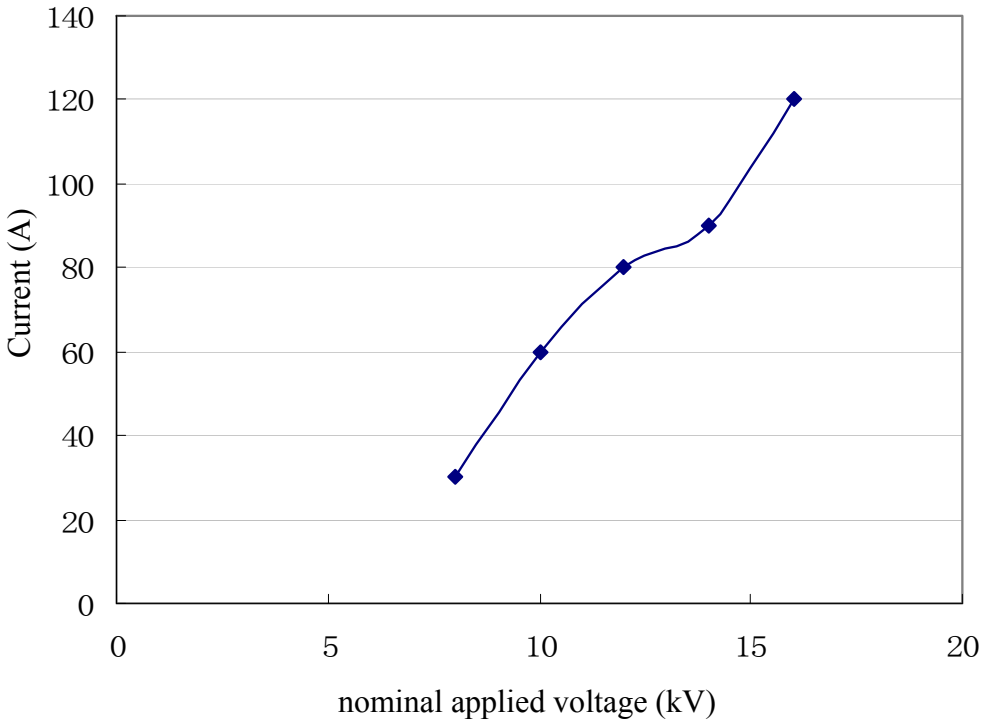

Fig. 3-6 Dependence of discharge current on nominal applied voltage. Note: discharge currents were calculated using the equivalent circuit model. Peak to peak values of discharge current and nominal applied voltage are given in the figure. Discharge conditions: pure Ar discharge at a flow rate of 10 SLPM, dielectric thickness of 2 mm, with 50% duty cycle, discharge frequency of 20 kHz.

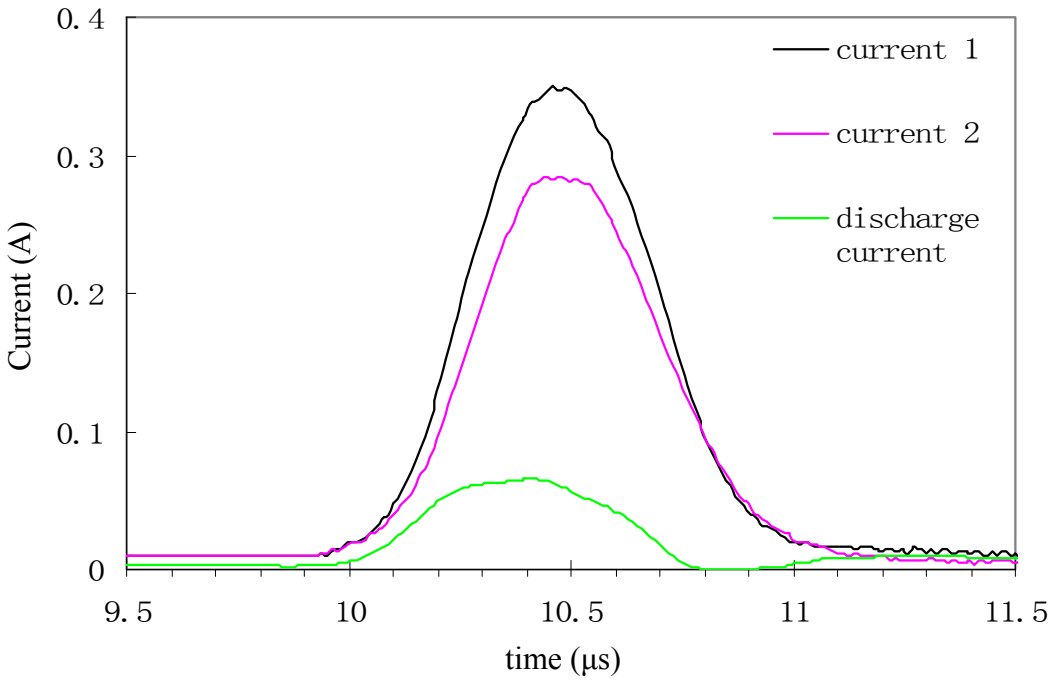

Fig. 3-7 Waveforms of total current (current 1), capacitive current (current 2), and discharge current during polarity change. Discharge conditions: pure Ar discharge at a flow rate of 5 SLPM, dielectric thickness of 2 mm, nominal applied voltage of 16.0 kV (peak to peak) with 50% duty cycle, discharge frequency of 20 kHz.

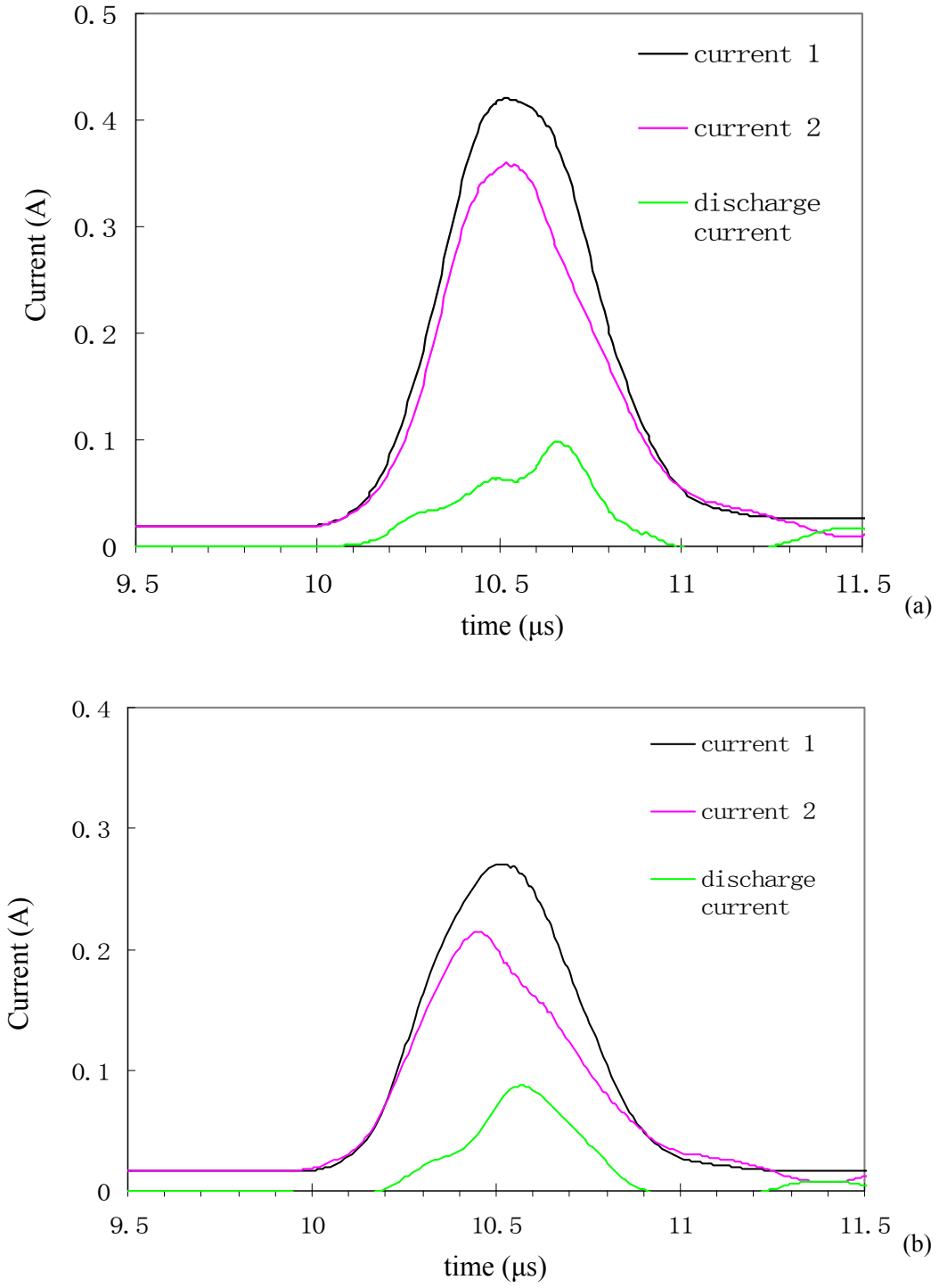

Fig. 3-8 Comparison of waveforms of total current (current 1), capacitive current (current 2), and discharge current during polarity change with different dielectric thicknesses. (a): thickness of 1 mm; (b): thickness of 5 mm. Discharge conditions: pure Ar discharge at a flow rate of 10 SLPM, nominal applied voltage of 16.0 kV (peak to peak) with 50% duty cycle, discharge frequency of 20 kHz.

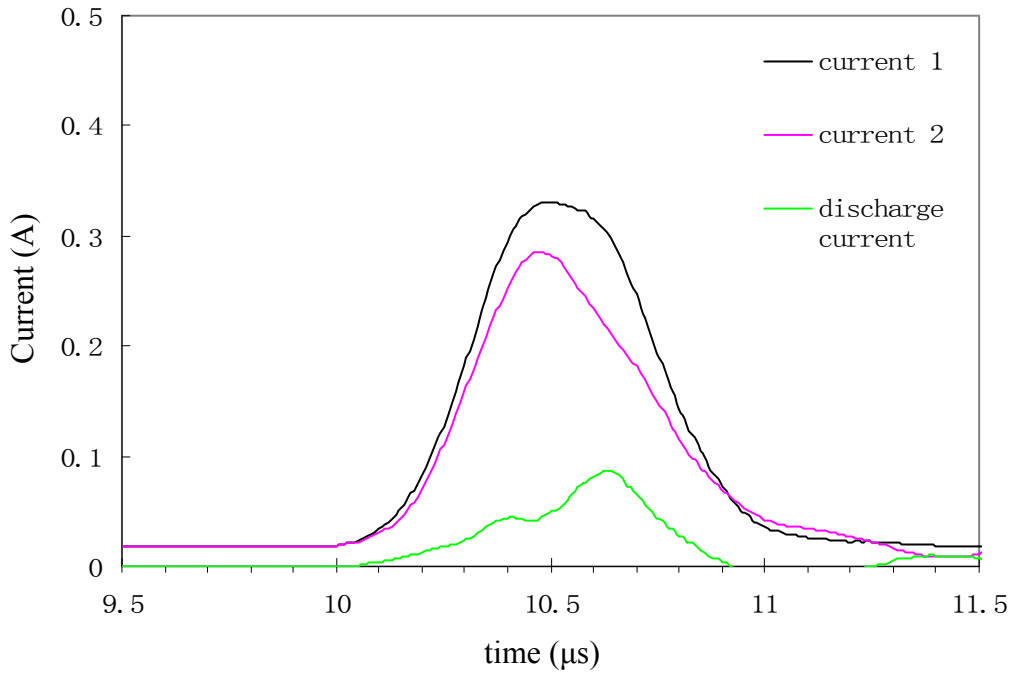

Fig. 3-9 Waveforms of total current (current 1), capacitive current (current 2), and discharge current during polarity change with mini-CAPPLAT plasma torch. Discharge conditions: pure Ar discharge at a flow rate of 10 SLPM, dielectric thickness of 1 mm, nominal applied voltage of 16.0 kV (peak to peak) with 50% duty cycle, discharge frequency of 20 kHz.

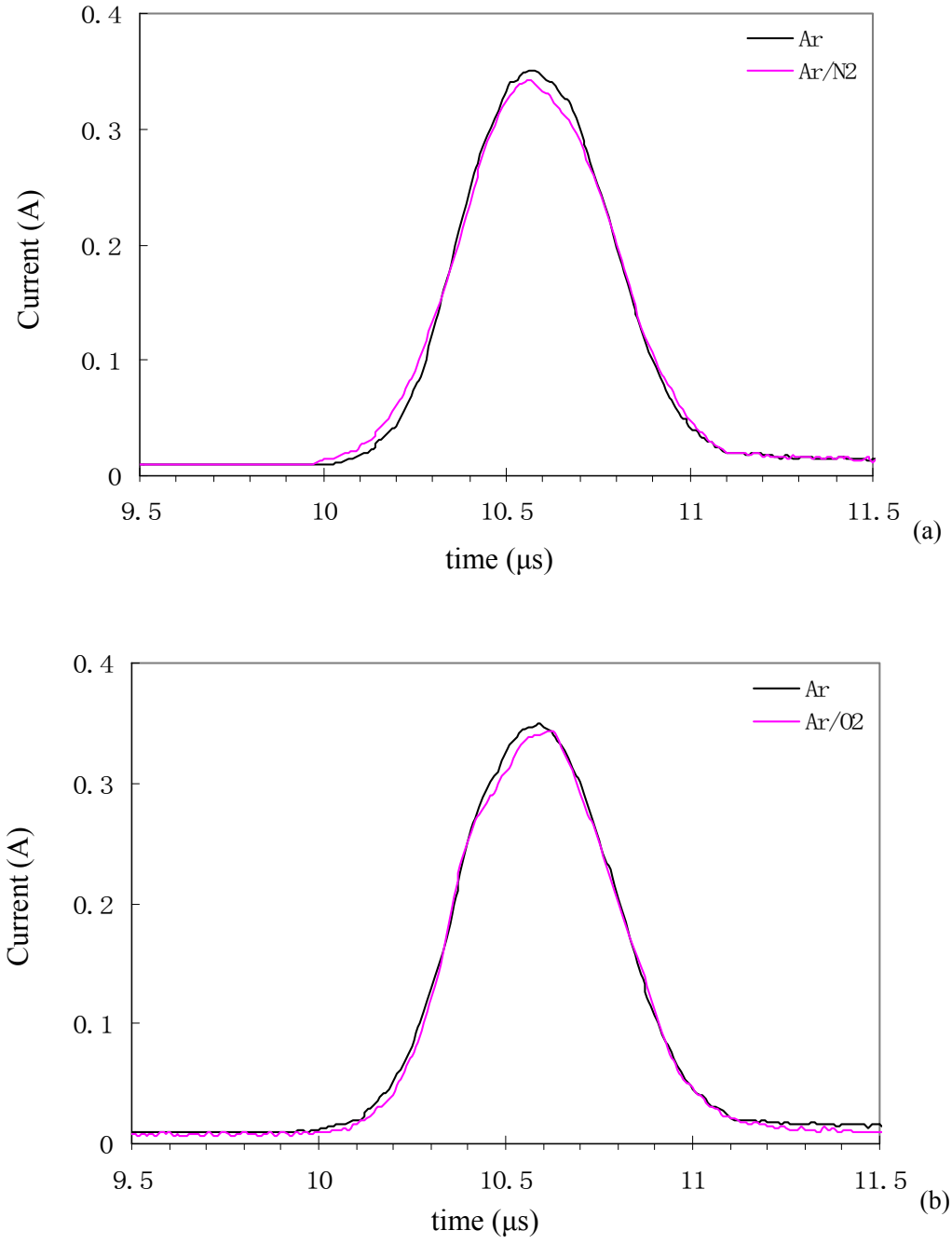

Fig. 3-10 (a): Comparison of waveforms of total current (current 1) in Ar discharge before and after N_2 injection during polarity change; (b): Comparison of waveforms of total current (current 1) in Ar discharge before and after O_2 addition during polarity change. Discharge conditions: Ar flow rate of 10 SLPM, additive gas (N_2 or O_2) flow rate of 0.5 SLPM, dielectric thickness of 2 mm, nominal applied voltage of 16.0 kV (peak to peak) with 50% duty cycle, discharge frequency of 20 kHz.

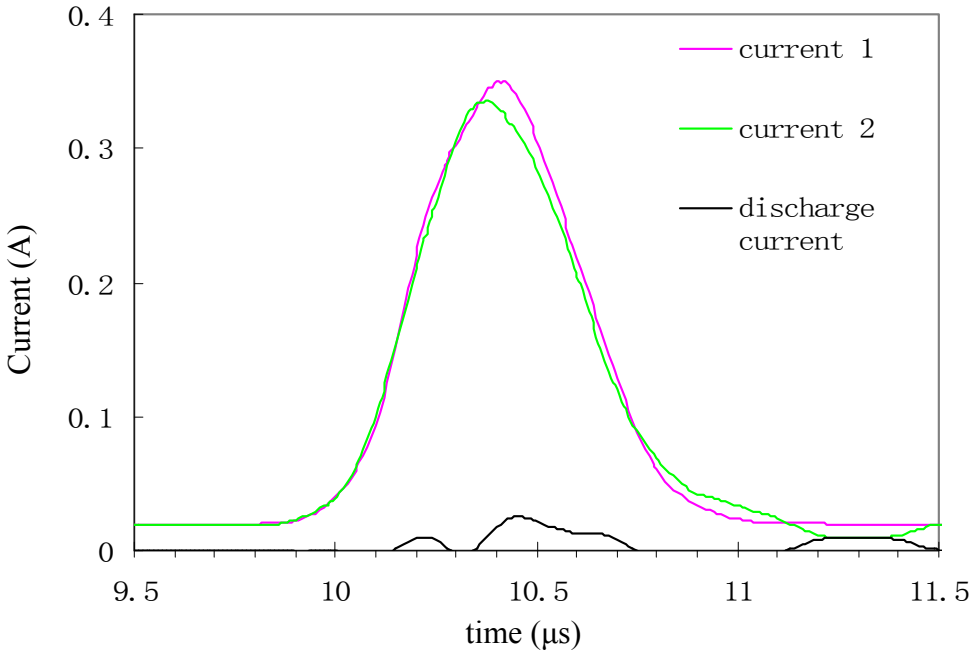

Fig. 3-11 Waveforms of total current (current 1), capacitive current (current 2), and discharge current during polarity change with reverse connection mode. Discharge conditions: pure Ar discharge at a flow rate of 10 SLPM, dielectric thickness of 2 mm, nominal applied voltage of 16.0 kV (peak to peak) with 50% duty cycle, discharge frequency of 20 kHz.

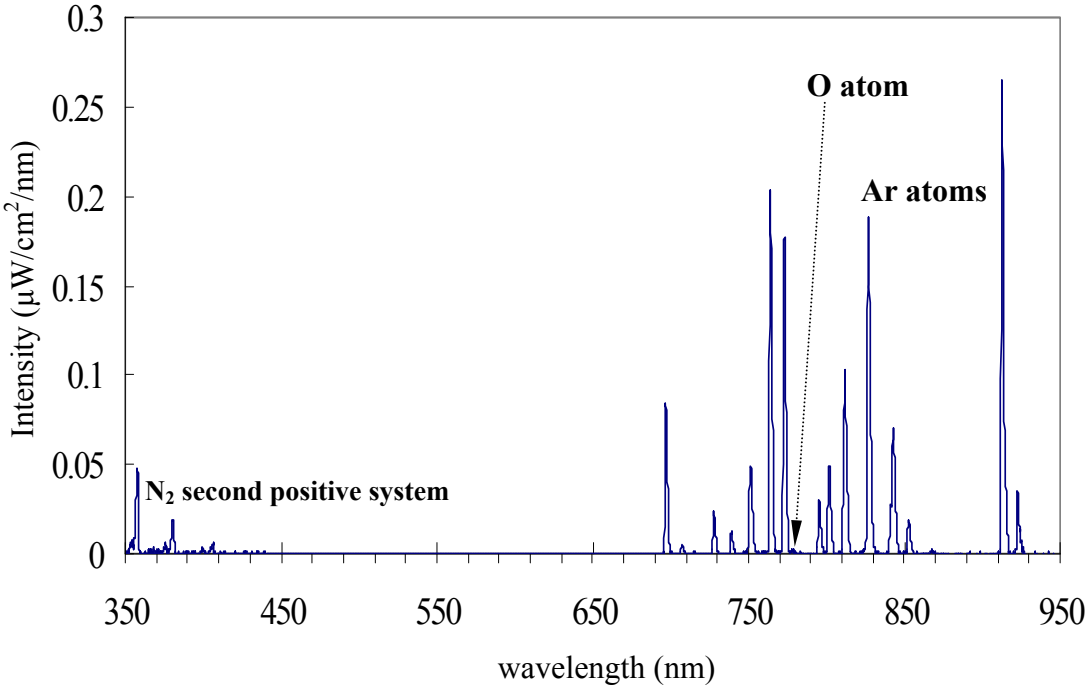

Fig. 3-12 Typical optical emission spectrum of CAPPLAT Ar plasma jet measured by USB4000 spectrometer at a distance of 5 mm from the end of torch. Discharge conditions: pure Ar discharge at a flow rate of 10 SLPM, dielectric thickness of 2 mm, nominal applied voltage of 16.0 kV (peak to peak) with 50% duty cycle, discharge frequency of 20 kHz.

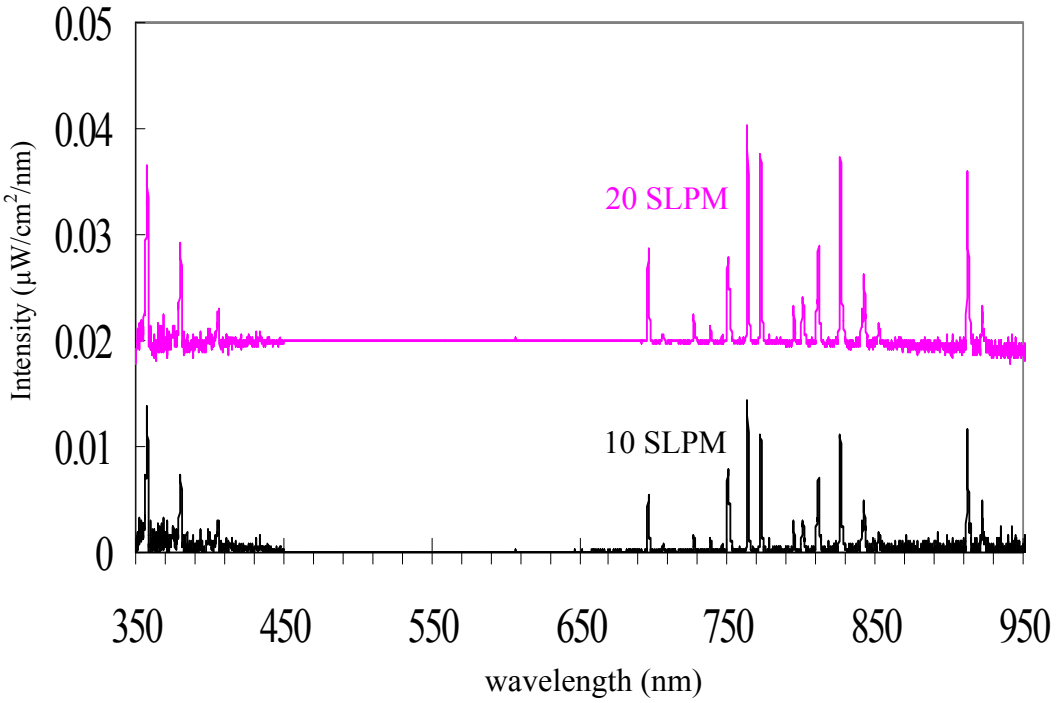

Fig. 3-13 Comparison of optical emission spectra of CAPPLAT Ar plasma jets at different Ar flow rates, measured by USB4000 spectrometer at a distance of 5 mm from the end of torch. Discharge conditions: pure Ar discharge, dielectric thickness of 2 mm, nominal applied voltage of 10.0 kV (peak to peak) with 50% duty cycle, discharge frequency of 20 kHz.

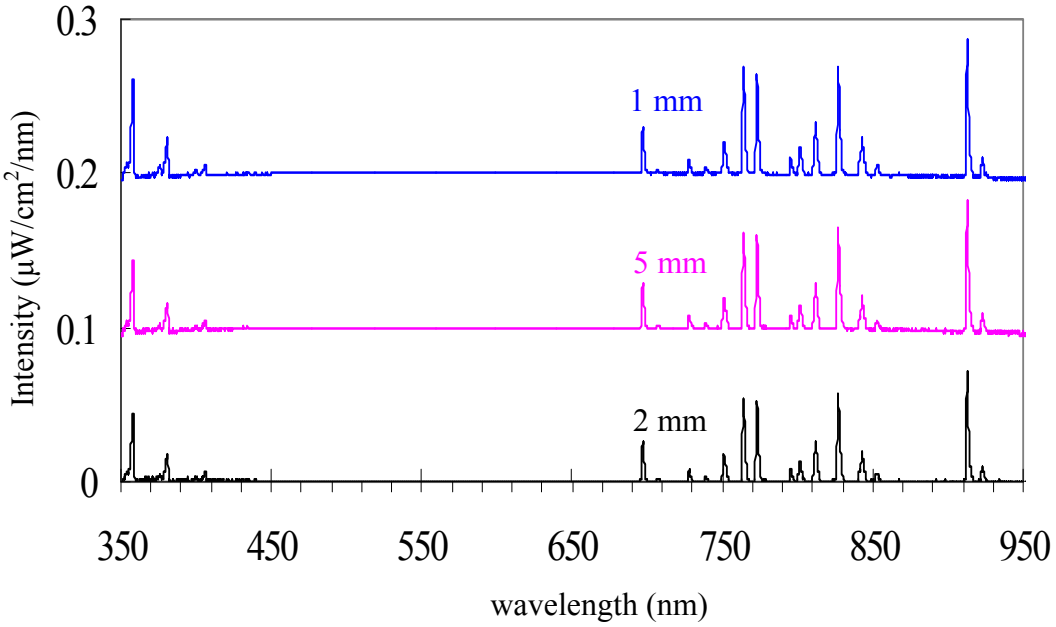

Fig. 3-14 Comparison of optical emission spectra of CAPPLAT Ar plasma jets with different dielectric thicknesses, measured by USB4000 spectrometer at a distance of 5 mm from the end of torch. Discharge conditions: pure Ar discharge at a flow rate of 10 SLPM, nominal applied voltage of 12.0 kV (peak to peak) with 50% duty cycle, discharge frequency of 20 kHz.

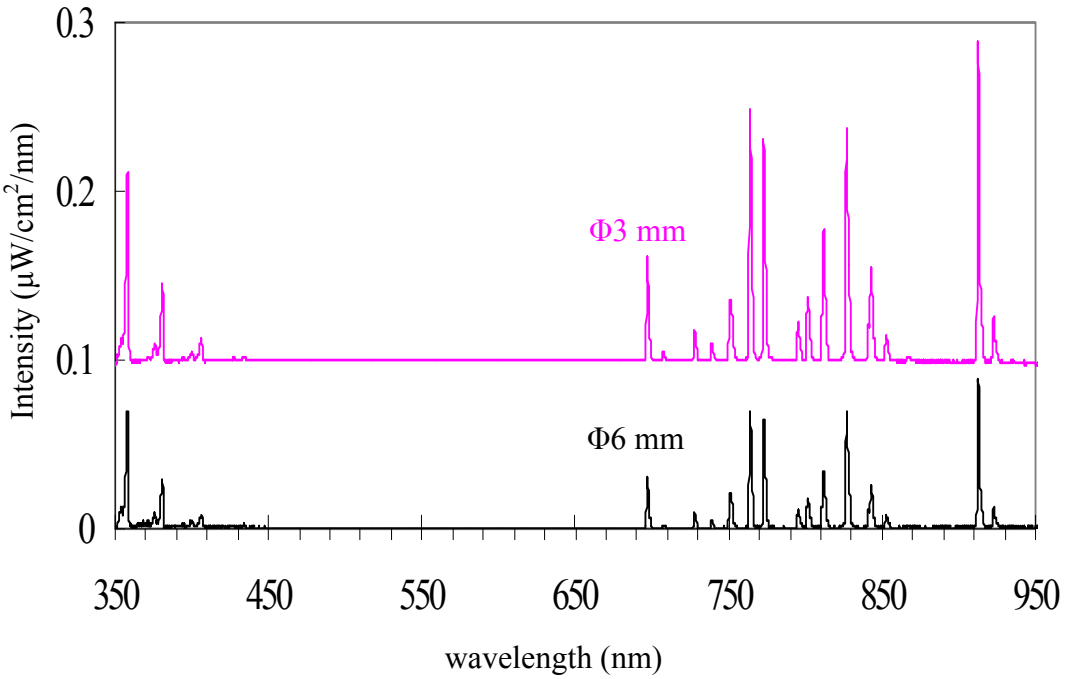

Fig. 3-15 Comparison of optical emission spectra of CAPPLAT Ar plasma jets with different torch inner diameters, measured by USB4000 spectrometer at a distance of 5 mm from the end of torch. Discharge conditions: pure Ar discharge at a flow rate of 10 SLPM, dielectric thickness of 1 mm, nominal applied voltage of 12.0 kV (peak to peak) with 50% duty cycle, discharge frequency of 20 kHz.

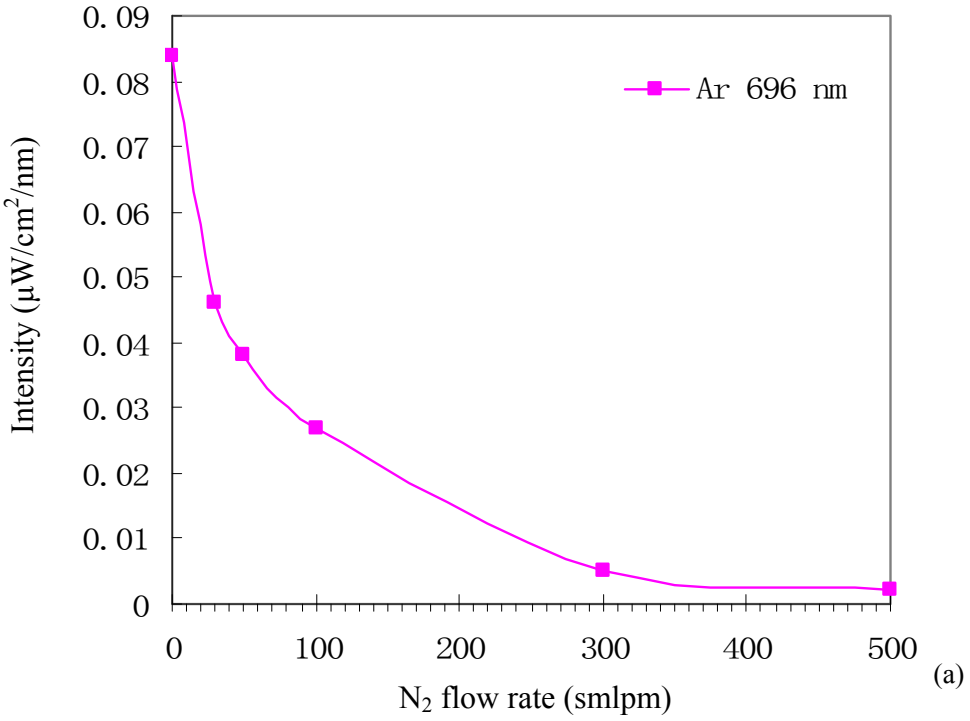
0. 09
0. 08
0. 07
0. 06
0. 05
0. 04
0. 03
0. 02
0. 01
0
Intensity (μW/cm²/nm)
Ar 696 nm
0
100
200
300
400
500
N₂ flow rate (smlpm)

(a)

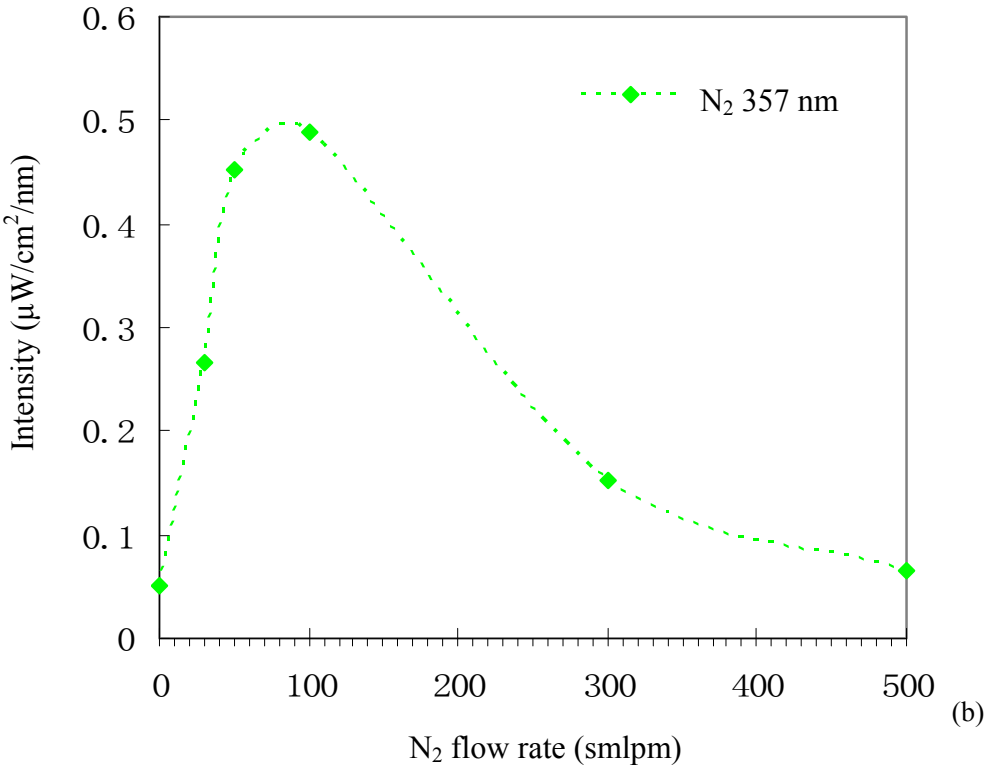
0. 6
0. 5
0. 4
0. 3
0. 2
0. 1
0
Intensity (μW/cm²/nm)
N₂ 357 nm
0
100
200
300
400
500
N₂ flow rate (smlpm)

(b)

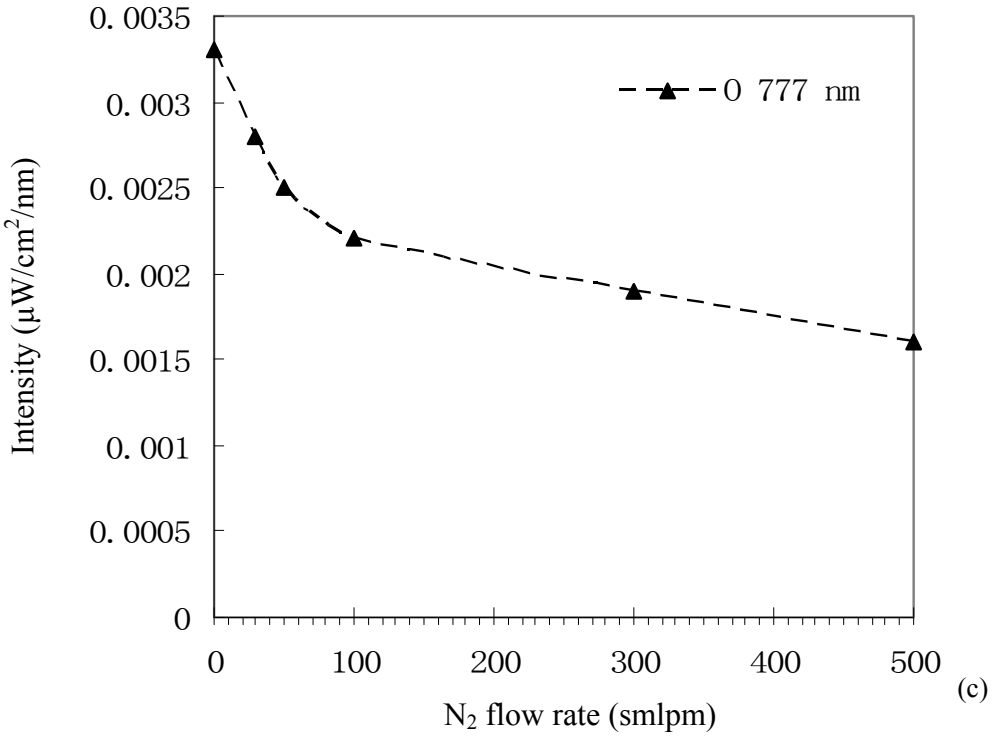

Fig. 3-16 Changes in emission intensities of excited Ar atoms at 696 nm (a), N_2 ($C^3\prod_u$ — $B^3\prod_g$) at 357 nm (b), and excited O atoms at 777 nm (c) with increasing concentration of N_2 additive gas at a distance of 5 mm from the end of the torch. Discharge conditions: Ar flow rate of 10 SLPM, dielectric thickness of 2 mm, nominal applied voltage of 16.0 kV (peak to peak) with 50% duty cycle, discharge frequency of 20 kHz. Note: excited Ar atoms at 696 nm and N_2 ($C^3\prod_u$ — $B^3\prod_g$) at 357 nm are selected as representatives for the excited Ar atoms and N_2 second positive system, respectively.

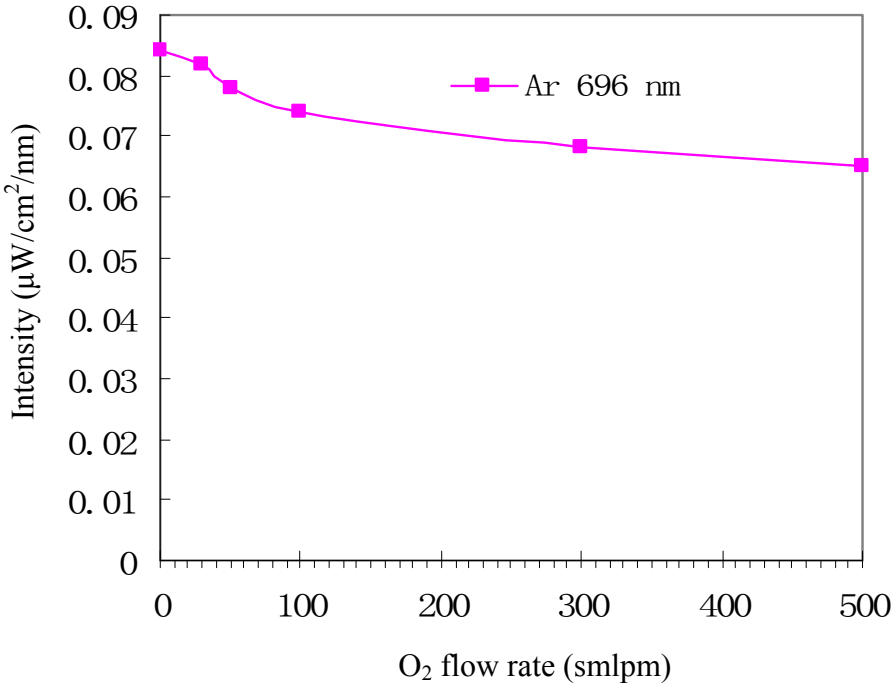
0. 09
0. 08
0. 07
0. 06
0. 05
0. 04
0. 03
0. 02
0. 01
0
Intensity (μW/cm²/nm)
Ar 696 nm
0
100
200
300
400
500
O₂ flow rate (smlpm)

(a)

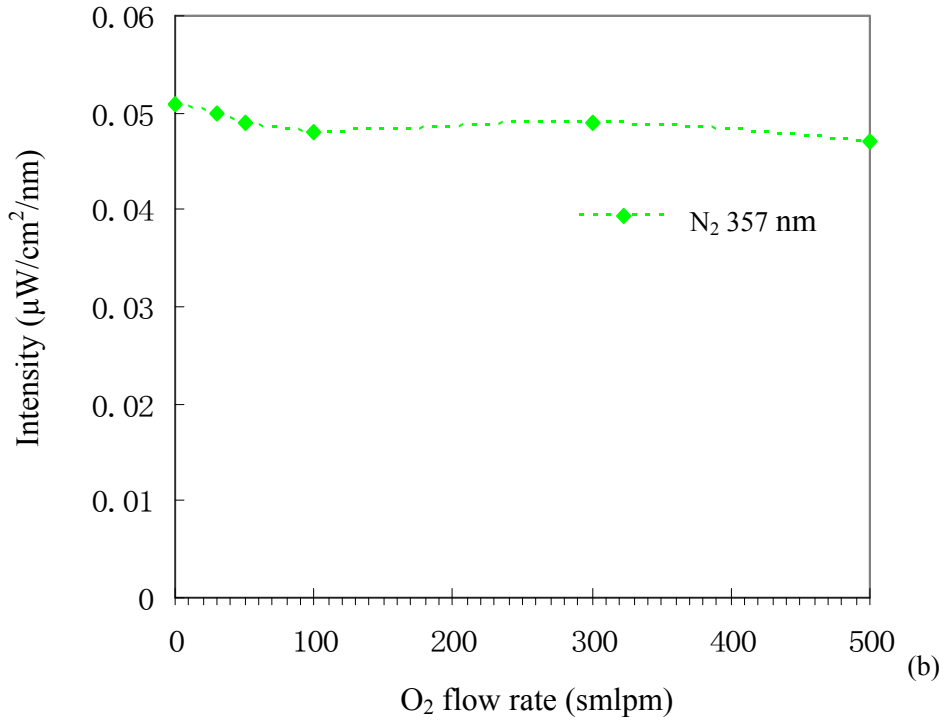
0. 06
0. 05
0. 04
0. 03
0. 02
0. 01
0
Intensity (μW/cm²/nm)
N₂ 357 nm
0
100
200
300
400
500
O₂ flow rate (smlpm)

(b)

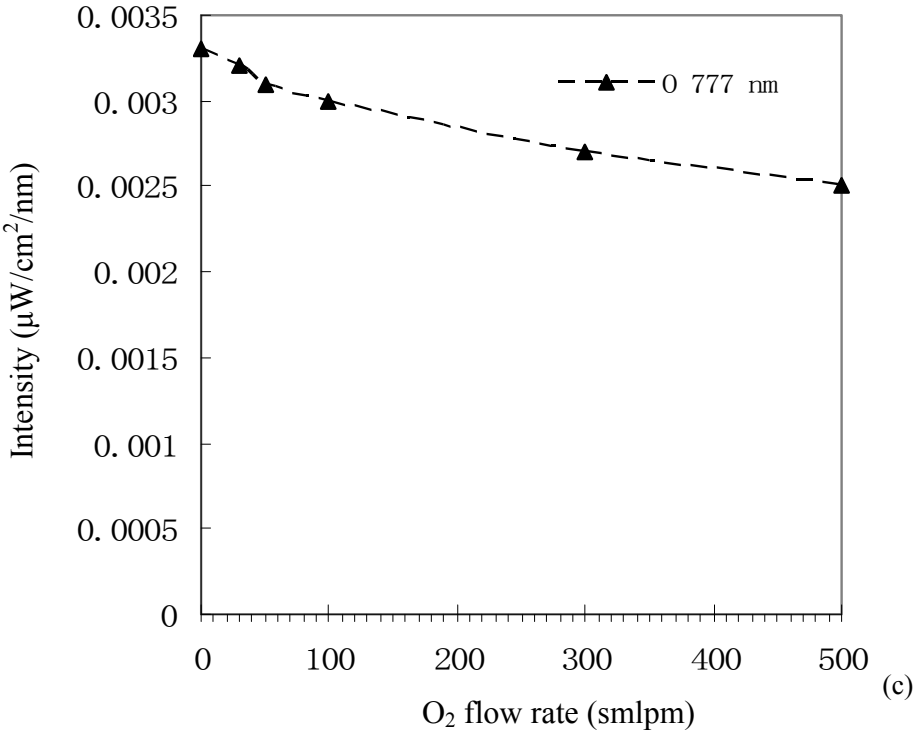

Fig. 3-17 Changes in emission intensities of excited Ar atoms at 696 nm (a), N_2 ($C^3\prod_u$ — $B^3\prod_g$) at 357 nm (b), and excited O atoms at 777 nm (c) with increasing concentration of O_2 additive gas at a distance of 5 mm from the end of the torch. Discharge conditions: Ar flow rate of 10 SLPM, dielectric thickness of 2 mm, nominal applied voltage of 16.0 kV (peak to peak) with 50% duty cycle, discharge frequency of 20 kHz. Note: excited Ar atoms at 696 nm and N_2 ($C^3\prod_u$ — $B^3\prod_g$) at 357 nm are selected as representatives for the excited Ar atoms and N_2 second positive system, respectively.

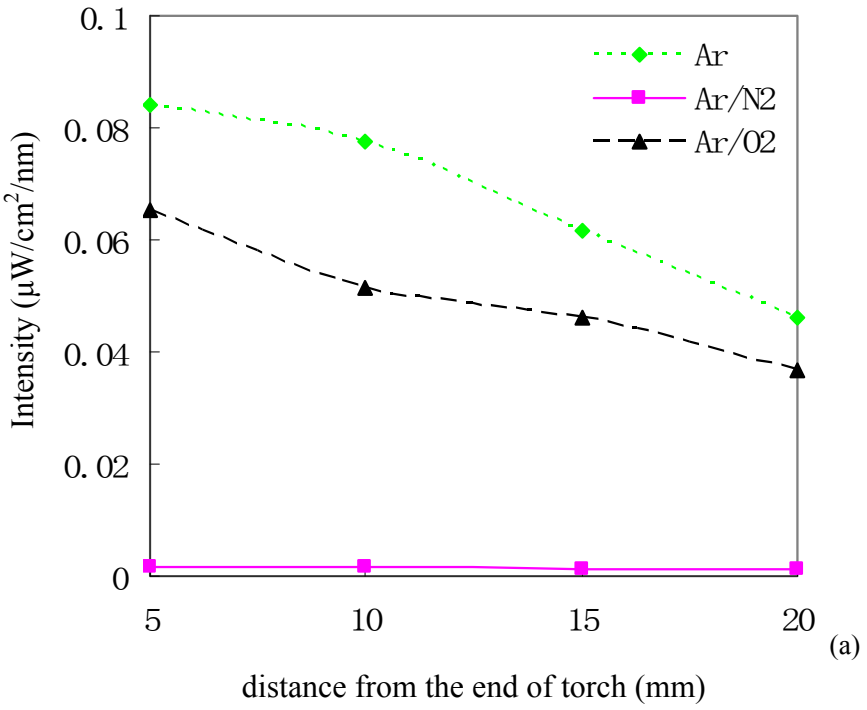
0. 1
0. 08
0. 06
0. 04
0. 02
0
Intensity (μW/cm²/nm)
Ar
Ar/N2
Ar/02
5
10
15
20
(a)
distance from the end of torch (mm)

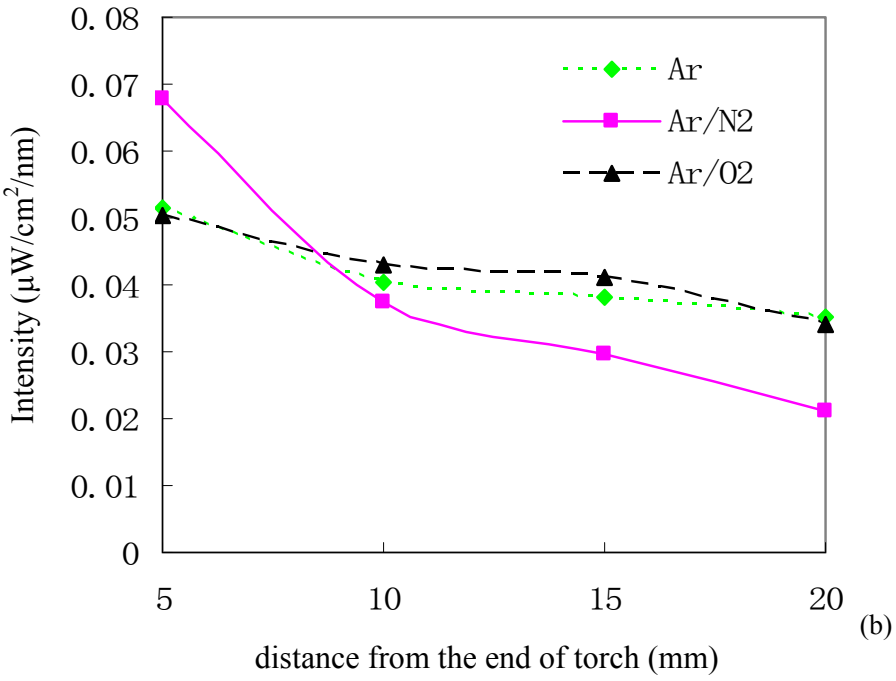
0. 08
0. 07
0. 06
0. 05
0. 04
0. 03
0. 02
0. 01
0
Intensity (μW/cm²/nm)
Ar
Ar/N2
Ar/02
5
10
15
20
(b)
distance from the end of torch (mm)

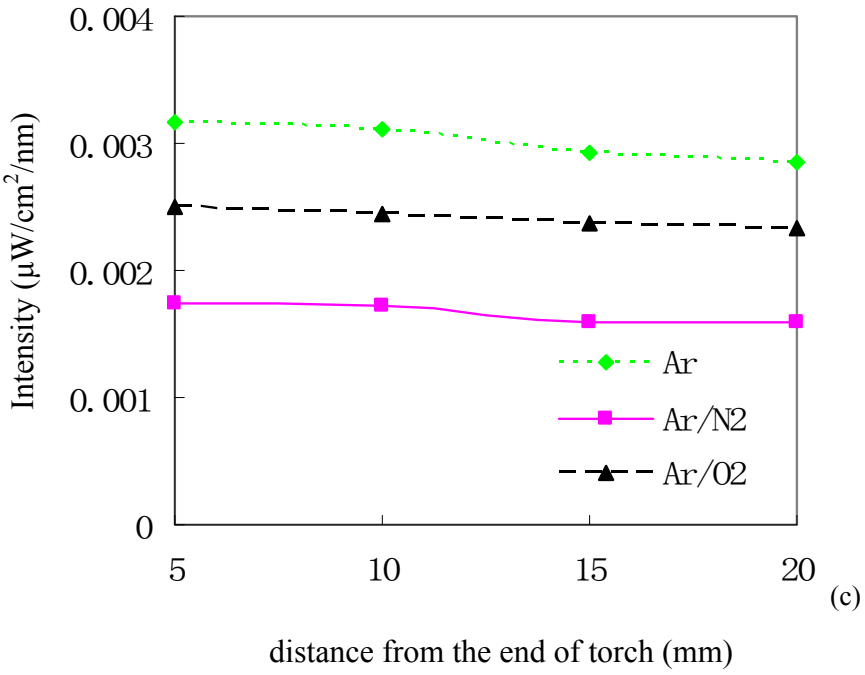

Fig. 3-18 Changes in emission intensities of excited Ar atoms at 696 nm (a), N_2 ($C^3\prod_u$ — $B^3\prod_g$) at 357 nm (b), and excited O atoms at 777 nm (c) in Ar, Ar/N_2, and Ar/O_2 plasmas at different axial positions. Discharge conditions: Ar flow rate of 10 SLPM, additive gas (N_2 or O_2) flow rate of 0.5 SLPM, nominal applied voltage of 16.0 kV (peak to peak) with 50% duty cycle, discharge frequency of 20 kHz. Note: excited Ar atoms at 697 nm and N_2 ($C^3\prod_u$ — $B^3\prod_g$) at 357 nm are selected as representatives for the excited Ar atoms and N_2 second positive system, respectively.

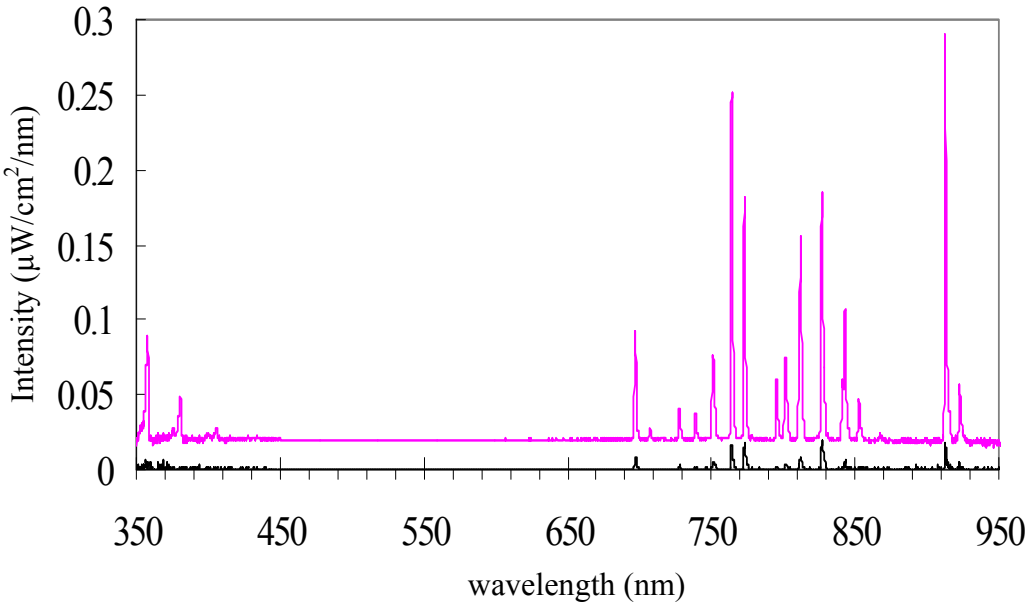

Fig. 3-19 Comparison of optical emission spectra of CAPPLAT Ar plasma jets with normal connection mode (red line) and reverse connection mode (black line), measured by USB4000 spectrometer at a distance of 5 mm from the end of torch. Discharge conditions: pure Ar discharge at a flow rate of 10 SLPM, dielectric thickness of 2 mm, nominal applied voltage of 16.0 kV (peak to peak) with 50% duty cycle, discharge frequency of 20 kHz.

Chapter 4 Comparison and Application of Two Types of Atmospheric Pressure Cold Argon Plasma Jets

1 Introduction

In chapter 2, we characterized the electrical properties of a RF capacitive cold Ar plasma jet (APC plasma jet) using a high-voltage probe and a current probe. Further, optical emission spectrometry (OES) was employed to identify the active species in this RF capacitive Ar plasma jet. In chapter 3, electrical and optical properties of a surface discharge Ar plasma jet (CAPPLAT plasma jet) were characterized. In order to get better understanding for the electrical and optical properties of these two different atmospheric pressure cold Ar plasma jets, both the physical and the chemical properties (such as jet length, jet temperature, discharge behavior and the mechanism of plasma chemical reactions) of APC Ar plasma jet and CAPPLAT Ar plasma jet were compared in this study. In particular, effects of an additive gas (N_2 or O_2) on the physical and chemical properties of these two Ar plasma jets were compared and discussed.

Nowadays, atmospheric pressure cold Ar plasma jet is the most promising tool for the polymer surface treatment since both the complicated vacuum system and the expensive He gas are unnecessary. Additionally, the plasma jet is not spatially confined by electrodes, which is very attractive for the treatment of complex shaped samples in the afterglow zone. On the other hand, high-density polyethylene (HDPE) is widely used in a variety of applications since it has good chemical resistance and high rigidity. However, in most cases (such as adhesion, printing, etc.), the hydrophilicity of HDPE surface is highly desirable to be improved since its wettability is not good for the practical use. To demonstrate an application of these two Ar plasma jets, high-density polyethylene (HDPE) surface treatment was performed using the CAPPLAT Ar plasma jet and the

APC Ar plasma jet. In particular, the effects of additive gas (N_2 or O_2) on the HDPE surface treatment were investigated and compared in detail.

2 Experimental set up and methods

2.1 Plasma devices

Two types of plasma devices were used in the experiments. One plasma device is a radio frequency (RF) capacitive plasma device and another plasma device is a pulsed surface discharge plasma torch. The RF capacitive plasma system is called APC plasma. APC plasma torch consists of two parallel perforated Al electrodes; the inner electrode is connected to a RF power source with a frequency of 27.12 MHz through an impedance matching network, and the outer electrode is grounded. In APC plasma torch, ceramic is used as an insulator between the two electrodes. The pulsed surface discharge plasma system is called CAPPLAT plasma. CAPPLAT plasma torch is composed of two co-axial cylindrical electrodes; the inner electrode is connected to a high-voltage pulsed power source with a frequency of several tens of kHz, and the outer electrode is grounded. In CAPPLAT plasma torch, a silicone tube (thickness: 2mm) was used as dielectric barrier between the two electrodes. The schematic illustrations of CAPPLAT plasma torch and APC plasma torch are shown in Fig. 3-1 and Fig 2-1, respectively. Both CAPPLAT and APC plasma devices are able to generate cold Ar plasma jet at atmospheric pressure. The main properties of the two plasma jets are listed in Table 4-1.

2.2 Preparation of HDPE samples and conditions for plasma surface treatment

HDPE pellets were purchased from Aldrich Chemistry. The melt index of the pellets is 12.00 g/min (190°C/2.16 kg, ASTMD 1238). The pellets were shaped into 5-mm-thick plates by a heat-molding machine at a molding temperature and pressure of 140°C and ca. 6.5 MPa, respectively.

The shaped plates were then cut into 12 mm × 38 mm bars for further investigations. Finally, the samples were purified by methanol in a supersonic oscillator and then dried at room temperature.

During the plasma surface treatment, the samples were placed on an X-Y axial movable stage driven by software (CP-310 Tool) and then exposed to the plasma at a certain scan speed. In order to compare the treatment effect of HDPE surface using the two plasma jets, the treatment distance and the treatment time were maintained at 5 mm and 5 s, respectively. Treatment distance is defined as a distance from the end of the torch to the sample's surface. In the experiments, scan speed was calculated from the treatment time and the diameter of the plasma jet. An invariable applied voltage (±8.0 kV) with a square-wave amplitude at a 50% duty cycle and a constant frequency of 20 kHz were used in the CAPPLAT discharge experiments. A constant RF power of 100 W with a frequency of 27.12 MHz was employed in the APC discharge experiments. Ar gas was used as the working gas with the both plasma devices. In order to investigate the effects of the additive gas (N_2 or O_2) on the HDPE surface treatment, trace of N_2 or O_2 was introduced as the additive gas into the two plasma jets, respectively. The flow rates of the working gas and the additive gas for CAPPLAT plasma and APC plasma are shown in Table 4-1. All flow rates were controlled by a mass flow controller. We should note that in APC plasma system, N_2 or O_2 as additive gas was injected directly into the Ar stream. However, in CAPPLAT plasma system, the injection approaches for N_2 and O_2 are different. In case of N_2 addition, similar to APC plasma system, N_2 gas was injected directly into the Ar stream. In case of O_2 addition, we attempted such direct injection approach; however, nearly no plasma jet was observed because of the considerable quenching effect of O_2. Therefore, we developed a new injection method. We added O_2 gas to the afterglow zone of the CAPPLAT plasma jet through a glass capillary placed at the center of the torch (see Fig. 3-1). In this case, O_2 mixed with the

CAPPLAT Ar plasma jet in the afterglow zone. The difference in the injection approaches for the N_2 and O_2 is shown in Fig. 3-2 (a) and (b).

2.3 Electrical measurement

Electrical characterizations were performed for both APC plasma jet and CAPPLAT plasma jet. The voltage applied to the RF discharge or to the surface discharge was measured using a 10:1 voltage probe (Tektronix P6139 10X Passive Probe 063-0870-05) and a 1000:1 high-voltage probe (Tektronix P6015A), respectively; the discharge current was monitored using a wide band current monitor (Pearson^{TM} current monitor) manufactured by Pearson Electronics Inc., Palo Alto, California, U.S.A. Further, a Tektronix TDS3012C digital phosphor oscilloscope was employed to record the waveforms of discharge voltage and discharge current.

2.4 Measurement of optical emission spectra

Optical emission spectra (OES) of CAPPLAT plasma jet and APC plasma jet were collected perpendicular to the plasma jet using an Ocean Optics USB4000 spectrometer (spectra range of 350–950 nm) with a resolution of 0.2 nm full width at half-maximum (FWHM); this was achieved using a personal computer equipped with relevant software (SpectraSuite) for both driving and acquisition. Prior to the OES measurement, the USB4000 spectrometer was calibrated using a standard halogen light source. Therefore, absolute irradiance of the active species in the plasma was obtained. During the OES measurement, the exposure time was 100 ms. Emission intensities of the active species were collected at a distance of 5 mm from the end of the torch through an optical fiber with a diameter of 100 μm.

2.5 Measurement of contact angle of water

Water contact angles (WCA) of HDPE samples were measured using a Kyowa contact angle

meter. For each sample, measurements were performed at 5 different points. The value of the WCA was obtained by averaging the results at these five points.

2.6 Measurement of XPS

XPS measurement was carried out by using a Perkin Elmer ESCA 5600 machine. Mg-Kα ray with a voltage of 15 kV and a power of 400 W was used as X-ray source. Take-off angle of photoelectron was fixed at 45°. The pressure in the chamber was kept at less than 5.0×10^{-8} Torr.

3 Results and discussion

3.1 Comparison of physical properties of APC and CAPPLAT plasma jets

3.1.1 Jet length

Under the normal operating conditions, Ar flow rate was maintained at 10 SLPM in CAPPLAT system; and Ar flow rate of 20 SLPM was employed in APC system. Then, the velocities of Ar stream in CAPPLAT and in APC can be calculated from the Ar flow rate and the torch diameter, respectively. It was found that the velocity of Ar stream in CAPPLAT jet is lower than in APC plasma jet. However, from Table 4-1, it is clearly seen that the jet length of CAPPLAT plasma is nearly one order of magnitude longer than APC plasma. On the other hand, considering the velocity of Ar stream and the life time of active species, the active species in CAPPLAT plasma jet is impossible to travel to the axial position at a distance of 35 mm from the discharge region at a speed of gas stream velocity. Obviously, the velocity of Ar stream is not the dependent factor for the determination of jet length. As we discussed in section 4.3 of chapter 1, photo-induced ionization should be considered in the formation of plasma jet. Actually, it was found that the traveling velocity of the plasma jet is several orders of magnitude faster than the gas flow velocity [1]. Using the model discussed in chapter 1, we can easily explain the difference in the jet lengths of CAPPLAT

and APC plasma. In chapter 1, we discussed the three requirements which must be fulfilled for the streamer propagation under low or zero electric field. (1) The number of new positive ions created by the avalanche must be equal to the number of ions in the original sphere (n^+); (2) The diffusion radius of the avalanche head must be smaller than r_0; (3) the avalanche must reach the required amplification before the two charge regions begin to overlap, (i.e., $2r_0 \leq r_2$) [2]. In APC system, the traveling of positive ions is very difficult since the polarity change is very fast (54.34 MHz). Therefore, the two charge regions are easily overlapped before the avalanche reaches the required amplification. This may probably be used to explain why the jet length of APC plasma is much shorter than CAPPLAT plasma.

3.1.2 Jet temperature

Under the normal operating conditions, Ar flow rate of 10 SLPM, nominal applied voltage of 16.0 kV (peak to peak) were employed in CAPPLAT system; and Ar flow rate of 20 SLPM, RF power of 100 W were employed in APC system, respectively. From Table 4-1, it can be seen that the jet temperatures of the two Ar plasma jets are quite different. As we discussed in chapter 3, a pulsed power supplier was employed in CAPPLAT system. A large and instantaneous pulse current forms when the high voltage was applied and switched off (see Fig. 3-5 (a)). The breakdown took place and the Ar plasma jet was generated under the strong pulse current and the high voltage. However, the duration of application of both voltage and current is quite short in a single period. This is why the temperature of the CAPPLAT plasma jet is as high as room temperature. On the other hand, a RF power supplier was employed in APC system. The dissipated power in the APC plasma is much higher than CAPPLAT plasma. It is why the temperature of APC plasma jet is relatively higher.

3.1.3 Effect of additive gas (N_2 or O_2) on electrical properties

As we discussed in chapter 2, at a higher input RF power (60 W ~ 105 W), the discharge of APC plasma jet became an abnormal glow discharge. This abnormal glow is an α-mode discharge [3-6]. In the α-mode, the discharge is sustained by bulk ionization. The electrons are oscillating with drifting amplitude and are trapped in the bulk plasma region [7-8]. It was found that the discharge voltage decreased and the current increased with the addition of the additive gas (N_2 or O_2) (see Fig. 2-8). On the other hand, the plasma temperature increased when the additive gas was added into APC plasma jet (see Fig. 2-9). We assumed that the direct collisions of additive gas molecules with energetic electrons changed the plasma impedance and the RF capacitive matching. However, through the observed waveforms of the discharge voltage and RF current, the addition of additive gas scarcely changed the discharge behavior of APC Ar plasma jet. On the other hand, through the electrical characterization, it was found that the discharge in CAPPLAT plasma jet is a glow-like (diffuse) barrier discharge and not filamentary barrier discharge (see Fig. 3-5). Surprisingly, both the discharge current and the plasma temperature scarcely changed when the additive gas was injected either directly into CAPPLAT Ar stream or into the plasma afterglow zone through a glass capillary. On the basis of this result, we proposed a simple discharge mechanism for CAPPLAT Ar plasma jet. First, Ar molecules are excited and ionized through collisions with energetic electrons. In this step, energy is transferred to the Ar particles and the Ar active species (Ar metastable atoms) are produced. Second, N_2 or O_2 molecules are excited through collisions with energetic Ar metastable atoms. Nitrogen active species (N_2 ($C^3\prod_u$)) and oxygen active species (O atoms) are then generated. This discharge mechanism is quite different from the APC Ar plasma jet. As we discussed in chapter 2, the direct collisions between additive gas molecules and energetic electrons play a very important role in the generation of nitrogen and oxygen active species in APC Ar plasma jet.

3.2 Comparison of chemical characteristics of APC and CAPPLAT plasma jets

3.2.1 Plasma chemical reactions in two Ar plasma jets

Comparison of optical emission spectra of the two Ar plasma jets in the wavelength range of 350-950 nm is shown in Fig. 4-1. It can be seen that categories of the active species in the two Ar plasma jets are identical but the emission intensities are quite different from each other. We can also see that peaks of Ar active species belonging to the excited Ar atoms (4p-4s transition) are predominant in the two plasma jets (in the wavelength of 690 nm to 950nm) [9, 10]. Peaks at 357 and 380 nm belonging to the N_2 second positive system (N_2 ($C^3\prod_u$ — $B^3\prod_g$)) were also observed. Additionally, the peak of O atoms at 777nm was detected in the two Ar plasma jets [9]. Both nitrogen active species (N_2 ($C^3\prod_u$ — $B^3\prod_g$)) and oxygen active species (O atoms) were detected in the two pure Ar plasma jets because impurities (N_2 and O_2) from the Ar gas or from the atmosphere are excited and dissociated. As we discussed in chapter 2 and chapter 3, emission lines of excited Ar atoms are generated through the following reactions:

$$e^* + Ar^0 \rightarrow Ar^m + e \quad (4\text{-}1)$$

$$e^* + Ar^m \rightarrow Ar^* (4p) + e \quad (4\text{-}2)$$

$$Ar^* (4p) \rightarrow Ar^* (4s) + h\nu \quad (4\text{-}3)$$

From Fig. 4-1, it can be clearly seen that the distribution of emission intensities of excited Ar atoms in the two Ar plasma jets is quite different from each other. We infer that the different gas rotational temperatures lead to the difference in the distribution of emission intensities of the active species in the two plasma jets. On the other hand, emission band of the nitrogen second positive system is generated though the following reactions [10]:

$$Ar^m + N_2 (X_1\Sigma^+_g) \rightarrow Ar^0 + N_2 (C^3\prod_u) \quad (4\text{-}4)$$

$$N_2 (C^3\prod_u) \rightarrow N_2 (B^3\prod_g) + h\nu \quad (4\text{-}5)$$

From Fig. 4-1, it can be clearly seen that the emission intensities of N_2 ($C^3\prod_u$ — $B^3\prod_g$) are relatively stronger in CAPPLAT plasma jet than in APC plasma jet. As we abovementioned, N_2 ($C^3\prod_u$) is mainly generated through the resonant reaction between the Ar metastables and ground-state molecular N_2 (see reaction (4-4)). In CAPPLAT plasma system, N_2 ($C^3\prod_u$) from both the discharge region and the afterglow zone is able to be transported to a certain distant position from the exit (a distance of 5 mm in the experiment). Additionally, the Ar stream velocity of CAPPLAT plasma is slower than APC plasma, which is helpful for the entry of N_2 into the plasma jet. On the other hand, in APC plasma system the electron temperature and the electron density are relatively higher than CAPPLAT plasma. Consequently, N_2 ($C^3\prod_u$) generated in the discharge region is quickly transformed to N_2^+ ($B^2\Sigma^+_u$) through the successive collisions with energetic electrons. Once the ionic nitrogen species (N_2^+ ($B^2\Sigma^+_u$)) is formed, it will be trapped in the discharge region by the polarity change with a very high frequency. Therefore, only N_2 ($C^3\prod_u$ — $B^3\prod_g$) from the afterglow zone can be observed in case of APC Ar plasma jet. It was why the emission intensities of N_2 ($C^3\prod_u$ — $B^3\prod_g$) are much weaker in APC plasma jet.

Interestingly, it can be clearly seen that the emission intensity of O atoms is much weaker in CAPPLAT plasma jet than in APC plasma jet. As we discussed in chapter 2, in the Ar discharge, excited O atoms at 777 nm can probably be generated through the following channels [9, 11-13]:

$$Ar^* + O_2 (X^3\Sigma^-_g) \rightarrow O (^1D) + O (^3P) + Ar^0 \quad (4\text{-}6)$$

$$e^* + O_2 (X^3\Sigma^-_g) \rightarrow e + [O (^1D) \text{ or } O (^1S)] + O (^3P) \quad (4\text{-}7)$$

$$e^* + O_2 (X^3\Sigma^-_g) \rightarrow 2e + O_2^+ (b^4\Sigma^-_g) \quad (4\text{-}8)$$

$$e^* + O_2^+ (b^4\Sigma^-_g) \rightarrow 2O (^3P) \quad (4\text{-}9)$$

It was reported that the most probable channel for the formation of O atoms was through collisions between the oxygen molecular ions (O_2^+) and electrons (see reaction (4-9)) [14]. Therefore, collisions of oxygen molecules with energetic electrons are the crucial channel for the formation of O atoms in Ar discharge (see reaction (4-8)). However, as we discussed in section 3.1.3, reaction (4-6) is the only channel for the generation of O atoms in CAPPLAT Ar plasma. It was because both nitrogen and oxygen active species are generated through collisions with Ar metastables in CAPPLAT plasma system. Different generation mechanisms in the two plasma jets lead to the different emission intensities of O atom at 777 nm.

3.2.2 Effect of additive gas (N_2 or O_2) on plasma chemical reactions

Effects of additive gas (N_2 or O_2) on optical properties of APC plasma jet and CAPPLAT plasma jet have been investigated in chapter 2 and chapter 3, respectively. Interestingly, the emission intensities of N_2 ($C^3\prod_u$ — $B^3\prod_g$) increased significantly when trace of N_2 gas was added into CAPPLAT Ar plasma (see Fig. 4-2 (a)); however, their emission intensities increased only slightly when the same amount of N_2 gas was added into APC Ar plasma (see Fig. 4-2 (b)). As we discussed in chapter 2, in the Ar discharge, the nitrogen molecular ions (N_2^+ ($B^2\Sigma^+_u$)) can probably be generated through the following channels [10, 15-16]:

$$e^* + N_2 (X^1\Sigma^+_g) \rightarrow N_2^+ (B^2\Sigma^+_u) + 2e \quad (4\text{-}10)$$

$$e^* + N_2 (C^3\prod_u) \rightarrow N_2^+ (B^2\Sigma^+_u) + 2e \quad (4\text{-}11)$$

$$Ar^+ + N_2 (X^1\Sigma^+_g) \rightarrow Ar^0 + N_2^+ (X^2\Sigma^+_g) \quad (4\text{-}12)$$

$$N_2^+ (X^2\Sigma^+_g) + e^* \rightarrow N_2^+ (B^2\Sigma^+_u) + e \quad (4\text{-}13)$$

We assumed that new nitrogen active species (such as N_2^+ ($B^2\Sigma^+_u$)) were generated in APC plasma after the addition of N_2 additive gas. Then N_2^+ ($B^2\Sigma^+_u$) was trapped in the discharge region by

the high-frequency polarity change. This assumption can explain why the emission intensities of N_2 ($C^3\prod_u$ — $B^3\prod_g$) increased only slightly when trace of N_2 gas was added into APC Ar plasma jet.

As we discussed above, the direct collisions between O_2 molecules and energetic electrons play a very important role in the generation of O atoms in APC Ar plasma jet. Therefore, when trace of O_2 gas was added into APC Ar plasma jet a lot of O atoms were generated through reactions (4-7) , (4-8) and (4-9) above. It is helpful to explain why the emission intensity of O atoms at 777 nm increased significantly with the addition of O_2 gas (see Fig. 4-2 (b)). However, in case of CAPPLAT plasma, the emission intensity of O atoms at 777 nm decreased inversely when O_2 gas was added into the afterglow zone of plasma jet through a glass capillary (see Fig. 4-2 (a)). As we discussed above, in CAPPLAT plasma jet the O atoms are mainly generated through reaction (4-6). The emission intensities of excited Ar atoms decreased when O_2 gas was added into the afterglow zone of the plasma jet, suggesting that more O atoms were produced through reaction (4-6). Therefore, we assumed that the newly generated O atoms were quickly transformed through the following reactions [17, 18]:

$$O\ (^1D) + O_2\ (X^3\Sigma^-_g) \rightarrow O_3 \qquad (4\text{-}14)$$

$$O_3 + O\ (^1D) \rightarrow 2O_2\ (X^3\Sigma^-_g) \qquad (4\text{-}15)$$

When O_2 gas was added we identified a much stronger ozone smell during the experiment, since the reaction rate of reaction (4-14) is much faster than reaction (4-15). This helps explain why the emission intensity of O atoms at 777 nm decreased inversely when O_2 gas was added into the afterglow zone of plasma jet through a glass capillary.

3.3 Application of APC and CAPPLAT Ar plasma jets

3.3.1 HDPE surface treatment by two Ar plasma jets

Comparison of WCA values of HDPE samples treated by CAPPLAT plasma and APC plasma is shown in Fig. 4-3. Comparing with untreated HDPE, the WCA value dropped significantly and a hydrophilic surface was formed when the HDPE surface was treated by the two Ar plasma jets, respectively. Interestingly, with the same treatment time and at the same treatment distance, nearly the same WCA value was obtained when the HDPE surface was treated by the two plasma jets, respectively. Figure 4-4 shows surface chemical compositions of HDPE samples measured by XPS. Compared to the untreated HDPE surface, oxygen element on the treated HDPE surface significantly increased. It suggests that a lot of O-containing functional groups were introduced onto the HDPE surface after the plasma treatment. These polar functional groups are responsible for the hydrophilicity enhancement of HDPE surface. Additionally, nitrogen element on HDPE surface changed slightly after the plasma treatment.

According to the OES, we can see that the emission intensities of O atoms in the two Ar plasma jets are quite weak, especially for CAPPLAT Ar plasma jet (see Fig. 4-1). However, according to XPS results, it was shown that a lot of O-containing functional groups were formed during the plasma treatment. Therefore, besides O atoms, other active species in the plasma jet, such as Ar metastable atoms and N_2 ($C^3\prod_u$), should also be considered for use in HDPE surface treatment. In actuality, we have successfully deposited poly (methyl methacrylate) (PMMA) films via CAPPLAT Ar plasma polymerization using methyl methacrylate monomer [19]. This suggests that energetic Ar metastables play an important role in the generation of radicals in the plasma. On the basis of this observation, we propose a probable process for HDPE surface treatment using the two Ar plasma jets. First, the HDPE surface is bombarded with the energetic active species (Ar metastable atoms, N_2 ($C^3\prod_u$), O atoms etc.) and large numbers of radicals are generated on the HDPE surface. Second,

these radicals react with O_2 molecules in the atmosphere and then numerous O-containing functional groups are formed on the HDPE surface.

3.3.2 Effect of additive gas (N_2 or O_2) on HDPE surface treatment

Figure 4-5 shows the effect of additive gas (N_2 or O_2) on HDPE surface treatment using CAPPLAT plasma jet and APC plasma jet. It can be seen that using the two Ar plasma jets, the effects of additive gas (N_2 or O_2) on the HDPE surface treatment are quite different from each other. The WCA value of treated HDPE surface increased slightly when trace of N_2 or O_2 was added into CAPPLAT Ar plasma jet. However, the WCA value of treated HDPE surface decreased significantly when the same amount of N_2 or O_2 was added into APC Ar plasma jet.

Changes in the roughness of HDPE surface during the plasma treatment are negligible in this study, since the plasma etching on the HDPE surface scarcely occurs in atmospheric pressure Ar plasma treatment. Therefore, it can be considered that the change in the WCA suggests the change in the number of functional groups on the HDPE surface. As is well known, $W_a = \gamma_L (1 + \cos\theta)$, where W_a is the work of adhesion on a polymer surface; γ_L is the interfacial tension of the tested liquid; and θ is the contact angle of the polymer surface. Further, W_a is proportional to the number of functional groups on the polymer surface, formed during the plasma treatment. As mentioned above, in addition to the O atoms, both Ar metastable atoms and N_2 ($C^3\prod_u$) contribute to the generation of functional groups. Namely, the number of functional groups on the polymer surface, formed during the plasma treatment, is proportional to the concentrations of all active species in plasma. Thus, we can construct the following expression.

$$W_a = \gamma_L (1 + \cos\theta) = C (a [Ar^*] + b [N_2^*] + c [O]), \quad (1)$$

where C is a constant; [Ar*], [N_2*] and [O] are the concentrations of excited Ar atoms, N_2 ($C^3\prod_u$)

and O atoms in the plasma; and a, b, and c are coefficients associated with [Ar*], [N_2*] and [O], respectively. As the concentrations of excited species are proportional to their emission intensities, equation (1) can be rewritten as equation (2), where I(Ar*), I(N_2*) and I(O) are the respective emission intensities in the plasma:

$$W_a = \gamma_L (1 + \cos\theta) = C' (a' I(Ar^*) + b' I(N_2^*) + c' I(O)), \quad (2)$$

From equation (2), we can see that the number of functional groups on the polymer surface, formed during the plasma treatment, is proportional to the effective total emission intensity of all active species in plasma. Then, equation (2) above is applied to HDPE samples treated with CAPPLAT Ar, CAPPLAT Ar/N_2, and CAPPLAT Ar/O_2 plasmas and the following equations are obtained.

$$\gamma_L (1 + \cos\theta_{Ar}) = C' (a' I(Ar^*)_{Ar} + b' I(N_2^*)_{Ar} + c' I(O)_{Ar}), \quad (3)$$

$$\gamma_L (1 + \cos\theta_{Ar/N2}) = C' (a' I(Ar^*)_{Ar/N2} + b' I(N_2^*)_{Ar/N2} + c' I(O)_{Ar/N2}), \quad (4)$$

$$\gamma_L (1 + \cos\theta_{Ar/O2}) = C' (a' I(Ar^*)_{Ar/O2} + b' I(N_2^*)_{Ar/O2} + c' I(O)_{Ar/O2}), \quad (5)$$

where θ denotes the WCA on the HDPE surface treated with CAPPLAT Ar, CAPPLAT Ar/N_2 and CAPPLAT Ar/O_2 plasmas, respectively. The subscripts indicate the plasma gases.

Hence, we can solve the above equations for coefficients a′, b′ and c′. Consequently, the ratio of a′ to b′ to c′ is obtained, which is approximately 1 : 4 : 398. This ratio suggests that Ar metastable atoms, N_2 ($C^3\prod_u$) and O atoms have different capabilities for the generation of functional groups on a polymer surface. Therefore, the effective total emission intensities of all active species in CAPPLAT Ar, CAPPLAT Ar/N_2 and CAPPLAT Ar/O_2 plasmas are expressed as follows:

$$I_{Ar} = a' I(Ar^*)_{Ar} + b' I(N_2^*)_{Ar} + c' I(O)_{Ar}, \quad (6)$$

$$I_{Ar/N2} = a' I(Ar^*)_{Ar/N2} + b' I(N_2^*)_{Ar/N2} + c' I(O)_{Ar/N2}, \quad (7)$$

$$I_{Ar/O2} = a' I(Ar^*)_{Ar/O2} + b' I(N_2^*)_{Ar/O2} + c' I(O)_{Ar/O2}. \quad (8)$$

Given that coefficient a′ is 1, from the ratio of a′ to b′ to c′, the effective total emission intensities of all active species in CAPPLAT Ar, CAPPLAT Ar/N_2 and CAPPLAT Ar/O_2 plasmas were calculated using the above expressions. Similarly, the effective total emission intensities of all active species in APC Ar, APC Ar/N_2 and APC Ar/O_2 plasmas were also calculated from the ratio of a′ to b′ to c′.

Since the number of functional groups on the polymer surface, formed during the plasma treatment, is proportional to the quantities of all active species in plasma, which is also proportional to the effective total emission intensity of all active species. Therefore, stronger effective total emission intensity means more functional groups are generated during the plasma treatment. Changes in effective total emission intensities of all active species in the two Ar plasma jets before and after the addition of the additive gas (N_2 or O_2) are shown in Fig. 4-6. In case of CAPPLAT plasma, it is apparent that the effective total emission intensity decreased slightly when trace of N_2 or O_2 was added (see Fig. 4-6). It suggests that the effective total quantities of energetic active species in CAPPLAT plasma decreased after the addition of N_2 or O_2. Based on the process proposed above, it is inferred that fewer radicals were generated on the HDPE surface when the additive gas (N_2 or O_2) was added into CAPPLAT Ar plasma. This is helpful to explain why the WCA value increased slightly when trace of N_2 or O_2 was added into CAPPLAT plasma. On the other hand, it can be seen that the effective total emission intensity increased significantly when trace of O_2 was added into APC plasma (see Fig. 4-6), suggesting that the effective total quantities of energetic active species increased remarkably after the addition of O_2. This may probably explain why the WCA value decreased significantly when trace of O_2 was added into APC Ar plasma. Interestingly, a

lower WCA value was also obtained when trace of N_2 was added into APC plasma, though the effective total emission intensity decreased significantly in this case (see Fig. 4-6). We monitored the treatment temperature during the plasma treatment. We should note that the treatment temperature (29 °C) scarcely changed when trace of additive gas (N_2 or O_2) was added into CAPPLAT plasma jet. On the other hand, the treatment temperature (120 °C) changed slightly when trace of O_2 gas was added into APC Ar plasma jet; however, the treatment temperature decreased to 106 °C when the same amount of N_2 gas was added. We assume that numerous newly generated nitrogen ionic species (N_2^+ ($B^2\Sigma^+_u$)) are trapped in the discharge region, which leads to a remarkable decrease in the radiation of active species in the plasma afterglow zone. This may probably explain the significant decrease in the treatment temperature when trace of N_2 gas was added into APC plasma. On the other hand, it was reported that the glass transition temperature (Tg) of the polymer surface is much lower than that of the bulk [20]. Thereby, surface molecular motion is much more active. During APC Ar plasma treatment, the treatment temperature is very close to the melt point of HDPE (about 130 °C). Therefore, the formed functional groups on the surface, with a very high free energy, are much easier to diffuse into the bulk in this case. During APC Ar/N_2 plasma treatment, more functional groups were easily remained on the HDPE surface because the treatment temperature is much lower than the melt point. This probably is helpful to explain why the WCA value decreased when trace of N_2 was added into APC plasma, though the effective total quantities of energetic active species decreased significantly in this case. High resolution XPS spectra for C1s peaks of HDPE samples treated by APC plasmas are shown in Fig. 4-7. Comparing with Fig. 4-7 (b), it is clearly seen that more heavier oxidized carbon species with binding energy of 287.5 eV and 289.0 eV, which are assigned to –C=O- and –O=C-O- bond, are observed on the APC Ar/N_2 plasma-treated

HDPE surface (See Fig. 4-7 (c)). It is completely consistent with our assumption above.

A summary for HDPE surface treatment by the two Ar plasma jets is shown in Table 4-2. From this summary, we can conclude that the effective total emission intensity and the treatment temperature are two very important factors for HDPE surface treatment. Stronger effective total emission intensity suggests more effective energetic active species in the plasma, which results in the generation of more polar functional groups on HDPE surface. On the other hand, the molecular motion on polymer surface is not negligible when the treatment temperature is relatively high. Especially, when the treatment temperature is close to the melt point of the polymer, a lot of formed functional groups diffuse into the bulk of the polymer during the plasma treatment.

3.3.3 Stability of HDPE surface treated by two Ar plasma jets

Changes in WCA values of HDPE samples with the aging time are shown in Table 4-3 and Fig. 4-8, respectively. It can be seen that the WCA values increased dramatically within 24 hours, and then increased gradually with the aging time. Many authors reported the mechanism of the increase in the WCA value or the loss in the wettability after polymer surface was treated by plasma [21-24]. It was reported that the scission of polymer chain occurs and then numerous low molecular weight organic materials (LMWOM) are formed during the plasma treatment. The tendency for the reorientation or migration increases with the decrease in molecular weight of polymer surface. Therefore, the hydrophobic recovery of treated HDPE surface attributes to the inward-diffusion, agglomeration or reorientation of mobile LMWOM on the surface. Interestingly, we should note that the WCA value increased slightly within 24 hours when the HDPE sample was treated by APC Ar plasma. This was because numerous O-containing functional groups already diffused into the bulk during the plasma treatment, since the treatment temperature is very close to the melt point of HDPE.

Additionally, we can see that comparing to the untreated HDPE surface a relatively stable hydrophilic surface was still remained even after an aging time of one month. It suggests that both CAPPLAT Ar plasma jet and APC Ar plasma jet are very effective for the HDPE surface treatment.

4 Conclusions

Both the physical and the chemical characteristics of the two Ar plasma jets (APC plasma jet and CAPPLAT plasma jet) were compared in this study. The electrical characteristics showed that the discharges of APC Ar plasma jet and CAPPLAT Ar plasma jet are glow (glow-like) discharges. As we mentioned in chapter 1, realizing stable Ar glow discharges at atmospheric pressure is very meaningful for the application of homogenous plasma treatment with lower costs since the complicated vacuum systems and the expensive He gas are unnecessary. On the other hand, the two Ar plasma jets are not spatially confined by electrodes and the jet length reaches several tens of millimeters (in case of CAPPLAT plasma jet). It is very helpful for the treatment of complex shaped samples in the afterglow zone. Additionally, it was shown that the jet temperatures of the two Ar plasma jets are relatively low, which is very attractive for the treatment of thermal sensitive materials.

To demonstrate an application of these two Ar plasma jets, CAPPLAT plasma jet and APC plasma jet were employed to the HDPE surface treatment. In particular, effects of the additive gas (N_2 or O_2) on the HDPE surface treatment were investigated and compared in detail. OES revealed that categories of the active species in the two Ar plasma jets are identical. However, the emission intensities of active species in the two Ar plasma jets are quite different. Using the two Ar plasma jets, a large number of O-containing functional groups were formed on the HDPE surface during the plasma treatment, though the concentration of O atoms in the two Ar plasma jets is rather low. On

the basis of this observation, we proposed a probable process for HDPE surface treatment using the two Ar plasma jets. First, the HDPE surface is bombarded with the energetic active species (Ar metastable atoms, N_2 ($C^3\prod_u$), O atoms etc.) and then large numbers of radicals are generated on the HDPE surface. Second, these radicals react with O_2 molecules in the atmosphere and then numerous O-containing functional groups are formed on the HDPE surface. From the process proposed above, we can see that in addition to the O atoms, both Ar metastable atoms and N_2 ($C^3\prod_u$) contribute to the generation of functional groups on HDPE surface. Considering the different capabilities of Ar metastable atoms, N_2 ($C^3\prod_u$) and O atoms for the generation of functional groups, we constructed and calculated the effective total emission intensity of all active species in the two Ar plasma jets. It was found that the effective total emission intensity is a very important factor for HDPE surface treatment. Stronger effective total emission intensity suggests more effective energetic active species in the plasma, which results in the generation of more polar functional groups on HDPE surface.

It proved that both CAPPLAT plasma jet and APC plasma jet are very effective for the HDPE surface treatment. However, the effects of the additive gas (N_2 or O_2) on the HDPE surface treatment are quite different from each other. It was shown that comparing to the pure Ar plasma treatment, the WCA value of treated HDPE surface increased slightly when trace of the additive gas (N_2 or O_2) was injected into CAPPLAT plasma. It was because the effective total quantities of energetic active species in CAPPLAT plasma decreased after the addition of additive gas (N_2 or O_2). On the other hand, the WCA value of treated HDPE surface decreased significantly when trace of O_2 was added into APC plasma; since the effective total quantities of energetic active species increased significantly after the addition of O_2. The WCA value of treated HDPE surface also decreased when trace of N_2 was added into APC plasma, though the effective total quantities of energetic active

species decreased in this case. It was because more O-containing functional groups were easily remained on the HDPE surface at a lower treatment temperature. It was inferred that the treatment temperature is another very important factor for HDPE surface treatment. The molecular motion on HDPE surface is not negligible when the treatment temperature is relatively high. Especially, when the treatment temperature is close to the melt point of HDPE, a lot of formed functional groups diffuse into the bulk during the plasma treatment.

References

[1] X. Lu, M. Laroussi, J. Appl. Phys. 2006, 100, 063302.

[2] G. A. Dawson,W. P. Winn, Zeitschrift fur Physik 1965, 183, 159.

[3] J. Laimer, H. Stŏri, Plasma Process. Polym. 2006, 3, 573.

[4] J. Park, I. Henins, H. W. Herrmann, G. S. Selwyn, Appl. Phys. Lett. 2000, 76, 288.

[5] S. Haslinger, J. Laimer, H. Stŏri, Vacuum 2008, 82, 142.

[6] S. Y. Moon, R. K. Rhee, D. B. Kim, W. Choe, Phys. Plasmas 2006, 13, 033502.

[7] X. Yang, M. Moravej, S. E. Babayan, G. R. Nowling, R. F. Hicks, Plasma Sources Sci. Technol. 2005, 14, 412.

[8] J. Laimer, H. Stŏri, Plasma Process. Polym. 2007, 4, 266.

[9] Q. S. Yu, H. K. Yasuda, Plasma Chem. Plasma Process. 1998, 18, 461.

[10] M. C. García, V. P. M. Martínez, Plasma Chem. Plasma Process. 2010, 30, 241.

[11] C. Lee, D. B. Graves, M. N. Lieberman, D. W. Hess, J. Electrochem. Soc. 1994, 141, 1546.

[12] B. Eliasson, U. Kogelschatz, ‘‘Basic Data for Modeling of Electrical Discharge in Gases: Oxygen’’, Research, Asea Brown Boveri Corporate, KLR-11C CH5405, 1986.

[13] D. Lee, J. Park, S. H. Hong,Y. Kim, IEEE Trans. Plasma Sci. 2005, 33, 949.

[14] V. Léveillé, S. Coulombe, Plasma Process. Polym. 2006, 3, 587.

[15] S. K. Dhali, P. F. Williams, J. Appl. Phys. 1987, 62, 4696.

[16] V. Nemchinsky, J. Phys. D: Appl. Phys. 2005, 38, 3825.

[17] S. T. Amimoto, A. P. Force, J. R. Wiesenfeld, Chem. Phys. Lett. 1978, 60, 40.

[18] J. Heicklen, “Atmospheric Chemistry”, Academic Press, New York, 1976.

[19] T. P. Kasih, S. Kuroda, H. Kubota, Plasma Process. Polym. 2007, 4, 648.

[20] X. Jiang, C. Z. Yang, Phys. Lett. A 2001, 281, 363.

[21] J. B. Lynch, P. D. Spence, J. Appl. Polym. Sci. 1999, 71, 319.

[22] S. Guimond, I. Radu, Plasmas Polym. 2002, 7, 71.

[23] A. Kuwabara, S. Kuroda, H. Kubota, Plasma Sci. Technol. 2007, 9, 181.

[24] M. Strobel, V. Jones, Plasmas Polym. 2003, 8, 61.

Tab. 4-1 Comparison of physical properties of CAPPLAT plasma jet and APC plasma jet.

Items	CAPPLAT plasma jet	APC plasma jet
Power supplier	AC square-wave pulsed power with frequency of 20 kHz	RF power with frequency of 27.12 MHz
Main gas flow rate	Ar gas at flow rate of 10 SLPM	Ar gas at flow rate of 20 SLPM
Additive gas flow rate	N_2 or O_2 at flow rate of 30 smlpm	N_2 or O_2 at flow rate of 30 smlpm
Jet length	35-40 mm	3-6 mm
Jet diameter	6 mm	25 mm
Jet temperature	22–35 °C	80–120 °C
Discharge behavior	Glow-like (diffuse barrier discharge)	Glow (RF α-mode discharge)

Tab. 4-2 Summary for HDPE surface treatment by two Ar plasma jets.

Plasmas	**Effective total emission intensity** ($\mu W/cm^2/nm$)	**Treatment temperature** (ºC)	**WCA** (º)	**O/C ratio** (%)
CAPPLAT Ar	4.82	29	36.6	22.5
CAPPLAT Ar/N_2	4.58	29	40.2	19.4
CAPPLAT Ar/O_2	4.76	29	38.8	22.2
APC Ar	16.12	120	36.1	22.7
APC Ar/N_2	7.89	106	28.7	28.9
APC Ar/O_2	33.16	123	23.6	34.8

Note: HDPE samples were treated for 5 seconds at a treatment distance of 5 mm. During APC plasma treatment, Ar flow rate and the additive gas (N_2 or O_2) flow rate were maintained at 20 SLPM and 30 smlpm, respectively. During CAPPLAT plasma treatment, Ar flow rate and the additive gas (N_2 or O_2) flow rate were maintained at 10 SLPM and 30 smlpm, respectively. Only active species in the wavelength range of 350 – 950 nm are counted in the effective total emission intensity. Temperatures of HDPE surface during the plasma treatment (treatment temperature) were monitored by a thermocouple. WCA was measured immediately after the plasma treatment. O/C ratio was calculated from the measurement of XPS.

Tab. 4-3 Changes in WCA values of HDPE samples treated by two Ar plasma jets.

Samples	**WCA-0** (days)	**WCA-1** (days)	**WCA-3** (days)	**WCA-7** (days)	**WCA-14** (days)	**WCA-21** (days)	**WCA-30** (days)
Untreated HDPE	90.6	90.6	90.6	90.6	90.6	90.6	90.6
CAPPLAT Ar	36.6	47.2	51.3	52.7	56.1	58.5	62.9
CAPPLAT Ar/N_2	40.2	50.8	51.8	53.2	56.3	61.6	63.5
CAPPLAT Ar/O_2	38.8	49.4	52.2	52.8	58.8	62.9	63.1
APC Ar	36.1	38.6	42.6	44.3	47.1	50.3	56.6
APC Ar/N_2	28.7	34.6	39.9	41.1	44.8	45.7	47.4
APC Ar/O_2	23.6	32.1	35.6	39.7	44.4	44.7	50.5

Note: investigation of changes in WCA values of plasma-treated HDPE samples was performed in the atmosphere at room temperature (25 ºC). WCA was measured at different aging time since the sample was treated by plasma. WCA-0 means that the WCA was measured immediately after the plasma treatment.

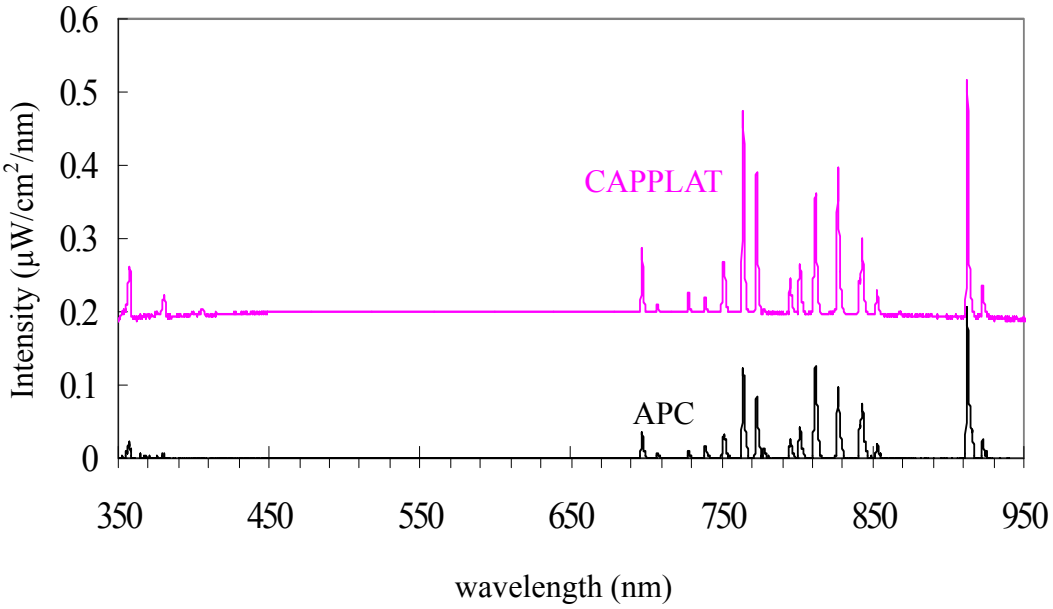

Fig. 4-1 Comparison of typical optical emission spectra of CAPPLAT Ar plasma jet and APC Ar plasma jet measured by Ocean Optics USB4000 spectrometer at a distance of 5 mm from the end of torch. CAPPLAT discharge conditions: pure Ar discharge at flow rate of 10 SLPM, applied voltage of ±8.0 kV with square-wave amplitude at 50% duty cycle and a frequency of 20 kHz. APC discharge conditions: pure Ar discharge at flow rate of 20 SLPM, RF power of 100 W with a frequency of 27.12 MHz.

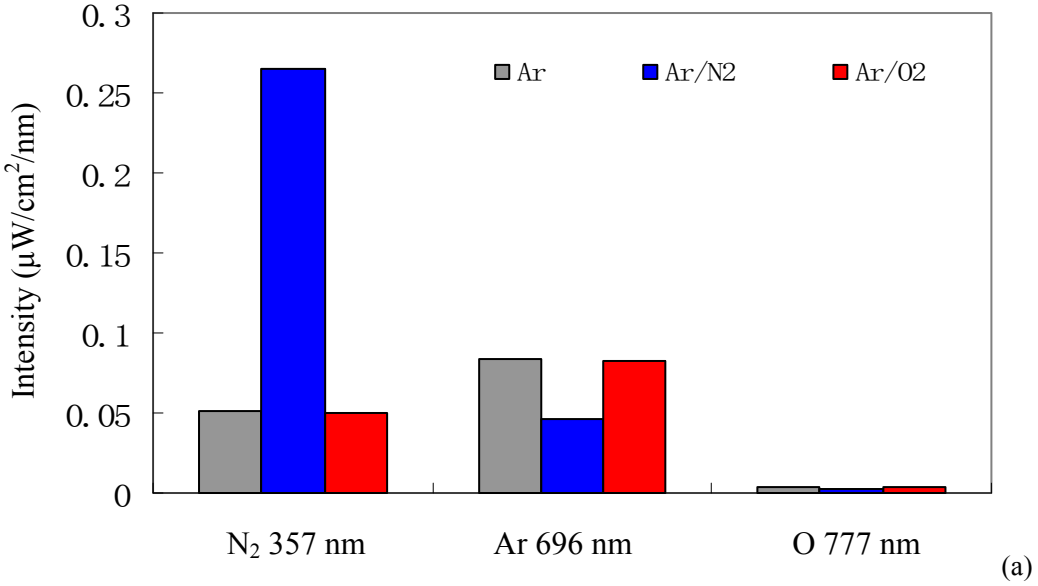

(a)

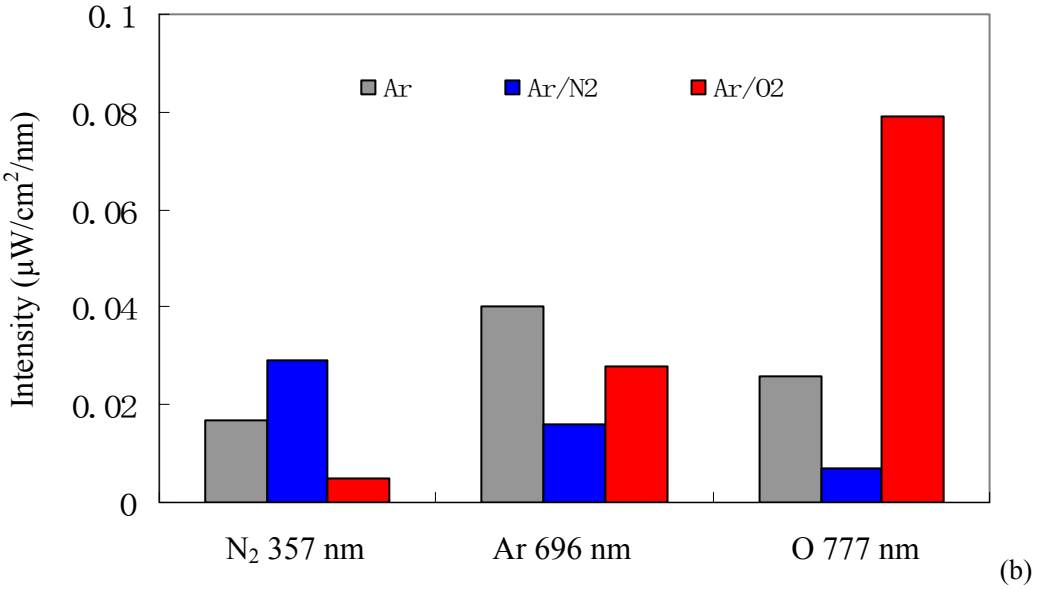

(b)

Fig. 4-2 Comparison of emission intensities of excited Ar atoms at 696 nm, N_2 ($C^3\prod_u$ — $B^3\prod_g$) at 357 nm and excited O atoms at 777 nm before and after the addition of additive gas (N_2 or O_2). (a): in case of CAPPLAT plasma jet; (b): in case of APC plasma jet. Note: discharge conditions employed in CAPPLAT plasma and APC plasma are the same as those shown in Fig. 4-1 above. N_2 ($C^3\prod_u$ — $B^3\prod_g$) at 357 nm and excited Ar atoms at 696 nm were selected as representatives for N_2 second positive system and excited Ar atoms, respectively.

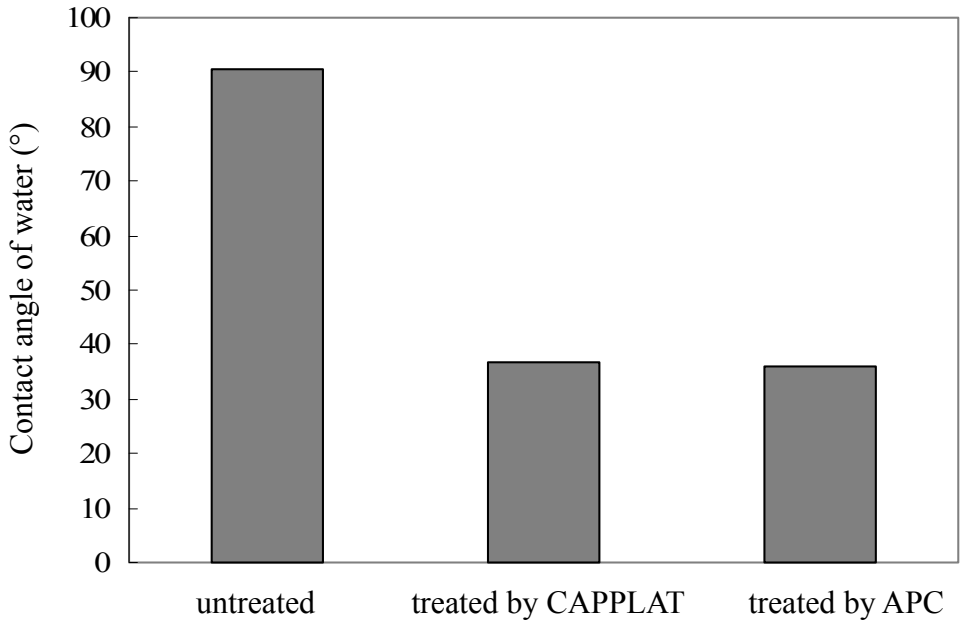

Fig. 4-3 Comparison of WCA values of HDPE samples before and after the plasma treatment. HDPE samples were treated by CAPPLAT pure Ar plasma jet and by APC pure Ar plasma jet, respectively. Treatment time and treatment distance were maintained at 5 s and 5 mm, respectively. Ar flow rates in CAPPLAT plasma system and APC plasma system were maintained at 10 SLPM and 20 SLPM, respectively.

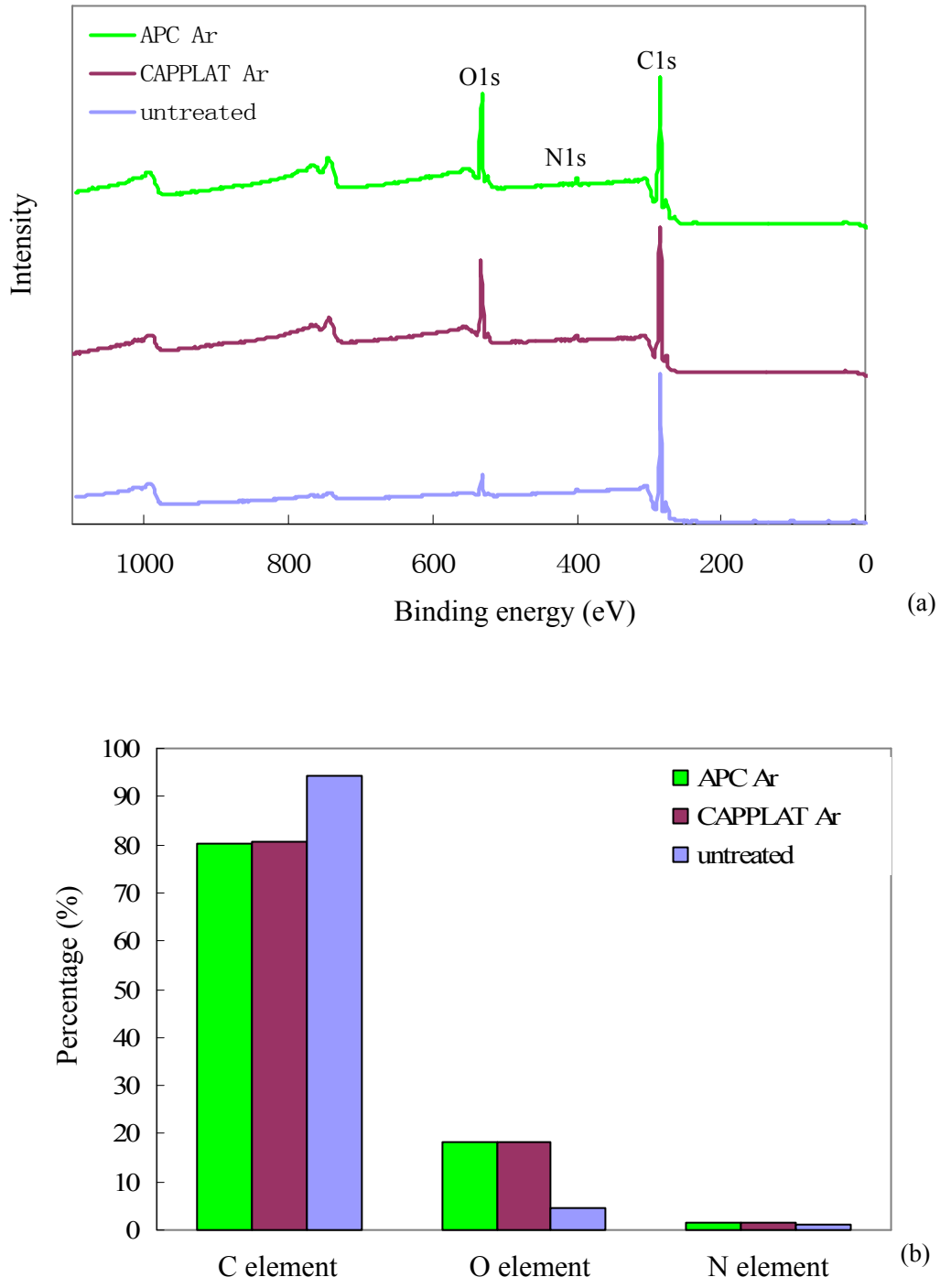

Fig. 4-4 Comparison of surface chemical compositions of HDPE samples before and after plasma treatment. (a): Comparison of typical XPS spectra; (b): Comparison of element percentages calculated from XPS measurement. HDPE samples were treated by CAPPLAT pure Ar plasma jet and APC pure Ar plasma jet, respectively. Treatment time and treatment distance were maintained at 5 s and 5 mm, respectively. Ar flow rates in CAPPLAT plasma system and APC plasma system were maintained at 10 SLPM and 20 SLPM, respectively.

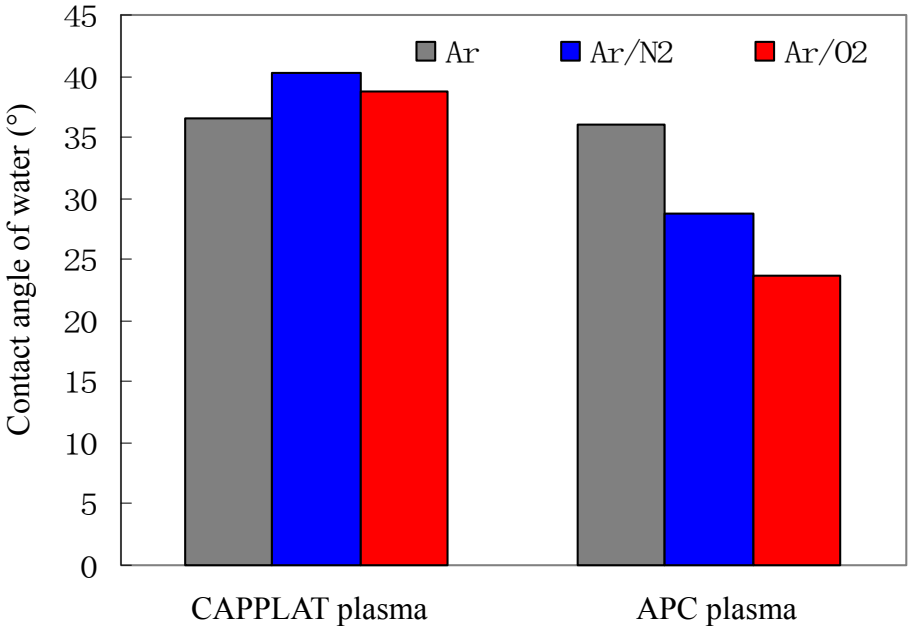

Fig. 4-5 Effect of additive gas (N_2 or O_2) on WCA of HDPE samples treated by CAPPLAT plasma jet and APC plasma jet, respectively. HDPE samples were treated for 5 seconds at a treatment distance of 5 mm. During CAPPLAT plasma treatment, Ar flow rate and the additive gas (N_2 or O_2) flow rate were maintained at 10 SLPM and 30 smlpm, respectively. During APC plasma treatment, Ar flow rate and the additive gas (N_2 or O_2) flow rate were maintained at 20 SLPM and 30 smlpm, respectively.

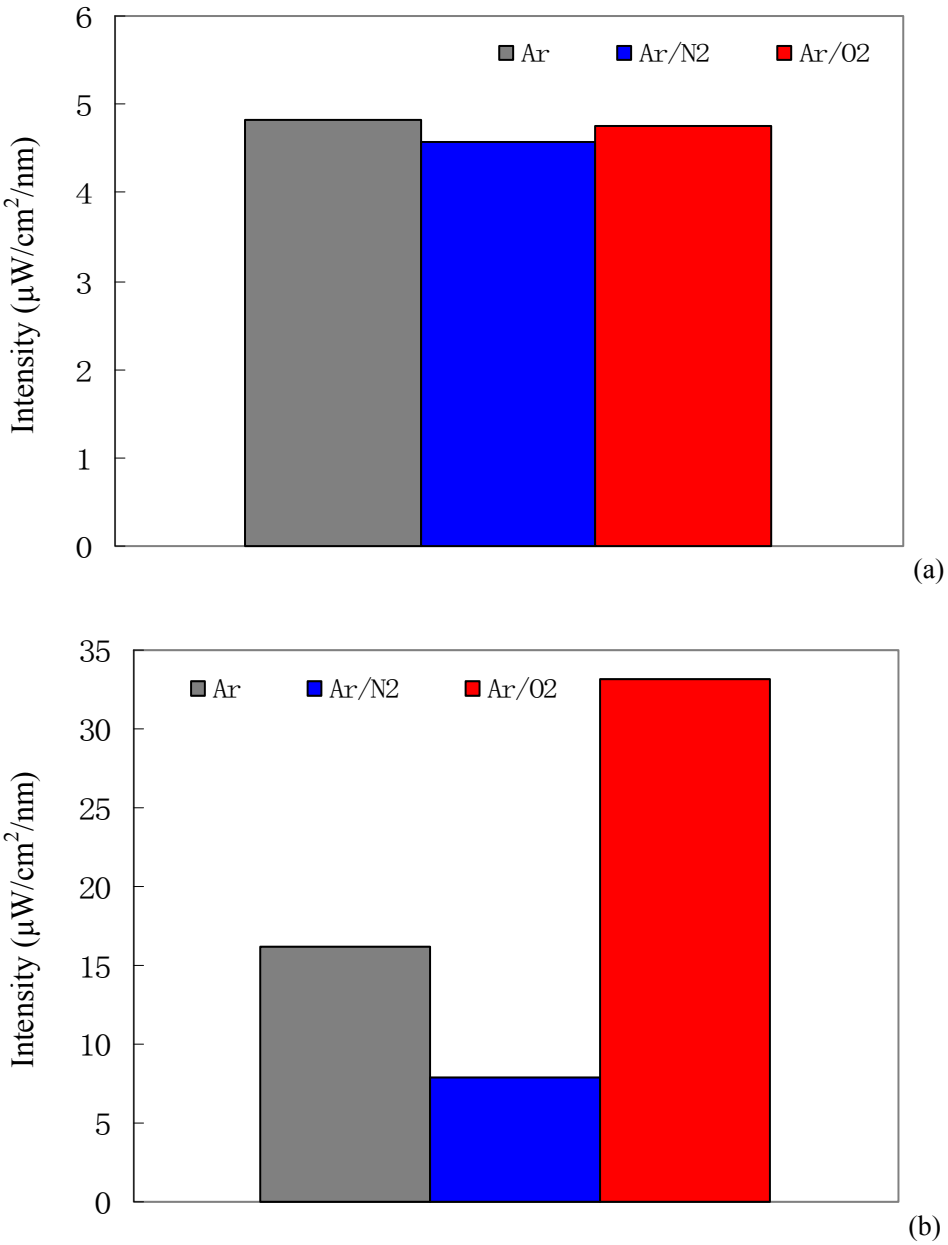

Fig. 4-6 Changes in effective total emission intensities of CAPPLAT plasma jet (a), and APC plasma jet (b), before and after the addition of additive gas (N_2 or O_2). Note: discharge conditions employed in CAPPLAT plasma and APC plasma are the same as those shown in Fig. 4-1 above. Flow rate of the additive gas (N_2 or O_2) was maintained at 30 smlpm for CAPPLAT plasma system and APC plasma system. Only active species in the wavelength range of 350–950 nm are counted in the effective total emission intensity.

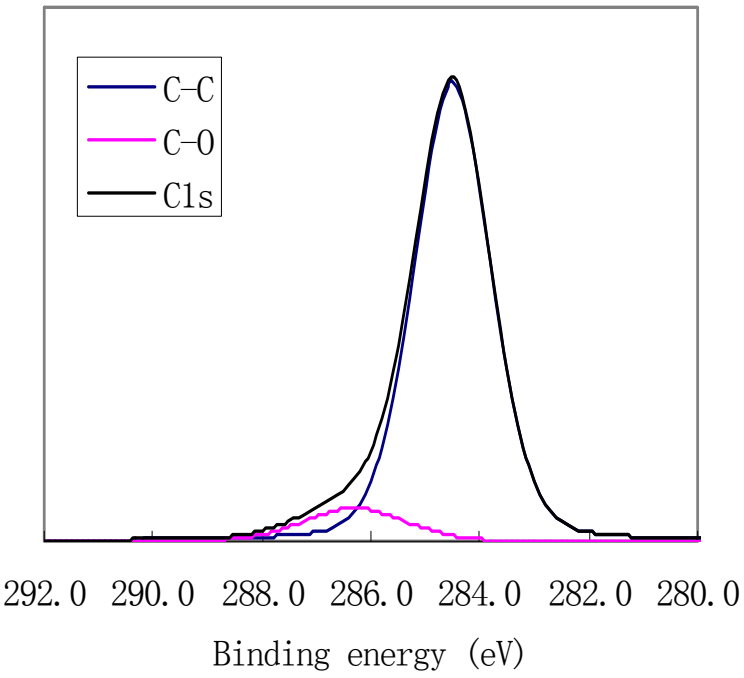
C-C
C-O
C1s
292.0 290.0 288.0 286.0 284.0 282.0 280.0
Binding energy (eV)

(a)

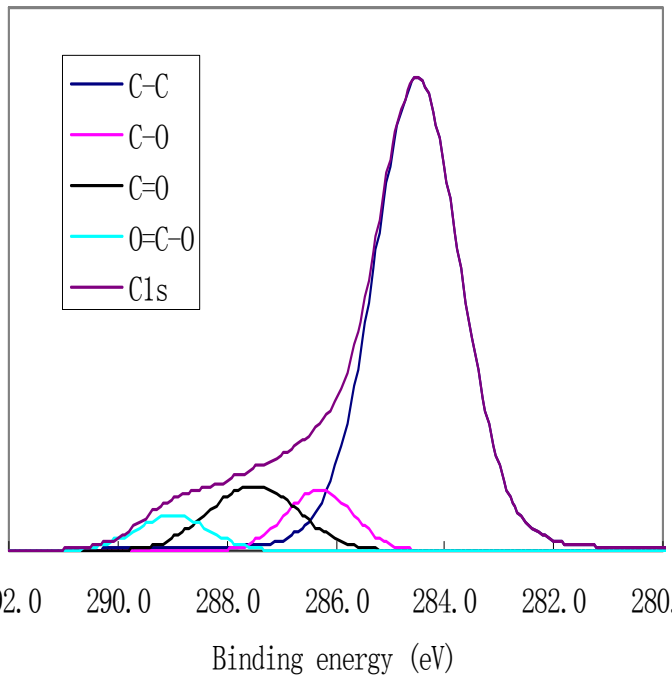
C-C
C-O
C=O
O=C-O
C1s
292.0 290.0 288.0 286.0 284.0 282.0 280.0
Binding energy (eV)

(b)

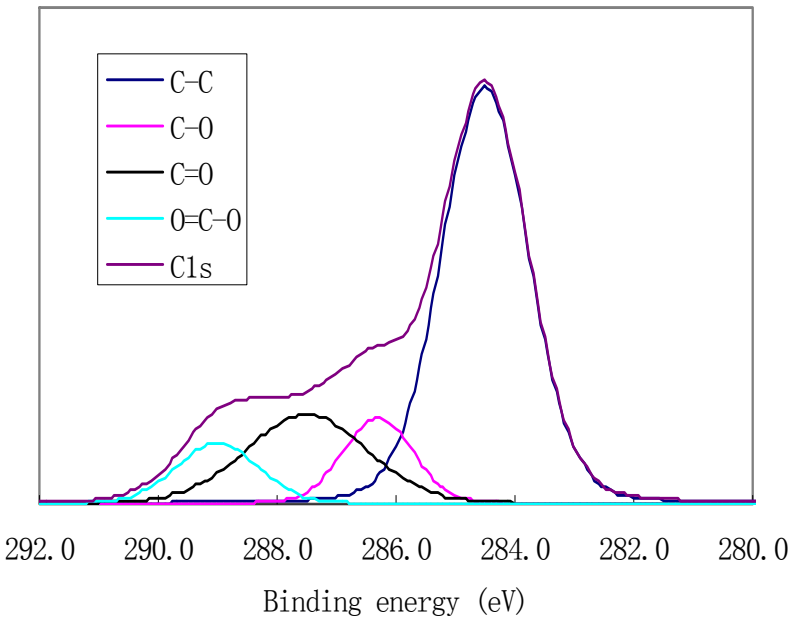

(c)

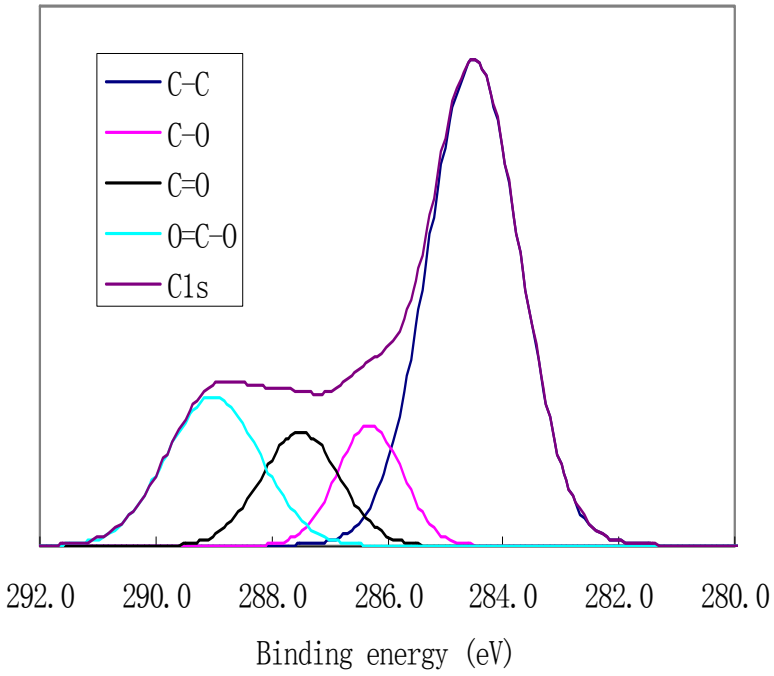

(d)

Fig. 4-7 High resolution XPS spectral analysis for C1s peaks of untreated HDPE (a), treated by APC Ar plasma (b), by APC Ar/N_2 plasma (c), and by APC Ar/O_2 plasma (d). Note: XPS measurement was performed immediately after HDPE samples were treated by plasma.

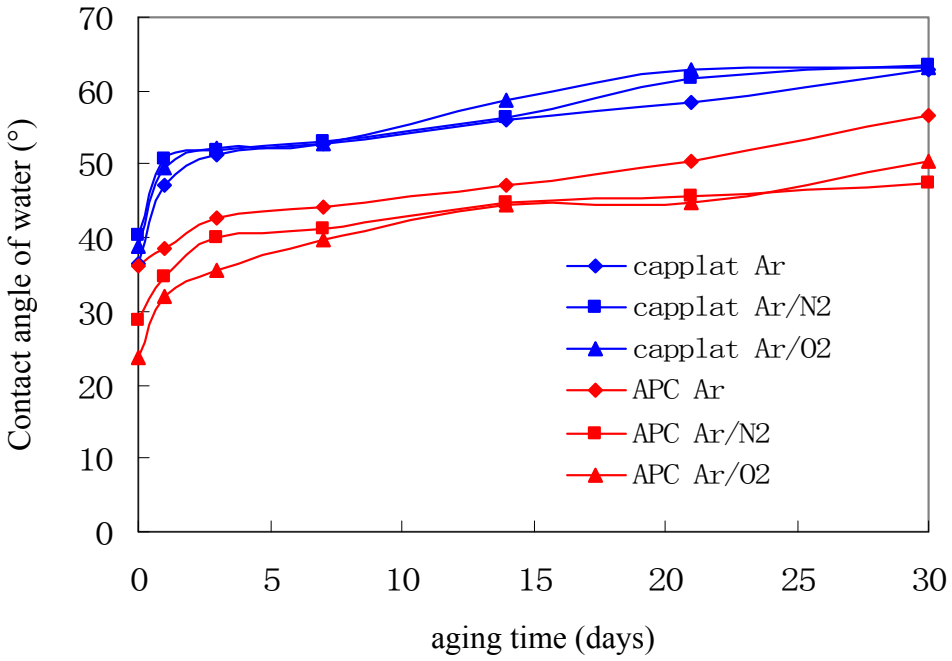

Fig. 4-8 Changes in WCA values of HDPE samples treated by CAPPLAT plasma jet and APC plasma jet. Note: investigation of changes in WCA values of plasma-treated HDPE samples was performed in the atmosphere at room temperature (25 ºC). WCA was measured at different aging time since the sample was treated by plasma.

Chapter 5 Summary

Realizing stable Ar glow discharges at atmospheric pressure is very meaningful for the application of homogenous plasma treatment with lower costs, since the complicated vacuum systems and expensive helium gas are unnecessary. A RF capacitive atmospheric pressure cold plasma device was developed by Cresur Corporation of Japan. This plasma device has been commercialized under the name of "APC". Using APC, a cold Ar plasma jet is able to be generated at atmospheric pressure. On the other hand, we have successfully developed a device that is able to generate a non-equilibrium atmospheric pressure Ar plasma jet of low temperature (22 to 35°C) using surface discharge fed by a high-voltage pulsed power source. This device has been commercialized under the name of "CAPPLAT" by Cresur Corporation of Japan. Though a variety of applications are being implemented, the electrical and the optical properties of these two atmospheric pressure cold Ar plasma jets have never been studied systematically. Therefore, it is highly desirable to get better understanding for the electrical and the optical properties of these two atmospheric pressure cold Ar plasma jets.

In chapter 2, electrical properties of APC Ar plasma jet were characterized using a high-voltage probe and a current probe. According to the observed waveforms of discharge voltage and RF current, the discharge behavior was confirmed. In particular, the effects such as additive gas (N_2 or O_2), torch diameter, and feeding gas flow rate on the electrical properties of APC Ar plasma jet were investigated in detail. It was found that APC Ar plasma jet is a stable abnormal glow discharge (the RF α-mode discharge), and this discharge behavior scarcely changed with different Ar flow rates and different torch diameters. Further, optical emission spectrometry (OES) was employed to identify the active species in APC Ar plasma jet. OES revealed that Ar active species belonging to the excited Ar

atoms (4p-4s transition) are predominant in this plasma jet (in the wavelength range of 690–950 nm). Peaks belonging to the N_2 second positive system (N_2 ($C^3\prod_u$ — $B^3\prod_g$)) were also observed. However, peaks belonging to the N_2 first negative system ((N_2^+ ($B^2\Sigma^+_u$ — $X^2\Sigma^+_g$)) (E ≈ 18.7 eV) were not detected. Additionally, an O atom peak was detected at 777 nm. Both the nitrogen and oxygen active species were detected in the pure Ar discharge because the impurities (N_2 and O_2) from the atmosphere were entrained into the plasma. Based on the electrical and optical characterizations, the chemical reactions of active species in APC Ar plasma jet were proposed. In particular, we investigated the effect of additive gas (N_2 or O_2) on the OES of APC Ar plasma jet. It was shown that the emission intensity of O atoms increased significantly when trace of O_2 gas was added. However, the emission intensities of N_2 ($C^3\prod_u$ — $B^3\prod_g$) increased only slightly when the same amount of N_2 gas was added. We assumed that the generated N_2 ($C^3\prod_u$) quickly transformed to N_2^+ ($B^2\Sigma^+_u$) through the successive collisions with energetic electrons, and then the newly created N_2^+ ($B^2\Sigma^+_u$) was trapped in the discharge region by a high frequency polarity change.

In chapter 3, electrical properties of CAPPLAT Ar plasma jet were characterized using a high-voltage probe and a current probe. Further, optical emission spectrometry (OES) was employed to identify the active species in CAPPLAT Ar plasma jet. In particular, the effects of additive gas (N_2 or O_2) on the electrical and optical characteristics of CAPPLAT Ar plasma jet were investigated in detail. According to the electrical characterization, it was found that CAPPLAT Ar plasma jet was a glow-like (diffuse barrier mode) discharge; and this discharge behavior scarcely changed with the injection of the additive gas either directly into the Ar stream or into the plasma afterglow zone through a glass capillary. On the basis of this observation, a simple discharge mechanism was proposed. According to this mechanism, in the first step, Ar molecules are excited and ionized

through collisions with energetic electrons. In this step, energy is transferred to the Ar particles, and Ar metastable atoms are generated. In the second step, Ar metastable atoms, the main energy carrier, are used to generate N_2 ($C^3\prod_u$) and O atoms through collisions with N_2 or O_2 molecules. On the other hand, OES characterization revealed that Ar active species belonging to the excited Ar atoms (4p-4s transition) are predominant in CAPPLAT Ar plasma jet (in the wavelength range of 690–950 nm). Peaks belonging to the N_2 second positive system (N_2 ($C^3\prod_u$ — $B^3\prod_g$)) were also observed. N_2 ($C^3\prod_u$ — $B^3\prod_g$) (E ≈ 11.1 eV) were generated through a resonant reaction between Ar metastables (E ≈ 11.5 eV) and ground-state molecular N_2. Additionally, an O atom peak was detected at 777 nm, with rather weak emission intensity. A small quantity of O atoms was generated through collisions between the excited Ar atoms and molecular O_2. CAPPLAT plasma jet was strongly modified when N_2 gas was injected directly into the Ar stream. In this case, Ar metastables were highly quenched; and N_2 ($C^3\prod_u$) became the main energy carrier. This resulted in a marked decrease in the emission intensities of excited Ar atoms and excited O atoms. When O_2 gas was added to the plasma afterglow zone through a glass capillary, no significant quenching effect was observed, since electrons and ions are not present in the afterglow zone. In this case, the emission intensities of excited Ar atoms decreased only slightly. Interestingly, the emission intensity of excited O atoms decreased with increasing concentration of added O_2. We presumed that the newly generated O atoms were quickly transformed to O_3 through combination with the added O_2 molecules.

In chapter 4, both the physical and the chemical characteristics of APC Ar plasma jet and CAPPLAT Ar plasma jet were compared. The electrical characteristics showed that the discharges of APC plasma jet and CAPPLAT plasma jet are glow (glow-like) discharges, which is very meaningful for the application of homogenous plasma treatment with lower costs since the complicated vacuum

system and expensive He gas are unnecessary. Additionally, it was shown that jet temperatures of these two Ar plasma jets are relatively low, which is very attractive for the treatment of thermal sensitive materials. OES characterization revealed that categories of the active species in APC plasma jet and CAPPLAT plasma jet are identical but the emission intensities of active species are quite different from each other. It was because the reaction mechanisms of active species in the two Ar plasma jets are different from each other. In CAPPLAT plasma jet, firstly energy is transferred to the Ar particles through collisions with energetic electrons; and then Ar metastables are generated. Second, Ar metastables, the main energy carrier, are used to generate nitrogen and oxygen active species through collisions with N_2 or O_2 molecules. However, in APC plasma jet, the direct collisions between N_2 or O_2 molecules with energetic electrons play an important role in the generation of nitrogen and oxygen active species.

To demonstrate an application of these two Ar plasma jets, high-density polyethylene (HDPE) surface treatment was performed using CAPPLAT Ar plasma jet and APC Ar plasma jet. In particular, the effects of additive gas (N_2 or O_2) on the HDPE surface treatment were investigated and compared in detail. It was concluded that the effective total emission intensity and the treatment temperature are two very important factors for HDPE surface treatment. Stronger effective total emission intensity suggests more effective energetic active species in the plasma, which results in the generation of more polar functional groups on HDPE surface. On the other hand, the molecular motion on polymer surface is not negligible when the treatment temperature is relatively high. Especially, when the treatment temperature is close to the melt point of the polymer, a lot of generated functional groups diffuse into the bulk of the polymer during the plasma treatment.

List of publications

1. Influences of Additive Gas on the Improvement of Hydrophilicity of Polymer Surface by a Cold Atmospheric Pressure Ar Plasma Jet

   Xiaomeng FEI, Shin-ichi KURODA, Yuki KONDO, Tamio MORI, Katsuhiko HOSOI

   Journal of Materials Life Society, accepted

   Related to Chapter 2 and Chapter 4

2. Influence of Additive Gas on Electrical and Optical Characteristics of RF Capacitive Atmospheric Pressure Cold Ar Plasma Jet

   Xiaomeng FEI, Shin-ichi KURODA, Yuki KONDO, Tamio MORI, Katsuhiko HOSOI

   Journal of Plasma Science and Technology, to be submitted

   Related to Chapter 2

3. Influence of Additive Gas on Electrical and Optical Characteristics of Non-equilibrium Atmospheric Pressure Ar Plasma Jet

   Xiaomeng FEI, Shin-ichi KURODA, Yuki KONDO, Tamio MORI, Katsuhiko HOSOI

   Journal of Plasma Science and Technology, submitted

   Related to Chapter 3

4. Comparison of High-density Polyethylene Surface Treatment Using Two Types of Cold Atmospheric Pressure Ar Plasma Jets

   Xiaomeng FEI, Shin-ichi KURODA, Yuki KONDO, Tamio MORI, Katsuhiko HOSOI

   Journal of Materials Life Society, accepted

   Related to Chapter 4

Acknowledgment

First of all, I wish to express my sincere gratitude to Professor Shin-ichi Kuroda, my supervisor, who provided much guidance and help for the accomplishment of this dissertation. Thank you for everything that you did for me during these years.

The heartfelt thanks are also given to Dr Kawai and Ms. Konoma for their kind encouragement and support during the study and the life in Japan.

I also wish to give special thanks to Professor Koumoto, Professor Tobita, Professor Takahashi, and Professor Kusumoto for their invaluable suggestions and comments to this dissertation.

A deep gratitude is also given to all the members of Kuroda Laboratory, especially to the members of plasma group, for their kind assistance and friendship.

Moreover, I wish to express my appreciation to Mr. Mori from Cresur Corporation for providing the plasma devices and the technical support.

Thanks are also given to Department of Culture, Sports, Education, Science and Technology of Japan for the supply of scholarship and all support.

Finally, I would like to give my special gratitude to my family and my friends for their support and encouragement in my life.